High Frequency Relaxation Kinetics in Metal and High-T_C Superconductor Nanocontacts

ILLYA KULYK

University of Groningen
Zernike Institute
for Advanced Materials

Cover: B. Verkin Institute for Low Temperature Physics and Engineering of the National Academy of Sciences, Ukraine

Cover design: Illya Kulyk

The work described in this thesis was performed in "Point-Contact Spectroscopy Laboratory" of ILTPE (B. Verkin Institute for Low Temperature Physics and Engineering) of the National Academy of Sciences, Ukraine and in the group "Surfaces and Thin Films" (part of the Zernike Institute for Advanced Materials) of the University of Groningen, the Netherlands.

Printed by: GrafiMedia, Facilitair Bedrijf, University of Groningen

Zernike Institute for Advanced Materials PhD. thesis series 2008-08

ISBN: 978-90-367-3499-8 (printed version)

ISBN: 978-90-367-3545-2 (electronic version)

ISSN 1570-1530

RIJKSUNIVERSITEIT GRONINGEN

High Frequency Relaxation Kinetics in Metal and High-T_C Superconductor Nanocontacts

Proefschrift

ter verkrijging van het doctoraat in de
Wiskunde en Natuurwetenschappen
aan de Rijksuniversiteit Groningen
op gezag van de
Rector Magnificus, dr. F. Zwarts,
in het openbaar te verdedigen op
maandag 8 september 2008
om 16:15 uur

door
Illya Kulyk

geboren op 17 mei 1961
te Tambov, Rusland

Promotor:	Prof. dr. P. Rudolf
Copromotor:	Prof. dr. I. K. Yanson

Beoordelingscommissie:	Prof. dr. A. Barone
	Prof. dr. ir. B. J. van Wees
	Prof. dr. J. M. van Ruitenbeek

Contents

Chapter 1

INTRODUCTION

1.1 Elementary Excitations and Quasiparticles in Solids

Following the explanation of physical effects in atoms, understanding the physical properties of metals is arguably the second most notable achievement of quantum mechanics. The translational symmetry of the crystalline lattice served as a key issue which enabled an exact solution for the electronic thermodynamic and kinetic properties and vibrational states of the atomic lattice. These solutions are known as the Bloch waves for electrons and as Debye vibrational modes (called phonons) for the lattice. For non-interacting particles, the distribution over the quantum states is given by the formula

$$f_p = \left[e^{(\varepsilon_p - \mu)/k_B T} + 1 \right]^{-1} \tag{1.1}$$

for electrons, and by the expression

$$N_q = \left[e^{\hbar\omega_q / k_B T} - 1 \right]^{-1} \tag{1.2}$$

for phonons, where p and q are the "crystal momenta" of electrons and phonons, respectively, and ε_p and ω_q are the corresponding energies of electron and phonon states; μ is the chemical potential of the electrons which equals the Fermi energy (the maximal energy of filled states) ε_F at temperature T=0. The typical Fermi energy of most metals is of the order of 10 eV, which corresponds to a temperature of about 100.000 K, while the typical phonon energy (the Debye energy) is of the order of 100 K.

The second key idea in the theory of solids was that of L. D. Landau [1] to include the effect of interaction between particles by transforming them into quasiparticles obeying the same statistics as the "bare" particles (the Fermi statistics for electrons and the Bose statistics for phonons). The interaction effect reduces the electron energy ε_p to the renormalized energy

$$\tilde{\varepsilon}_p = \varepsilon_p + \sum(p) \tag{1.3}$$

where $\Sigma(p)$ is called the electron mass operator, and the phonon frequency ω_q to the renormalized phonon frequency

$$\tilde{\omega}_q = \omega_q + \Pi(q), \tag{1.4}$$

where $\Pi(q)$ is the phonon polarization operator. The state of the metal is presented as a gas of "dressed" electrons and phonons with energies $\tilde{\varepsilon}_p$ and $\hbar\tilde{\omega}_q$ respectively. The important quantities explaining the thermal properties of metals are the electron density of states

$$N(\varepsilon) = \sum_p \delta(\varepsilon - \tilde{\varepsilon}_p) \tag{1.5}$$

and the phonon spectral density of states

$$F(\omega) = \sum_q \delta(\omega - \tilde{\omega}_q) \tag{1.6}$$

where $\delta(x)$ is the Dirac delta-function. The sums in (1.5) and (1.6) are accomplished by counting the electron and phonon states according to:

$$p_i = 2\pi\hbar n_i / L, \quad q_i = 2\pi n_i / L, \quad n_i = 0,\ 1,\ 2,\ \ldots \tag{1.7}$$

Methods of calculation of the electron and phonon spectra are presented in the Kittel's textbook [2].

1.2 Superconducting Junctions: the Josephson effect

The superconductivity of metals is the condensation of pairs of electrons with opposite momenta and spin orientations in a macroscopic coherent state. This phenomenon was discovered by H. Kamerling-Onnes [3] in 1911 as a complete loss of resistance of the metal at a certain temperature T=Tc (critical temperature). Later it was also shown that superconducting metals behave as ideal diamagnetics with zero magnetic field inside a metal, for applied fields H<Hc(T) – this phenomenon is called the Meissner effect [4].

The explanation of superconductivity was proposed by F. London [5] as the result of the rigidity of the wave function of

the superconductor, and phenomenologically described by V. L. Ginsburg and L. D. Landau [6]. Successively A. A. Abrikosov [7] showed that superconducting alloys display a mixed state in a certain range of magnetic fields, $H_{c1}<H<H_{c2}$ with a strong but reduced diamagnetism and a penetration of quantized magnetic vortices (fluxons) into the superconductor. The microscopic theory of superconductivity was developed by J. Bardeen, L.N. Cooper and J. R. Schrieffer (BCS theory [8]) as well as by N. N. Bogoliubov [9] and by L. P. Gor'kov [10] at approximately the same time with a model of attractive interaction between electrons caused by the exchange of virtual phonons. This is a Green-function language of a process in which an electron disturbs the phonon field around it, and this perturbation in the field is forwarded to another electron resulting in an attractive interaction between both. A detailed state-of-the-art description of superconductivity can be found in a book by M. Tinkham [11].

Superconductivity was considered a bulk property until B. D. Josephson predicted extraordinary phenomena in electron tunneling between superconductors [12], namely zero DC resistance between superconductors in a tunnel junction and the oscillation of tunneling current with a frequency

$$\omega = 2eV / \hbar \tag{1.8}$$

These effects were soon confirmed experimentally [13, 14], and resulted in an avalanche of theoretical, experimental and applied works on tunneling junctions.

Besides tunneling junctions, the supercurrent flow in a contact with a normal metal (the S-N-S contact) confirmed the intriguing prediction of A. F. Andreev [15] of the reflection of electron-hole type at a N-S boundary, and of the strongly phase-sensitive discrete spectrum of the superconducting quasiparticle [16].

The phase dependence of the supercurrent in a S-I-S junction (the tunneling contact) was calculated by V. Ambegaokar and A. Baratoff [17]:

$$J_{S-I-S} = (\pi\Delta / 2eR_N)\sin(\varphi) \tag{1.9}$$

where Δ is the energy gap of superconductor, and φ is the phase of the superconductive order parameter.

The phase dependence of the supercurrent in a S-C-S junction (constriction-type contact) was predicted to be non-sinusoidal by I. O. Kulik and A. N. Omel'yanchuk [18]:

$$J_{S-C-S} = (\pi\Delta / eR_N)\sin(\varphi / 2)\tanh(\Delta\cos(\varphi / 2) / 2T) \tag{1.10}$$

It was shown that it has twice the magnitude of the supercurrent at T=0 compared to the tunneling contact with the same contact resistance in the normal state R_N.

Extensive reviews [19-24] and books [25-28] on the contact properties in normal and superconducting states are available.

1.3 High-T_C Superconductivity

After many years of intense study (1911-1986), superconductivity reached the maximal critical temperature of 18 K. In the year 1986, J. G. Bednorz and K. A. Müller [29] found a new class of materials (perovskite type ceramic compounds) with much higher critical temperatures of up to 36 K, a value which quickly increased to 90 K, and later on to 120 K. These ceramics are

$$La_{1-x}Ba_xCuO_4 \qquad T_c = 36K$$
$$YBa_2Cu_3O_{7-x} \qquad T_c = 90K$$
$$Tl_2Ba_2Ca_2Cu_3O_{10} \qquad T_c = 120K$$

All these materials are layered compounds with strong valence forces in the layers and weak Van der Waals interactions between the layers. This is possibly the key for understanding the origin of a new type of superconductivity. Many theoretical mechanisms have been proposed to understand this type of superconductivity [30, 31] but a consensus has not yet been reached.

All bulk properties of these new superconductors appear to be the same as those of low-T_C superconductive metals: zero resistance below T_C; ideal diamagnetism and a mixed state with a vortex structure; macroscopic quantum coherence properties and the Josephson effect. Experiments indicate that the superconducting state is gapless and most probably, in the context of the BCS theory of superconductivity, corresponds to a *d*-wave pairing of electrons rather than to *s*-wave pairing in the conventional superconductors. This in particular is supported by experiments with orientation dependent tunneling between adjacent sides of single high-T_C crystals [32, 33].

Point-Contact Spectroscopy is a tool to determine whether the Electron-Phonon Interaction (EPI) mechanism and electron pairing may be as effective for high-T_C superconductors as for low-T_C ones.

1.4 Motivation for High Frequency Point-Contact Spectroscopy

One of the main endeavours of modern solid state physics is understanding the processes of relaxation of non-equilibrium quasiparticle excitations that determine kinetic and resonance phenomena: electrical and thermal conductivity, galvanic and thermo-magnetic effects, high frequency (HF) behaviour etc. These topics have become more important with the development of nanoscience and technology.

Direct static experiments are commonly influenced by all mechanisms of relaxation. More selective information can be obtained from dynamic measurements with a pulsed probe signal. The period of the pulse should be much less than the relaxation time, and its energy not more than one quantum of the excitation, otherwise the analysis will be complicated by multi-quantum and reabsorption effects. Such a selective approach permits determination of the individual contributions from various relaxation processes.

The method of extremely short thermal pulses (10^{-9} s) for the study of non-equilibrium phonon relaxation is widely known. Non-equilibrium electron processes are more complicated because of much smaller characteristic times. Point-Contact Spectroscopy (PCS) offers the possibility to investigate the properties of quasiparticle excitations, not by a pulsed approach, but with the response to a harmonic signal. The response of the electrical conductivity to irradiation in a wide range (10^3 –10^{15} Hz) is under study for NanoContact (NC) samples with diameters of 10–10^2 nm. The fundamental work of I. K. Yanson [34] on contacts of geometric size lower than the electron relaxation length (i. e., NCs) forms the basis for this new technique. The

relaxation of the local electronic excitation in such structures manifests itself as a strong non-linearity in their current-voltage characteristics (IVC). Nowadays, this method has found application in the study of such different phenomena as thermoelectric effect, galvanomagnetic effect, quantum localisation, electric fluctuations, single atom contacts etc.

From another point of view, the nonlinear electrical conductivity of NCs enables their application as nonlinear radiotechnical elements for the detection of electromagnetic radiation. Given the very small dimensions of NCs (in comparison with the skin depth), the external field is practically homogeneous in the contact zone up to optical frequencies.

The aim of the work reported in this thesis was to study the kinetics of the relaxation processes in NCs for a wide range of excitation energies and a wide range of frequencies. Along with the classical low frequency PCS, a new method of video response of NCs was developed for measuring the response to high frequency electromagnetic radiation. The latter was applied also to the study of high-T_C superconducting ceramics.

References

1. A. A. Abrikosov. Fundamental Theory of Metals, North Holland, 1988

2. C. Kittel. Introduction to Solid State Physics, 7th edition. Wiley, New York, 1996

3. H. Kamerlingh-Onnes. Leiden Comm. 120b, 122b, 124c (1911)

4. W. Meissner and R. Ochsenfeld. Short initial announcements. Naturwissenschaften 21, 787 (1933)

5. F. London. Superfluids, vol. 1. Wiley, New York, 1950

6. V. L. Ginsburg and Landau. On the theory of sperconductivity. Zh. Eksp. Teor. Fiz. 20, 1064 (1950)

7. A. A. Abrikosov. On the magnetic properties of superconductors of the second group. Sov. Phys. JETP 5, 1174 (1957)

8. J. Bardeen, L. N. Cooper and J. R. Schrieffer. Theory of sperconductivity. Phys. Rev. 108, 1175 (1957)

9. N. N. Bogoliubov. A new method in the theory of superconductivity. Sov. Phys. JETP 34, 41 (1958)

10. L. P. Gorkov. On the energy spectrum of superconductors. Sov. Phys. JETP 7, 505 (158)

11. M. Tinkham, Introduction to Superconductivity, 2nd edition. McGraw-Hill, New York, 1996

12. D. Josephson. A possible new effect in superconductive tunneling. Phys. Lett. 1, 251 (1962); Adv. Phys. 14, 419 (1965)

13. P. W. Anderson and J. M. Rowell. Possible observation of Josephson superconducting tunneling effect. Phys. Rev. Lett. 10, 230; 11, 200 (1963)

14. I. K. Yanson, V. M. Svistunov, and I. M. Dmitrenko. Experimental observation of tunnel effect for Cooper pairs with emission of photons. Sov. Phys. JETP 21, 650 (1965)

15. A. F. Andreev. The thermal conductivity of the intermediate state in superconductors. Sov. Phys. JETP 19, 1228 (1964)

16. I. O. Kulik. Macroscopic quantization and the proximity effect in S-N-S junctions. Sov. Phys. JETP 30, 944 (1970)

17. V. Ambegaokar and A. Baratoff. Tunneling between superconductors. Phys. Rev. Lett. 10, 486; 11, 104 (1963)

18. I. O. Kulik and A. N. Omelyanchouk. Contribution to the microscopic theory of the Josephson effect in superconducting bridges. Sov. Phys. JETP Lett. 21, 96 (1975)

19. N. Agrait, A. L. Yeyati, and J. M. van Ruitenbeek. Quantum properties of atomic-seized conductors. Phys. Reports – Review Section of Physics Letters, 377, 81 (2003)

20. A. A. Golubov, M. Yu. Kupriyanov, and E. Ilichev. The current-phase relation in Josephson junctions. Rev. Mod. Phys. 76, 411 (2004)

21. A. Feher, A. A. Mamaluj, A. Ya. Dulfan, E. S. Syrkin, and A. G. Shkorbatov. Low temperature phonon transport in 3D point-contacts. Sov. J. Low Temp. Phys. 31, 921, 2005

22. D. V. Averin and K. K. Likharev, in: Mesoscopic Phenomena in Solids, edited by B. L. Altshuler, P. A. Lee, and R. A. Webb. Elsevier, Amsterdam, 1991

23. M. A. Kastner. The single-electron transistor. Rev. Mod. Phys. 64, 849 (1992)

24. E. N. Bogachek, I. O. Kulik, and A. G. Shkorbatov. Ballistic charge-carrier kinetics and phonon drag in semiconducting point contacts. J. Phys. Condens. Matter 3, 8877 (1991)

25. A. Barone and G. Paterno. Physics and Applications of the Josephson Effect. Wiley, New York, 1982

26. I. O. Kulik, I. K. Yanson. The Josephson Effect in Superconductive Tunneling Structures. Keter Press, Israel Program for Scientific Translation, Jerusalem, 1972

27. K. K. Likharev. Dynamics of Josephson Junctions and Circuits. Gordon and Breach, New York, 1986

28. Y. Imry. Introduction to Mesoscopic Physics. Oxford Univ. Press, Oxford, 1997

29. J. G. Bednorz and K. A. Muller. Possible high-T_c superconductivity in the Ba-La-Cu-O system. J. Phys. B 64, 189 (1986)

30. High Temperature Superconductivity, edited by J. W. Lynn. Springer-Verlag, New York, 1990

31. Physical Properties of High Temperature Superconductors, edited by D. M. Ginsberg. World Scientific, Singapore, 1994

32. V. B. Geskenbein, A. I. Larkin, and A. Barone. Vortices with half magnetic-flux quanta in heavy-fermion superconductors. Phys. Rev. B 36, 235 (1987)

33. D. A. Wollman, D. J. Harlingen, W. C. Lee, D. M. Ginsberg, and A. J. Leggett. Experimental determination of the superconducting pairing state in YBCO from the phase coherence of YBCO-Pb DC SQUIDs. Phys. Rev. B 71, 2134 (1993)

34. I. K. Yanson. Nonlinear effects in the electrical conductance of point contacts and electron-phonon interaction in normal metals. Sov. Phys. JETP, 39, 506 (1974)

Chapter 2

NON-STATIONARY PROPERTIES OF METAL NANOCONTACTS

2.1 Abstract

Studying the nonlinear behaviour of the electrical conductivity of Nanocontacts (NCs) at low temperatures, where by NC we mean a nanoscopic bridge between massive metal electrodes with a characteristic diameter, d, of 10-100 nm, has nowadays become a simple but effective method for investigating the inelastic scattering processes of the electrons on different quasiparticle excitations in solids.

As known from the theory of Point-Contact Spectroscopy (PCS), the second derivative of the IVC of a NC is quite similar to the phonon spectrum of the metal, and this provides a simple and reliable method for studying this important property. The splitting of the Fermi surface exactly for the bias voltage applied to the NC, eV, serves as the energy probe that permits to realize the PCS.

There are three different regimes of PCS, distinguished by the relation between the diameter of the NC and the mean free paths of electrons (elastic l_i and inelastic l_ε), namely the ballistic, the diffusive and the thermal regime. The features of these different current states of PCS are discussed below in section 2.2.

Recording the second derivative of the current-voltage characteristics (IVC) of a NC provides the information about the Electron-Phonon Interaction (EPI) in the metal. The relaxation of the electrons occurs through the generation of non-equilibrium phonons in the NC and the reabsorption of non-equilibrium phonons by electrons is responsible for the background on the point-contact spectra. These considerations relate to the stationary conductivity of the NCs but quite important information may be obtained from measuring the spectra when the NC is exposed to high frequency (HF) electromagnetic radiation. The characteristic parameters of these processes are the relaxation times of the corresponding quasiparticle subsystems (electrons, phonons). The reabsorption of phonons decreases when the oscillation frequency of the electrons exceeds the characteristic phonon relaxation frequency. Therefore, the characteristic relaxation times of phonons in metals can be determined directly from the HF PCS measurements.

2.2 The Principles of the Point-Contact Spectroscopy of Metals

As already mentioned, a NC is a nanoscopic bridge between massive metal electrodes. From the theoretical point of view, there are two basic models of such contacts which are illustrated in Fig. 2.1 a) and b). In the "orifice" model, the contact is described as the circular hole in the isolating layer between two metal spaces. The main parameter of such a contact is the diameter, d. In the "channel" model, the contact is approximated as a long thin bridge that connects massive metal electrodes. In the latter model, there are two characteristic parameters: the length L and the diameter d of the contact. Other models describe the contact with more common hyperboloid zones that may be

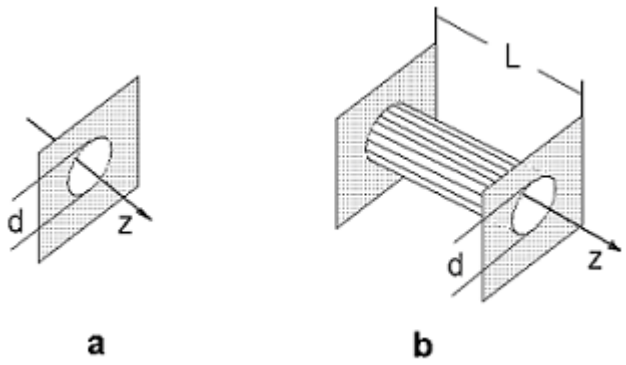

Fig. 2.1 Models of a nanocontact: a – an orifice in the dielectric wall; b – a long channel between two massive metal electrodes.

transformed into the previous models. The model type does not change the physics of the processes in the NC.

The subject of this study is the nonlinear behaviour of the electrical conductivity of NCs at low temperatures. Maxwell calculated the resistance of an electric contact of diameter d much larger than the electron mean free path l [1]:

$$R_M = \frac{\rho}{d}, \text{ for } d >> l, \tag{2.1}$$

where ρ is the resistivity of the metal.

In the case of the reverse relation between the characteristic dimensions, the resistance of the contact, according to Sharvin [2], is given by:

$$R_S = \frac{16}{3\pi}\frac{\rho l}{d^2}, \text{ for } d << l. \tag{2.2}$$

In the general case of any relation between *d* and *l*, Wexler [3] discovered the interpolation formula:

$$R_{pc} = R_S + \Gamma\left(l/d\right)\frac{\rho}{d} = R_S\left[1+\frac{3\pi}{16}\Gamma\left(l/d\right)\frac{d}{l}\right], \quad (2.3)$$

where $\Gamma(l/d)$ is a monotonous function of the parameter *l/d*; $\Gamma(0)=1$ and $\Gamma(\infty)=0{,}694$.

For the scattering of the electrons by phonons we can write

$$l = v_F\tau_{e-ph} \quad (2.4)$$

where v_F is the Fermi velocity and $\tau_{e\text{-}ph}$ is the characteristic time of scattering events, also called electron – phonon relaxation time. So, we have for the resistance of the NC:

$$R_{pc}\left(eV\right) = R_S\left[1+\frac{3\pi}{16}\Gamma\left(l/d\right)\frac{d}{v_F\tau_{e-ph}\left(eV\right)}\right]. \quad (2.5)$$

From the energy dependence of the electron – phonon relaxation time follows that [4]

$$\tau_{e-ph}^{-1} = \frac{2\pi}{\hbar}\int_0^{eV}\alpha^2F\left(\omega\right)d\omega \quad (2.6)$$

Hence $\tau_{e\text{-}ph}$ is determined by the Eliashberg function $\alpha^2F(\omega)$. The function $\alpha^2F(\omega)$ is the multiplication of the square of the electron–phonon interaction matrix element (normalised over the

Fermi surface), α, with the phonon density of states, $F(\omega)$. When differentiating (2.5) and considering (2.6), we obtain:

$$\frac{dR_{pc}}{dV}(eV) = \frac{3\pi^2}{8} R_S \frac{ed}{\hbar v_F} \Gamma(l/d)\alpha^2 F(eV). \quad (2.7)$$

So the second derivative of the IVC of a NC, $d^2V/dI^2=(dR/dV)\cdot R$, will be quite similar to the phonon spectrum of the metal.

As shown theoretically [5, 6], the processes of inelastic scattering of electrons from any quasiparticle excitation in the NC, that depends on the electrons energy, will cause irregularities in the d^2V/dI^2 spectra at the characteristic quasiparticle energies. The exact theoretical analysis of the NC "orifice" model presents the Fermi surface for the electrons in the proximity of the orifice as shown in Fig. 2.2.

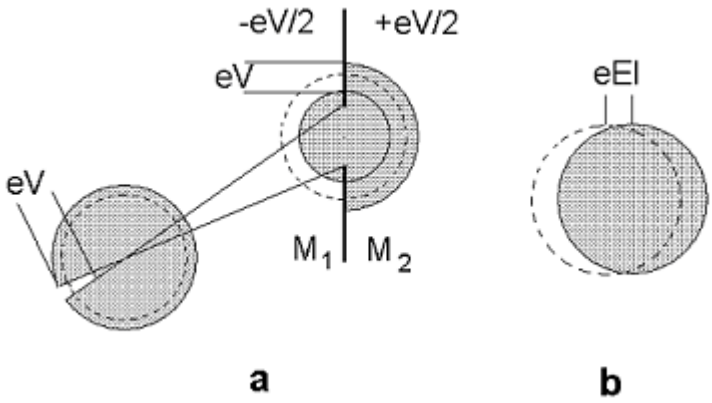

Fig. 2.2 Non-equilibrium functions of the distribution of the electron momenta: a - in two different points of the ballistic nanocontact; b – for the homogeneous current state.

The dashed line represents the equilibrium Fermi surface for an isotropic electron distribution. The hatched space corresponds to the occupied electron states; its volume does not depend on the coordinates because of the charge neutrality condition. The splitting of the Fermi surface exactly for the eV value serves as the energy probe that permits to realize the PCS of the elementary excitations in metals. In the absence of such a narrow spot for the current state, such a probe does not exist (Fig. 2.2, b). Moreover, the accessible electron energy, in this case limited by heating of the metal, is quite small ~ eVl/L (here L is the length of the macroscopic sample).

Scattering of the electrons in the contact brings about a relaxation of the distribution shown in Fig. 2.2 (a). The generation of phonons results in a decrease in the conductivity of the NC. As shown above, the second derivative of the IVC of the contact may be written for T=0 as

$$R^{-1}\frac{dR}{dV}=\frac{8ed}{3\hbar v_F}\alpha_{pc}^2F(eV)=\frac{8ed}{3\hbar v_F}g_{pc}(eV) \quad (2.8)$$

The NC function of the EPI is given as

$$g_{pc}(eV)=\alpha_{pc}^2F(eV)\,. \quad (2.9)$$

The NC EPI is different from the thermodynamic Eliashberg function $g(eV)=\alpha^2F(\varepsilon)$ because of the presence of the geometric form-factor K, that takes in account the kinematics of electron scattering in the NC. The EPI functions (thermodynamic, transport and NC ones) determine the physical properties of metals [4]: electrical and thermal conductivity, superconductivity and the most important integral parameter of the metal, the constant of the EPI, λ:

$$\lambda = 2\int_0^{\infty} g(\omega)\frac{d\omega}{\omega}. \qquad (2.10)$$

When the temperature of the contact is $T\neq 0$, the phonon irregularities of the spectra will be broadened because of the thermal distortion of the Fermi distribution, and (2.8) will transform into:

$$-R\frac{d^2I}{dV^2}(eV) = R^{-1}\frac{dR}{dV}(eV) = \frac{8ed}{3\hbar v_F}\int_0^{\infty} g_{pc}(\varepsilon)\chi\left(\frac{\varepsilon - eV}{k_BT}\right)d\varepsilon \qquad (2.11)$$

where

$$\chi(y) = \frac{1}{k_BT}\frac{d^2}{dy^2}\left(\frac{y}{e^y - 1}\right). \qquad (2.12)$$

The function of thermal distortion $\chi(y)$ limits the precision of PCS to the value of $\Delta\varepsilon = 5{,}44\ k_BT$.

Up to now we have considered the case of pure contacts and the corresponding formulae were obtained for the generation of phonons in the ***ballistic regime*** of PCS, when $d<<l_i,\ l_\varepsilon$, where l_i and l_ε indicate the elastic (impulse relaxation) and inelastic (energy relaxation) mean free path of electrons, respectively. In the zeroth approximation, the resistance of the contact is determined by the Sharvin expression (2.2).

A specific feature of ballistic NCs is the decrease of the shot noise with respect to bulk conductors. This phenomenon is due to coherent phonon generation in ballistic NCs [7, 8, 9].

Another regime of PCS, when the contact diameter is much larger than l_i, but much smaller than the characteristic energy relaxation length $\Lambda=(l_i l_\varepsilon)^{1/2}/3$, is referred to as the ***diffusive regime***. The main formulae for this regime were reported elsewhere [10, 11]. The trajectories of electrons in the case of a diffusive current regime are no longer straight lines because of the elastic scattering of electrons by impurities in the contact. There is still the splitting of the Fermi surface exactly for eV in the proximity of the contact, as in the ballistic case (see Fig. 2.2, a). The difference with the ballistic case consists in the partial occupation of states outside the left semi-sphere and the partial emptying of states inside the right one. This is the reason for the reduced contribution of inelastic scattering process to the resistance of the contact. In a zeroth approximation, the resistance of the contact is determined by the Maxwell equation (2.1). In a first order approximation, the inelastic component of current, I_{in}, with respect to the elastic one, I_{el}, is given by [12]:

$$\frac{I_{in}}{I_{el}} \sim \frac{d}{l_\varepsilon}\frac{l_i}{d} \tag{2.13}$$

The PC spectrum is still given by the expression (2.8), but with a more complicated K-factor.

The third regime of PCS, the so-called *dirty* or ***thermal regime*** is realised in contacts with large diameters ($d>>l_i,\ l_\varepsilon$). At any point in the contact, equilibrium between the electron and phonon systems is achieved, with the local temperature $T(r)$ deriving from the balance between Joule heating and loss of heat by the electronic thermal conductivity. As shown by calculations [1], the temperature T_0 in the centre of the contact is:

$$T_0 = \left(T_b^2 + \frac{V^2}{4L} \right)^{1/2} \tag{2.14}$$

where L=0,026 mV^2/K^2 is the Lorenz number. When the temperature in the centre of the contact is much larger than the temperature of the cooling medium, T_b (usually it is the temperature of the liquid Helium bath), the relation between the temperature of the contact and the applied voltage is given by

$$eV = \frac{2\pi}{\sqrt{3}} k_B T \,, \tag{2.15}$$

or, simply,

$$V\left[mV\right] \sim 3,2\ T\left[K\right]. \tag{2.16}$$

In the thermal regime, the phonon irregularities in the PC spectrum are strongly broadened. Additionally, at large bias voltage a constant background signal arises due to scattering of the electrons by non-equilibrium phonons generated with increasing NC temperature. This phenomenon will be considered in detail later in this thesis.

It is important to mention that a NC with nonlinear IVC can be made as a four-terminal structure, in a way that the current passing between one pair of terminals changes the resistance between another pair of terminals. Such a structure can also work as a NC transistor [13].

2.3 Relaxation Processes in Nanocontacts and their Characteristic Relaxation Times

The experimentally measured second derivatives of the IVC are not equal to zero at energies higher than the maximum phonon energy, $eV \geq \hbar\omega_D$ (ω_D – Debye frequency), as it should be if (2.8) was a rigorous description. When considering the ballistic and diffusive regimes in the discussion above, we assumed that the phonon system remains in equilibrium. But in the current state, the relaxation of the electrons occurs via the generation of non-equilibrium phonons which escape through the massive electrodes that form the contact. The characteristic inelastic free path for these phonons is $l_{ph\text{-}e} \sim l_{e\text{-}ph} \sim v_F/\lambda\omega_D$. Therefore, in the ballistic regime, where both the elastic mean free path of the phonons, l_r, and that of the electrons, l_i, *are much larger than d*, only a small part of the non-equilibrium phonons (in the order of $d/l_{e\text{-}ph}$) is reabsorbed by the electron flux. That is the reason [14] for the small intensity of the background signal in the PC spectra in the ballistic regime.

The nature of the background could be explained qualitatively [15] in a following way. At large bias voltage, the quantity of the non-equilibrium phonons increases proportionally to the current density. This causes an increase in the reabsorption of non-equilibrium phonons by means of electrons scattering from those phonons. The resistance of the nanocontact will grow with the bias, and the second derivative of the IVC is no longer equal to zero [14, 16, 17, 18, 19]:

$$-R\frac{d^2I}{dV^2}(eV) = R^{-1}\frac{dR}{dV} =$$

$$= \frac{8ed}{3\hbar v_F}\left[g_{pc}(\omega) + \frac{\gamma}{2}\frac{eV}{eV+\hbar\omega_0} g_{pc}(\omega) + \gamma\int_0^{\infty} \frac{g_{pc}(\omega)\,d\omega}{\omega+\omega_0} \right], \tag{2.17}$$

where γ=0,58 (for the "orifice" geometry of the contact), $\omega_0=\omega_D(l_{ph\text{-}e}l_r)/d^2$ the frequency of the phonons escaping from the contact zone, defined by their inelastic and elastic mean free paths. The last two parts in (2.17) are the background signal on the second derivative of the IVC. The first one has a structure similar to $g_{pc}(eV)$, but with another form-factor; it refers to the stimulated phonon generation. The second one is the monotonous part of the background signal, caused by reabsorption of non-equilibrium phonons. In the case of a weak reabsorption process, when $\omega_0>>\omega_D$, the expression (2.17) transforms into

$$-R\frac{d^2I}{dV^2}(eV) = R^{-1}\frac{dR}{dV}(eV) = C\left\{ g_{pc}(eV) + b\int_0^{eV} g_{pc}(\omega)\frac{d\omega}{\omega} \right\} \tag{2.18}$$

Here the coefficient b is obtained by requiring that the PC spectrum is equal to zero when $eV\geq\hbar\omega_D$.

In addition to the monotonous background signal, smaller irregularities at higher frequencies which are multiples of maximal phonon frequencies ω_1, ω_2 and their combinations may be observed.

All of the above considerations relate to the stationary conductivity of the NCs, but important information can be obtained from measuring the PC spectra at high frequencies. The dynamics of the EPI and of the phonon reabsorption represent fundamental properties of metals. The characteristic parameters

of these processes are the relaxation times of the corresponding quasiparticle subsystems (electrons, phonons).

The shortest characteristic times for the NCs are associated with the relaxation of the electron subsystem. One of these is determined by the time for electron transport through the NC zone, $\tau_0 \sim d/v_F \sim 10^{-14}$ s (at $d \sim 10$ nm). Another one is related to the non-elastic scattering of the electrons from high-energy (Debye) phonons, $\tau_{e\text{-}ph} \sim 10^{-13}$ s. The lowest characteristic frequency is determined by the slow processes of the thermal relaxation of NCs: $\tau_T \sim cd/\lambda \sim 10^{-8}$–$10^{-9}$ s (where c is the specific heat and λ the thermal conductivity for metals).

The corresponding measurements at high frequencies significantly enlarge the investigation capabilities of PCS. They permit to study the energy dependence of the different scattering processes in metals and to determine experimentally the frequency parameters of these phenomena. With PCS experiments, these characteristic frequencies could be measured directly, as the relaxation times of NCs conductivity in HF fields. A special method [20] for the determination of the relaxation times for non-equilibrium excitations in metals has been claimed in a specific patent.

2.4 The Influence of High-Frequency Electromagnetic Rradiation on the Characteristics of Nanocontacts

When the inelastic mean free path of phonons is much higher than the contact diameter ($l_{ph\text{-}e} >> d$), and their elastic mean free path is smaller than the contact diameter ($l_r < d$), the PC spectrum is defined by the reabsorption of non-equilibrium phonons [18]. The distribution of the non-equilibrium phonons is a function of the bias voltage applied to the contact. In the case of complete

reabsorption of the non-equilibrium phonons, in the centre (z=0) of the NC the distribution of phonons will be

$$N_\omega(z=0) = \frac{eV - \hbar\omega}{4}(eV - \hbar\omega), \qquad (2.19)$$

and it will gradually decrease with the distance from the contact. The distribution (2.19) has the sharp edge at the phonon energy $\hbar\omega = eV$. The effective temperature of the phonon subsystem is

$$T_{eff} \approx \frac{eV}{4k_B}. \qquad (2.20)$$

A similar expression was presented previously for the thermal regime of the NC (2.16). This value does not regard the temperature of electrons; only for the thermal regime of PCS electrons could be characterised by an equilibrium temperature (2.16), that is quite similar to the one defined by (2.20) for non-equilibrium phonons.

The substantial differences between the electron and phonon subsystems are their characteristic relaxation frequencies. For the electrons they are very high [18, 21]:

$$f_{e-ph} \approx \lambda\omega_D \approx 10^{13} s^{-1}; \quad f_e \approx v_F / d \approx 10^{14} s^{-1}, \qquad (2.21)$$

where λ is the EPI constant, and f_e the frequency of the electron transport across the contact zone. The corresponding values for phonons are:

$$f_{ph-e} \approx \lambda \frac{s}{v_F}\omega_D \approx 10^{10} s^{-1}; \quad f_{ph} \approx s/d \approx 10^{11} s^{-1}, \qquad (2.22)$$

where s is the speed of sound. On this basis the frequency dispersion of the conductivity of the NCs in the HF range was theoretically predicted [18,19] and the modification of the spectrum with the applied voltage $V(t)=V_0+V_1cos(\Omega t)$ was analysed. For frequencies $f=\Omega/2\pi>f_{ph\text{-}e}$, the change occurs for the background component of the spectrum and is caused by non-equilibrium phonons. This is clear if one considers the fact that the amplitude of the oscillating part of the non-equilibrium distribution function for the phonons (generated by the transported electrons) depends on the relation between the oscillation frequency of the electron subsystem and that of the phonon relaxation. The reabsorption of phonons decreases when the frequency of the electron oscillation starts to be larger than the phonon relaxation frequency. For this reason, the signal detected on the contact also decreases as soon as its part derived from the electron-phonon scattering becomes smaller.

The background reduction coefficient $\eta=\gamma_{HF}/\gamma_{LF}$ could be introduced as the ratio of the background signal levels for high and low frequency, at $V_0>\hbar f_D/e$. The parameter γ is the spectral signal normalized to the acoustic (transverse) phonons T-maximum. η is obtained theoretically by

$$\eta(f)=\left[1+\left(f\Big/f_{ph-e}\right)^2\right]^{-1}, \qquad (2.23)$$

where the $f_{ph\text{-}e}$ is the average characteristic frequency of homogeneous relaxation of the entire multitude of phonons by electron-phonon scattering, mainly related to the high-energy phonons.

As can be seen from (2.23), the background component of the spectrum decreases with increasing frequency and goes to zero at

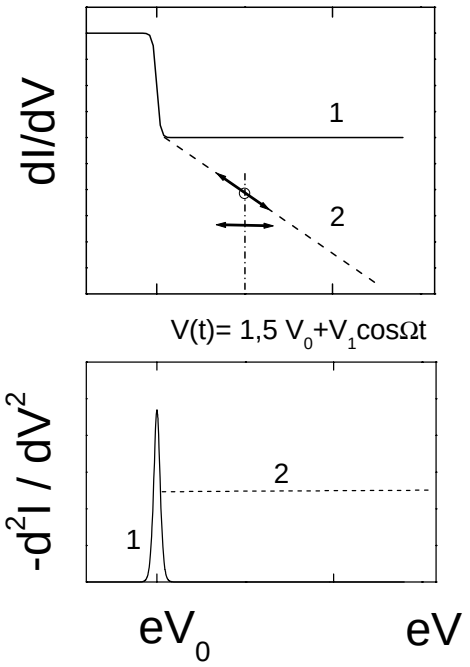

Fig 2.3 The first and the second derivative of the I-V characteristic of a nanocontact without the reabsorption of non-equilibrium phonons (1) and with the reabsorption of non-equilibrium phonons (2).

$f>>f_{ph\text{-}e}$. The physical processes in the NC are illustrated in Fig. 2.3 for a metal with the Einstein model phonon spectrum $g(\varepsilon)=\delta(\varepsilon - eV_0)$. At the bias voltage V_0, spontaneous generation of non-equilibrium phonons by the transported electrons begins and the conductivity of the NC drops (line 1). The electron relaxation is quite rapid (about 10^{-13} s), such that the quantity of generated phonons and, correspondingly, the dependence represented with line 1, remain the same up to frequencies of $\sim 10^{13}$ Hz. If reabsorption of non-equilibrium phonons is taken into

consideration, the conductivity of the NC should decrease with bias, due to the growth of electron-phonon scattering events (line 2). Consequently, the second derivative of the IVC will not be zero for $V>V_0$.

References

1. R. Holm. Electrical Contacts Handbook. Berlin, Göttingen and Heidelberg, 1958

2. Yu. V. Sharvin. A possible method for studying of Fermi surfaces**.** Sov. Phys. JETP, vol. 21, p. 655 (1965)

3. G. Wexler. The size effect and the non-local Boltzmann transport equation in orifice and disk geometry. Proc. Phys. Soc., 1966, v.89, N 4, p. 927-941

4. G. Grimvall. The electron-phonon interaction in normal metals. Phys. Scr., 1976, v.14, N 1/2, p. 63-78

5. A. N. Omel'yanchuk, I. O. Kulik, R. I. Shekhter. Contribution to the theory of nonlinear effects in the electric conductivity of metallic junctions. Sov. Phys. JETP Lett. vol. 25, No. 10, pp. 437-440 (1977)

6. I. O. Kulik, A. N. Omel'yanchuk, R. I. Shekhter. Electrical conductivity of point micro-bridges and phonon and impurity spectroscopy in normal metals. Sov. J. Low Temp. Phys., vol. 3, N 12, pp. 740-748 (1977)

7. A. I. Akimenko, A. B. Verkin, and I. K. Yanson. Point-contact noise spectroscopy of phonons in metals. Sov. J. Low Temp. Phys. 54, 247 (1984)

8. I. O. Kulik and A. M. Omelyanchouk. Non-equilibrium fluctuations in normal-metal point contacts. Sov. J. Low Temp. Phys. 10, 158 (1984)

9. M. Blanter and M. Buttiker. Shot noise in mesoscopic conductors. Phys. Reports-Review Section of Physics Letters. 336, 1 (2000)

10. I. O. Kulik, R. I. Shekhter, A. G. Shkorbatov. Point-contact spectroscopy of electron-phonon coupling in metals with small electron mean free path. Sov. Phys. JETP, vol. 54, N 6, pp. 1130-1137 (1981)

11. I. O. Kulik, I. K. Yanson. Microcontact phonon spectroscopy in the dirty limit. Sov. J. Low Temp. Phys., 1978, v.4, pp. 569-60

12. I. O. Kulik. Ballistic and non-ballistic regimes in point-contact spectroscopy. Sov. J. Low Temp. Phys. vol. 18, N 5, p. 302 (1992)

13. R. Ellialtioglu and I. I. Kaya. Conductance in metallic submicron cross-junctions, in: Quantum Mesoscopic Phenomena and Mesoscopic Devices in Microelectronics. NATO Science Series. vol. 559. Kluwer, Dordrecht, 2000

14. I. O. Kulik, A. N. Omel'yanchuk, I. G. Tuluzov. Processes of the second order with respect to the electron-phonon interaction in point contacts of normal metals. Sov. J. Low Temp. Phys., vol. 10, pp. 484-490 (1984)

15. I. K. Yanson, I. O. Kulik, A. G. Batrak. Point-contact spectroscopy of electron-phonon interaction in normal metal single crystals. Sov. J. Low Temp. Phys. vol. 42, N 5-6, p. 527 (1981)

16. A. P. van Gelder. On the structure of the d^2J/dV^2 characteristics of point contacts between metals. Solid State Communs., 1980, v.35, N 1, p. 19-21

17. I. O. Kulik, A. N. Omel'yanchuk, I. K. Yanson. Non-equilibrium phonons in the point-contacts between the normal metals. Sov. J. Low Temp. Phys. **7**, 129 (1991)

18. I. O. Kulik. Non-equilibrium current states in the metal micro-contacts. Sov. J. Low Temp. Phys. 11, 516 (1985)

19. I. F. Itskovich, R. I. Shekhter. Non-equilibrium phonons in conducting point-contacts. Sov. J. Low Temp. Phys. 11, 649 (1985).

20. I. O. Kulik, I. K. Yanson, O. P. Balkashin, Yu. A. Pilipenko, I. I. Kulik. The method for determination of the non-equilibrium excitations' relaxation time. USSR Patent No. 1581138, March 22, 1990

21. I. O. Kulik. Frequency dependence caused by Nonequilibrium phonon relaxation in the conductivity of metallic micro-contacts. JETP Lett., vol. 41, N 7, p. 370 (1985)

Chapter 3

NANOCONTACT TECHNOLOGY

3.1 Abstract

The two classical preparation methods for NCs are the "pin-to-plate" and the "shift" method explained below. The preparation of the surface of the electrodes is quite important: the surface layer which was damaged during cutting and polishing of the sample must be eliminated and a thin oxide layer has to be created on the metal surface.

The low temperature part of the equipment comprises liquid He cryostats, He gas pumping lines and exchangeable special cryogenic inserts for the creation and regulation of the NCs. Cryostats of two different types were used, one for the low frequency and HF measurements, and another one for the IR and optical irradiation experiments.

For the wide frequency range experiments, a coaxial line, a waveguide and a polished hollow optical light guide were mounted for the simultaneous connection of the different sources. For the 10^8–10^{11} Hz range high frequency triodes and frequency adjustable klystron generators were used; for the far-IR range, a special optically pumped laser was constructed. For irradiation in the IR and optical range, we employed CO_2 and He-Ne lasers, respectively. The radiation from every source was applied to the sample alternatively, and the corresponding response signal registered. At the end of each measurement cycle, the low frequency spectrum of the NC was routinely checked, to prove

that the given contact was stable and, consequently, its characteristics unchanged during the whole cycle of measurements.

The NC was connected to the measuring circuit according to a 4-electrode scheme. For measurement of minor non-linearities in the IVC of the NCs we registered the dI/dV characteristics by detection of the harmonics of a small oscillating current. which was generated on the contact together with the bias voltage linearly changing with time; for these measurements we applied the modulation method.

The PC spectrometer comprises several independent channels for the detection and registration of different kinds of signals on the NC.

3.2 Methods for Creating Nanocontacts

In the first NC experiments, the contacts were made in a non-controlled way by electric breakdown or by mechanical breaking of tunneling thin film structures. Nowadays NCs can be prepared by electron-beam lithography and ion etching or with a "break junction" technology. These methods allow for the creation of NCs of controlled dimensions.

In the work presented here, the NCs were created by the classical "pin-to-plate" method that permits the use of almost any kind of material for NCs. This simple technique [1] provides quite stable contacts in an easy way, by means of touching a polished plate with a sharp pin. In the alternative "shift" method, the contact is realised between two sides of crossed rectangular bars of metal, which can be moved one along the other. The shifting of the bars or the pressing of the pin electrode on the plate is realised with a precision mechanism employing differential screws, that has several degrees of freedom. Good mechanical stability is guaranteed by the relatively large contact

area of several microns (the radius of the curvature of the pin). The electric contact is realised just between the metal nanopins on the contact area, in the point where the surface oxide film is cracked. The typical diameters of the obtained NCs were in the range of 10-100 nm. Good mechanical stability of such a system can be achieved by shaping part of the pin wire into a damping curve, and by varying the force applied to the electrodes. Due to its mechanical stability, with this method long cycles of experimental measurements of different properties of the same NC can be performed.

The additional advantage of the "pin-to-plate" contacts is their optimal electrodynamic compatibility with mm-range irradiation: the wire electrode acts as an antenna and permits measurements at low irradiation power level. For the experiments that deal with Sb NCs, contacts of the "shift" type made of Sb monocrystalline bars were used.

As already mentioned in the introduction, for the "pin-to-plate" type of NCs the preparation of the surface of the electrodes is important: the surface layer which was damaged during cutting and polishing of the sample must be eliminated and a thin oxide layer has to be created on the metal surface; the latter has to be strong enough to support the stress force of the pin electrode and to guarantee the mechanical stability of the structure.

The methods of chemical treatment for the metals applied here were chosen according to the specific NC literature and general chemical reference literature [2, 3]. The shaping of the wire pins (0,05-0,2 mm diameter) made of Cu was performed with orthophosphorous acid. The diameter of the resulting pin was 1-2 μm, as controlled by an optical microscope. At a distance of 2-10 mm from the pin, the wire was fashioned into a damping S-shape curve. With increasing applied force, the electric resistance of the NC drops, and the quality of spectra, in most cases, improves as long as the diameter of the NC is not too large. For the low

resistance NC, the ballistic or diffusion current regime often transforms into the thermal regime of the conductivity by momentarily increasing of the current through the contact.

For the experiments with the Sb monocrystalline bars by the "shift" method, 2x2x10 mm size bars were spark-cut from bulk crystals. The axis of the contacts was oriented along the binary axis *C* of the Sb elementary cell. The bars of high purity Sb (relative resistance ratio $R_{300K}/R_{4,2K}\approx$6500–7000) were chemically etched using a HF:CH_3COOH:HNO_3 1:2:3 mixture before creating the NCs.

3.3 Description of the Experimental Set-Up

3.3.1 Cryogenic Equipment

The low temperature part of the equipment comprises liquid He cryostats with liquid N_2 protection screens, He gas pumping lines and exchangeable cryogenic inserts for the creation and regulation of the NCs. Cryostats of two different types were used, one for the low frequency and HF measurements, and another for the experiments with IR and optical irradiation. By pumping the He gas a temperature of 1,5 K could be reached which enabled measurements in superfluid He-II, below T_λ=2,17 K. These conditions avoided bubble formation in the liquid He when irradiating the sample with the optical laser. In some experiments the measurements were performed in over-pressurized liquid He to avoid bubble formation at temperatures above the λ-point in normal liquid He. For the microwave (MW)

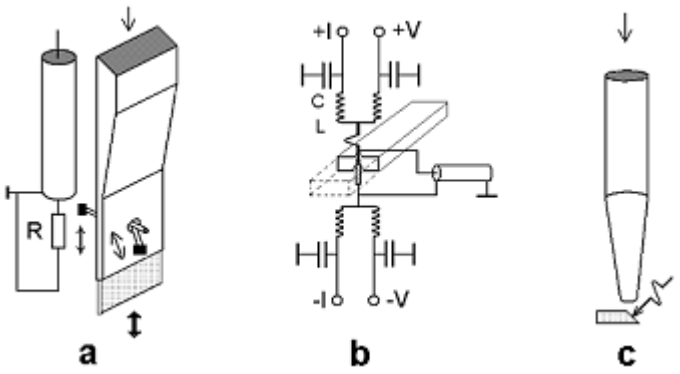

Fig. 3.1 The schemes of the creation of nanocontacts: a – "shift" type nanocontact in the waveguide; b - "pin-to-plate" nanocontact in the waveguide; c – "pin-to-plate" nanocontact at the output of the hollow optical light guide.

and optical measurements, cryogenic windows made of Germanium or crystalline quartz were used.

The schemes of the different inserts are presented in Fig. 3.1. The detection of MW radiation (10^8–10^{11} Hz) and the measurement of its second harmonics were carried out with the insert based on the rectangular waveguide (10x23 mm^2 in section), presented in Fig. 3.1, a. In the lower part of this insert, the cross section of the waveguide was gradually reduced down to 2x23 mm^2. The NC electrodes were introduced through the lateral holes and were mounted in two independent holders with precision displacement mechanics. It was possible to shift the electrodes with respect to one another and to vary the force applied to the electrode bars. Such a method allows for the creation of NCs at different points of the bars and to choose the NCs with the optimal characteristics in terms of the resistance of the NCs. Matching between the MW irradiation and the NC was optimised by moving the shortcutting plug at the bottom of the

waveguide. The high frequency radiation was conducted to the NC either by the waveguide, or by the coaxial cable charged with the 75 Ohm resistive coupling loop placed nearby the contact (Fig. 3.1 a, see also Fig. 3.2, a below). Fig. 3.1, b presents the insert which gives the additional possibility of mixing two MW signals. The NC was connected to the measuring devices with LC-filters, for uncoupling the DC current and the intermediate frequency signal (60–100 MHz); the latter was picked up with a standard coaxial cable.

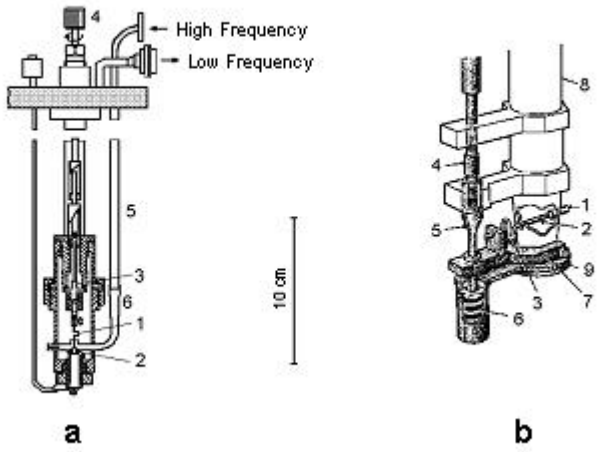

Fig. 3.2: a) The cryogenic insert for microwave irradiation: 1, 2 –electrodes of the nanocontact; 3 – differential screw; 4 – rotating movement; 5 – circular-section part of the waveguide; 6 – rectangular (1,8x3,6 mm^2) part of the waveguide;
b) The cryogenic insert for experiments in the IR and optical range: 1, 2 – electrodes of the nanocontact; 3 – S-shaped curve of the wire for damping; 4 - differential screw; 5 – axial movement; 6 – spring; 7 – bracket; 8 – hollow light guide; 9 – closure cap with a temperature sensor.

For experiments in the IR and optical range an insert with a polished hollow optical light guide (Fig. 3.1, c) was used.

The physical constructions of the cryogenic inserts are presented in Fig. 3.2. In Fig. 3.2 (a) the microwave insert is shown; the construction of the optical insert is demonstrated in Fig. 3.2, b.

3.3.2 Measurement of I-V Characteristics and their Derivatives

The NC was connected to the measuring circuit with four probes (see Fig. 3.1 b). For measurement of minor non-linearities in the IVC (the derivatives of the IVC) of the NCs, detection of the harmonics of the small oscillating current was used, generated on the contact together with the bias linearly changing with time.

If the current through the NC is presented as $I=I_0+i\cos(\omega t)$, $i<<I_0$, $\omega<<1/\tau_0$ (where I_0 is the bias current, and τ_0 is the characteristic relaxation time), the voltage on the contact will be

$$V(I) = V_0(I_0) + i\frac{dV}{dI}\cos(\omega t) + \frac{i^2}{2}\frac{d^2V}{dI^2}\cos^2(\omega t) + \ldots =$$
$$= V_0(I_0) + i\frac{dV}{dI}\cos(\omega t) + \frac{i^2}{4}\frac{d^2V}{dI^2} + \frac{i^2}{4}\frac{d^2V}{dI^2}\cos(2\omega t) + \ldots \tag{3.1}$$

If the amplitude of the modulation current is small enough and additional terms indicated by the dots in the sum (3.1) may be neglected, the output signal at the basic frequency will be proportional to the first derivative of the IVC, dV/dI, and that at the double frequency will be proportional to the second derivative of the IVC, d^2V/dI^2. The dependence of these values

on the bias voltage (energy), $V_1(eV_0)$ and $V_2(eV_0)$, represent the NC differential resistance and the point-contact spectrum, respectively. The signals at the basic frequency ω and at the double frequency 2ω can be easily measured experimentally.

For these measurements the modulation method was used. The modulation current ***i*** was applied to the NC from the acoustic generator. The frequency of modulation was in the range 463-1863 Hz in different experiments. The acoustic generator was converted to the current source by connection to the sample via the RC-circuit. The amplitude of the oscillation was quite small, in order to make the 1st harmonic of generated signal as small as 0,1–1 mV in order to avoid modulation broadening of the point-contact spectra. Amplification of the 1st harmonic signal was performed by a synchronous detector with a sensibility of 0,3 μV. Measurement of the 2nd harmonic signal at acoustic frequencies was realised with a sharp-band RLC filter and selective amplifier with a phase detector.

3.3.3 Measurements of the Nanocontact Response to Electromagnetic Radiation

For a NC in a HF field [4], the average IVC can be written as

$$\bar{I}(V) = \sum_{n=-\infty}^{\infty} J_n^2\left(\frac{eV_1}{\hbar\Omega}\right) I_0\left(V_0 + n\frac{\hbar\Omega}{e}\right) \qquad (3.2)$$

where V_1 and Ω are the amplitude and frequency of the signal generated by irradiation from an external source. In the case $\hbar\Omega << eV_1$ the expression (3.2) can be presented as the classic detection formula for the average current through the contact :

$$\bar{I}(V) = \frac{\Omega}{\pi} \int_0^{\pi/\Omega} I_0(V_0 + V_1 \cos \Omega t) dt \qquad (3.3)$$

In this case, the response of the contact (determined as the difference of the IVC of the contact with and without the irradiation) will be proportional to the 2nd derivative of the IVC curve:

$$\delta I(V_0) \equiv \bar{I}(V) - I_0(V_0) = \frac{V_1^2}{4} \frac{d^2 I_0}{dV^2}(V) . \qquad (3.4)$$

In the case of relatively high frequencies $\hbar\Omega >> eV_1$ the interaction between the electromagnetic field and the contact should be considered as the quantum process of absorption and emission of photons with an energy $\hbar\Omega$. It can be shown for this case that the expression (3.2) transforms into:

$$\delta I(V_0) = \left(\frac{eV_1}{2\hbar\Omega} \right)^2 \left[I_0\left(V_0 + \frac{\hbar\Omega}{e} \right) - 2I_0(V_0) + I_0\left(V_0 - \frac{\hbar\Omega}{e} \right) \right] \qquad (3.5)$$

The usual experimental protocol involved the measurement of the voltage response, related to the current response as $|V_d| = |\delta I| \, (dV / dI)$.

When irradiating the NC with IR or visible light, the video response signal is quite small (~1 μV) and can thus be influenced by the thermal bolometric effect caused by the irradiation power. In this case, a synchronous detection scheme was applied with a modulation of the impinging beam in the low frequency range ($\omega/2\pi$~10-3·10^3 Hz) and a rotating disc having equidistant holes

drilled along the circumference. With this modulated beam the induced current in the NC is:

$$I(t) = I_0 + i\Theta(\cos\omega t)\cos\Omega t, \quad \omega << \Omega \qquad (3.6)$$

where $\theta(x)$ is the Heavyside theta function. The voltage video response (at the modulation frequency ω) of the NC can be written as:

$$V_d \sim i^2 \left(d^2V / dI^2\right)\theta\left(\cos\omega t\right) / 4 \qquad (3.7)$$

The PC spectrometer has several independent channels for the detection and registration of different kinds of signals on the NC:

- direct current I_0 and direct voltage V_0 signal
- amplitudes of the 1st V_1 and 2nd V_2 harmonics of the low frequency modulation signal
- amplitude of the voltage response V_d under MW irradiation
- video response signal V_d under optical or IR laser irradiation.

Due to the different coupling coefficients and different transmission characteristics of the waveguides for different frequency ranges, the response signals of NCs have different effective power levels. To compare the results obtained for the different probe frequencies, the PC spectra were normalised for the intensity of the peak signal corresponding to transverse phonons.

To apply a classical or a quantum approach for the interpretation of the response signal, the energy of the photon should be compared with the interval ΔeV, related to the width of the non-linearity peak. The characteristic parameter for Cu (the half-width of the T-phonon peak) is equal to 11 meV.

All current sources used had an internal resistance that was much greater than the characteristic resistance of the NCs at zero bias (about tens of Ohm). For HF irradiation of the contact, the wave impedance of free space ($120\pi \approx 377$ Ohm) is also quite large compared with the typical resistance of the NCs.

At the end of each measurement cycle, the low frequency spectrum of the NC was routinely checked, to verify that the contact was stable and, consequently, its characteristics unchanged during the cycle of measurements. The measurement accuracies for I, V_2 and V_d signals were typically of 1 μA, 20 nV and 30 nV, correspondently.

3.3.4 Electromagnetic Radiation Sources

The parameters of the electromagnetic radiation sources, used for the investigations reported in this thesis are presented in Table 3.1.

For the wide frequency range experiments, a coaxial line and a waveguide were mounted for simultaneous connection of different generators. The radiation from each source was sent to the sample alternatively, and the corresponding response signal registered.

For the 10^8–10^{11} Hz range high frequency triodes and frequency adjustable klystron generators were used. For measuring the response signal, a klystron in the regime of external modulation was used; a low frequency meander modulation (2433 Hz) with an amplitude of ~80 V was applied to the reflector of the klystron.

Wave length, λ	Frequency, Hz, $f = \Omega/2\pi$	Quantum energy, meV, $\hbar\Omega$	Radiation source	Output power, mW
3 m 30 cm	10^8 10^9	$4\cdot10^{-4}$ $4\cdot10^{-3}$	High Frequency triode	500
6,31 cm 3 cm 5 mm 3,75 mm	$4{,}75\cdot10^9$ 10^{10} $6\cdot10^{10}$ $8\cdot10^{10}$	0,02 0,041 0,25 0,33	Klystron	10
1,22 mm 571 μm 118,8 μm 70,5 μm	$2{,}46\cdot10^{11}$ $5{,}25\cdot10^{11}$ $2{,}52\cdot10^{12}$ $4{,}25\cdot10^{12}$	1,02 2,17 10,43 17,6	Optically pumped far-IR laser	1 5 100 25
10,6 μm	$2{,}83\cdot10^{13}$	117	CO_2 laser	1000
3,39 μm 1,15 μm 0,63 μm	$8{,}84\cdot10^{13}$ $2{,}61\cdot10^{14}$ $4{,}75\cdot10^{14}$	366 1078 1960	He–Ne laser	30

Table 3.1 Parameters of electromagnetic radiation sources used in experiments.

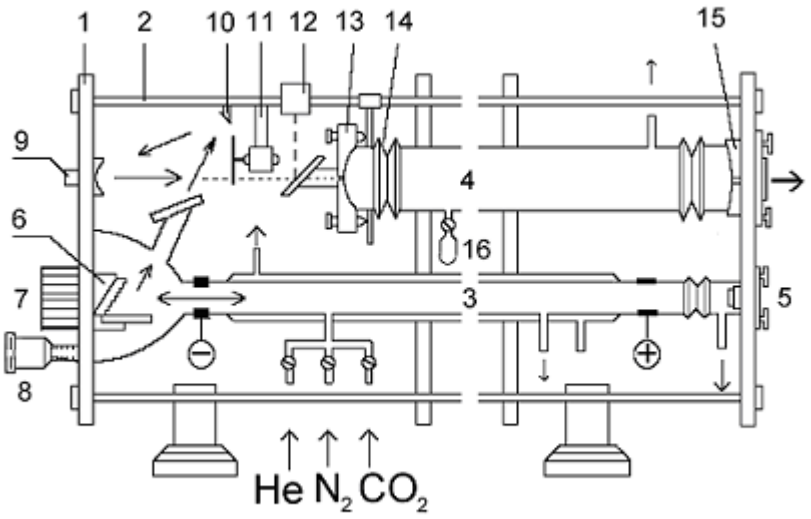

Fig. 3.3 Scheme of the optically pumped far-IR laser. For the explanation of the numbers, see text.

For the far-IR range, a specially constructed optically pumped laser was employed. It is pumped by a powerful (30-40 W) IR CO_2-laser that excites transitions between the rotational levels of the gas molecules of the far-IR laser. The scheme of this laser is presented in Fig. 3.3.

The CO_2-exciting laser and the far-IR laser were mounted in a unique module (190x34x27 cm^3), with INOX flanges (1) and INVAR staffs (2). The CO_2-laser cylinder (3) has an inner diameter of 14 mm and a 160 cm discharge length. At one end the piezo-driven adjustment head (5) with a mirror (R=8 m) is mounted. The other end houses the diffraction grating (6) having a period of 0,01 mm. The generation mix of $He:N_2:CO_2$=1:0,57:0,64 with a total pressure of 150-160 mm Hg was continuously pumped through the laser cylinder. Adjustment of the CO_2-generation lines was realised by a micrometric screw

(8). The Cu radiator (7) is attached to the grating for thermal stabilisation of the generation frequency. After modulation by the disc chopper (11), the excitation irradiation is reflected by the plain mirror (10) and the spherical one (9) with the R=60 cm, and consequently focused on the input mirror flange (13) of the far-IR resonator cylinder (4).

The input window (KCl) is mounted at an angle of 45° with respect to the beam axis. This gives the possibility to split the input beam and control the CO_2-excitation power with the detector (12). The input (13) and output (15) mirrors are made of Cu and have axial holes of 1,5 and 5 mm, respectively. Both mirrors are mounted on adjustment units (14). The output from the resonator cylinder is closed by a quartz crystal plate that is transparent in the far-IR range but completely removes the CO_2-irradiation of the excitation laser. The active gas for far-IR generation (methyl alcohol CH_3OH) enters the resonator cylinder from a vessel (16) through a needle valve, and is continuously pumped away to maintain a pressure of $(5–10)\cdot10^{-2}$ mm Hg in the cylinder. The generated wavelength was measured with a Michelson interferometer.

For irradiation in the IR and optical range, CO_2 and He-Ne lasers (see Table 3.1) were used, respectively. To irradiate the NC in this range of frequencies, we employed a cryogenic insert with a hollow tubular light guide (Fig. 3.2, b) with an Al spherical mirror (F=1 m) mounted at the top end. The orientation of the mirror was adjusted to reach the maximum response signal from the NC.

The “antenna” geometry of the “pin-to-plate” NCs is very advantageous for HF coupling. From another point of view, the extremely small area of the NCs (~$10–10^3$ nm^2) makes their electric capacity very small. Consequencely, the contact capacitance shorting effect is negligible. This fact enlarges the effective working range of the NCs up to optical frequencies.

For the NCs the skin-effect can be neglected, since the skin depth for frequencies of ~10^{14} Hz is about 10-20 nm. Thus irradiation of the NCs can be considered homogeneous in depth.

References

1. A. V. Khotkevich and I. K. Yanson. Atlas of Point Contact Spectra of Electron-Phonon Interaction in Metals. Kluver Academic Publishers, Boston/Dordrecht/London (1995)

2. L. Ya. Popilov, L. P. Zaitseva. Electropolishing and Electrolytic Etching of Metallographic Sections [in Russian]. Metallurgizdat, Moscow (1963), 410 p.

3. V. S. Kovalenko. Metallographic Reagents [in Russian], Metallurgiya, Moscow (1981), 120 p.

4. A. N. Omel'yanchuk, I. G. Tuluzov. Non-linear electrical conductivity of metal microcontacts in an alternating electric field. Sov. J. Low Temp. Phys., 1983, v.9, 142

HIGH FREQUENCY RELAXATION KINETICS IN METAL AND HIGH-T_C SUPERCONDUCTOR NANOCONTACTS

Chapter 4

HIGH FREQUENCY RESPONSE OF NANOCONTACTS WITH SHORT ELECTRON MEAN FREE PATH

4.1 Abstract

The thermal regime, realised in contacts with small electron mean free path, is the most simple to interpret. The experiments on the frequency dispersion in NCs in the thermal regime were performed for Cu and Sb contacts.

In the thermal regime, when the elastic and inelastic mean free paths of the electrons are much smaller than the diameter of the NC, the IVC is defined by the temperature dependence of the resistivity of the metal.

For thermal NC exposed to external electromagnetic radiation, the frequency of thermal relaxation of the NC defines the nature of the response signal. Experiments were performed in two ranges, for frequencies of the incident irradiation, Ω, smaller than the thermal relaxation frequency of the NC, ν_T, and for $\Omega>\nu_T$. The obtained results are discussed in the light of theoretical models. Our calculated results agree well with the experimental data. The experimental results permitted to calculate the thermal relaxation frequency for a Sb NC.

A theoretical calculation of ν_T for a Cu NC was also performed. The experimentally obtained response signal to microwave radiation was in good correspondence with theory.

Special attention was dedicated to the response of Cu NCs in the thermal regime when exposed to light in the IR and visible range. The contribution of NC's surrounding zone to the bolometric response in optical frequency range was taken into account to obtain an agreement between calculations and experimental data.

4.2 Thermal Relaxation Kinetics for Sb Nanocontacts

A relatively simple case of NC behaviour in alternating electromagnetic fields is the thermal regime of electron transport through the contact. In this regime, the IVC are defined by the temperature dependence of the resistivity of the metal. In stationary conditions, the temperature of the constriction zone is directly related to the applied bias voltage, according to (2.14).

When the applied voltage changes with a frequency close to the thermal relaxation frequency of the NC, a corresponding variation of the IVC can be expected. From measurements in the range $\Omega\tau_T \sim 1$, it is possible to define the characteristic frequency of the thermal relaxation of the contact $f_T \sim 1/\tau_T$.

As shown in Fig. 4.1, low frequency measurements of the PC spectra of Sb in the wide energy range [1] show that at bias $eV_0 \approx 175$ mV, a peak occurs, which is much higher than the low energy spectral singularities. All of the curves in Fig. 4.1 are normalised to the low-energy singularities of the spectrum. Icreasing the bias voltage, as a rule leads to NC instability and finally to a jump-like decrease in the resistance. Figure 4.1 shows that the higher the frequency, the lower is the amplitude of the mentioned maximum; in the 0,8–80 GHz range a plateau is reached.

The contact instability and the clear non-linearity of the IVC at high voltages point to a thermal effect, caused by the bias current

in the contact, as origin of the above-mentioned peak. The simple relation between the applied bias voltage and the temperature of

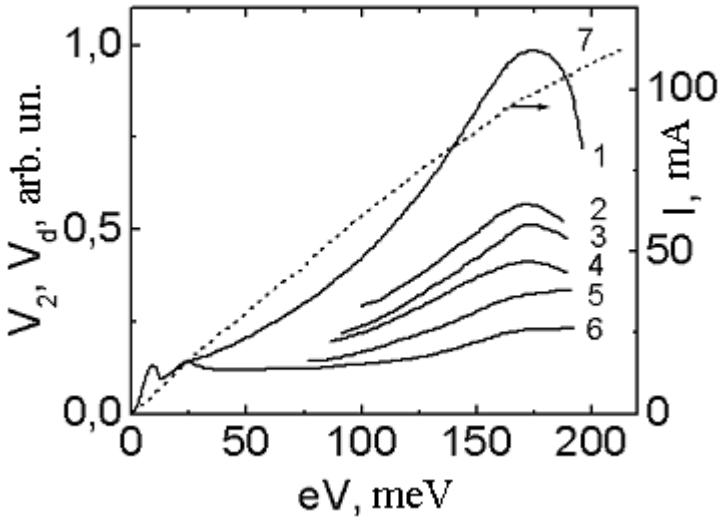

Fig. 4.1 The point-contact spectra of a Sb nanocontact over a wide energy range, measured at acoustic frequency at ~1 kHz (1) and at 0,033 GHz (2); 0,08 GHz (3); 0,155 GHz (4); 0,170 GHz (5) and at 80 GHz (6). The dashed line (7) presents the I-V characteristics of the nanocontact.

the contact in the thermal regime explains the dramatic change of the contact: indeed, the peak occurs when Sb becomes soft (≈406 K), at about 0,45 of the melting temperature. The corresponding bias voltage, V_S, taken from (2.14) is ≈131 mV. The difference with the experimental value (≈175 mV) can be due to the fact that at low energies the contact is still in the spectral regime (with characteristic singularities as presented in Fig. 4.1 at low energies) and gradually moves into the thermal regime with increasing bias. This kind of NC transformation could shift the observed V_S value upward. However, the high V_S value can also

be attributed to the temperature dependence of the Lorenz number.

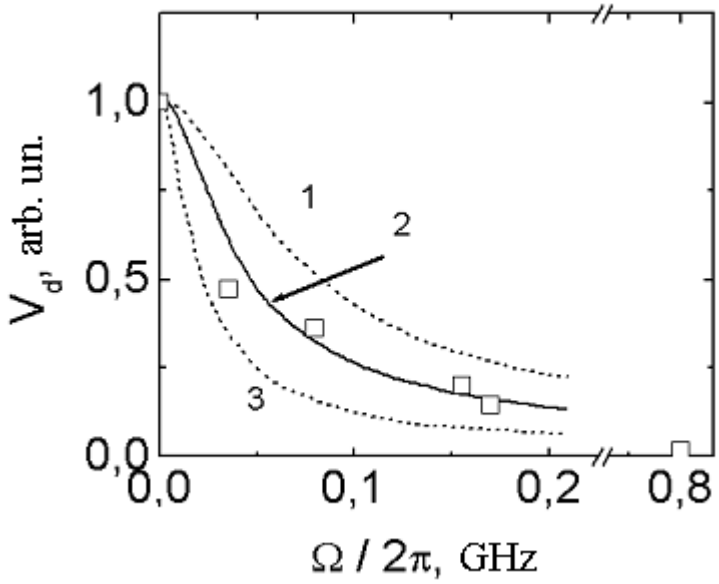

Fig. 4.2 Frequency dispersion of the thermal peak's amplitude from the Sb point-contact spectra. The calculated for the different f_T (thermal relaxation frequency) values curves approximate the experimental points: curve 1 for the f_T=0,3 GHz, curve 2 for the f_T=0,17 GHz and curve 3 for the f_T=0,08 GHz.

The higher the radiation frequency with respect to the nanocontact thermal relaxation frequency f_T, the smaller the temperature increase of the NC. The stationary temperature of the contact will increase and the measured HF response will become proportional to the first derivative [2]. This transition from one detection regime to another one was observed at f ≈0,17 GHz (Fig. 4.1). The points in Fig. 4.2 represent the experimental response values at eV≈175 meV, with detraction of the response level for f=80 GHz. The curves were calculated as the bolometric

NC response for the different constants $\tau_T \sim 1/f_T$, in accordance with

$$\delta(f) = \left[1 + (2\pi f \tau_T)^2\right]^{-1/2}. \qquad (4.1)$$

As it can be seen from the Fig. 4.2, the best agreement with the experiment data is for f_T=0,17 GHz.

Using the Wexler formula (2.3) and taking the zero-bias resistance of this Sb NC (R_0=1,5 Ohm), a contact diameter $d \approx 160$ nm can be calculated. The thermal relaxation frequency, f_T, for the given NC can be estimated as $f_T \approx s l_i / d^2$. Taking a reasonable value for the electron mean free path [3] for the NC in the thermal regime, namely $l_i \approx 5$ nm, the temperature relaxation frequency is found to be f_T =0,22 GHz.

By further considering the contact as a ball with diameter d and using the formula $f_T \approx \lambda / c\rho d^2$, with thermal conductivity λ=0,17 J/(cm·s·K), specific heat c=0,05 Cal/(g·K) and Sb density ρ=6,62 g/cm^3, we obtain f_T=0,12 GHz. This value is also quite close to the experimental one. With these different estimates that give quite close results, we can attribute the background peak at the Sb PC spectra to Joule heating of the contact by the transport current.

4.3 Theoretical Analysis of Relaxation Kinetics in the Thermal Regime

Experimentally, the spectra of NCs exposed to radiation in a wide frequency range are obtained by means of a small amplitude alternating voltage ($V(t)=V_0+V_1\cos(\Omega t)$, $V_1 << V_0$) applied to the contact. When using the current source (instead of

voltage source), the derivatives of IVs are dertermined by means of the small alternating current.

The theoretical analysis of the response of the NCs in the thermal regime [2] shows that the characteristic parameter is the frequency of the NC temperature relaxation $\nu_T \sim sl_i/d^2$ (s – speed of sound). With increasing modulation frequency, a transition occurs from synchronous detection (rectifying) of the external signal at $\Omega < \nu_T$ to bolometric detection when $\Omega > \nu_T$. In the first case, the temperature of the contact changes with applied voltage, while in the second case, the alternating external signal is converted into stationary heating of the contact. In this regime, the response becomes a rather smooth function of the bias voltage, V_0. The formulae for the NC response to HF radiation are [4]:

a) at low frequencies ($\Omega < \nu_T$)

$$\delta I(V_0) = -C\frac{V_1^2}{4}\int_0^\infty g_{tr}(\omega) S\left(\frac{|eV_0|}{\omega}\right)\frac{d\omega}{\omega},$$

$$S(x) = \frac{2\pi}{3}\frac{d^2}{dx^2}\int_0^{\pi/2} sh^{-2}\left(\frac{\pi}{\sqrt{3}x\sin y}\right)dy, \qquad (4.2)$$

where $C = \sqrt{3}\cdot\pi m/ne\hbar\rho_i R$. In this case the response signal is proportional to the 2nd derivative of the IVC, as we noted before (3.4).

b) at high frequencies ($\Omega > \nu_T$)

$$\delta I(V_0) = -C\frac{V_1^2}{4}\int_0^\infty g_{tr}(\omega) S_1\left(\frac{|eV_0|}{\omega}\right)\frac{d\omega}{\omega},$$

$$S_1 = \frac{2\pi}{3}\frac{d}{dx}\int_0^{\pi/2} sh^{-2}\left(\frac{\pi}{\sqrt{3}x\sin y}\right)\frac{dy}{x}. \qquad (4.3)$$

In this case radiation from the external source induces a HF current in the contact which heats up the NC while the bulk electrodes remain cool. Theoretical analysis shows [5] that in this situation the response of the contact will be similar to the 1st derivative of the IVC.

The situation changes when irradiating in the optical range, since in these conditions the heating also impacts the bulk electrodes (zone covered by the spot of the focused laser beam). At large generated voltages $V_0^2/4L >> T_0^2$ and consequently at high temperatures of the NC, when the function $\rho_{ph}(T)$ is linear ($\rho_{ph}(T)=\alpha T$), we obtain

$$\delta I(V) = -\frac{\alpha\sqrt{L}\left(T_1^2 - T_0^2\right)}{R\rho_i}. \qquad (4.4)$$

So, the response signal δI in the case of irradiation in the optical range is no longer dependent on the bias voltage, V_0. These theoretical considerations will be proven experimentally (see below).

4.4 Experimental Results for Cu Nanocontacts

The solid line in Fig. 4.3 shows the Cu-Cu NC response under irradiation with a frequency $\Omega/2\pi$=79 GHz. Using the value ρ_i=9·10^{-6} Ohm·cm, the resistance of the contact R=3,33 Ohm and (ρl_i=5.3·10^{-12} Ohm·cm^2), we obtain for the elastic mean free path for this NC l_i~6 nm, and a diameter of d~27 nm.

With these data the frequency of thermal relaxation is derived for this NC f_T~13 GHz (considering the speed of sound s=4,7·10^5 cm/s for Cu). This value is much lower than the frequency of the

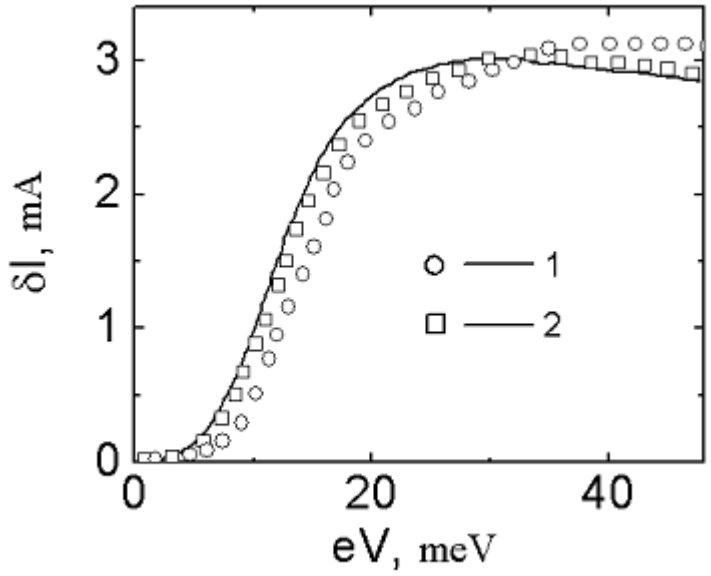

Fig. 4.3 The response of the Cu nanocontact to irradiation at the frequency $\Omega/2\pi=7{,}9\cdot10^{10}$ *GHz: 1 – calculation with* $g_{tr}(\omega)$*, 2 – calculation with* $g_{pc}(\omega)$*, continuous line – the experimental data.*

impinging radiation. So, for the calculation of the response for this NC the formula (4.3) can be used. To make the calculations correspond to the experimental data, a V_1 value of 4,7 mV was chosen for the calculations with $g_{tr}(\omega)$and V_1 value of 3.2 mV for the calculations with $g_{pc}(\omega)$.

The solid line in Fig. 4.4 presents the experimental results obtained for the Cu-Cu NC irradiated with the He-Ne laser. The laser beam was focused through the glass substrate on the back side of the Cu film. The inset in Fig. 4.4 shows the PC spectrum of this contact. The film thickness was ~1 μm. Identical

dependences were obtained with direct irradiation of the NC (front side). This experimental fact confirms the thermal nature of the response. As one can see, the signal V_d monotonously

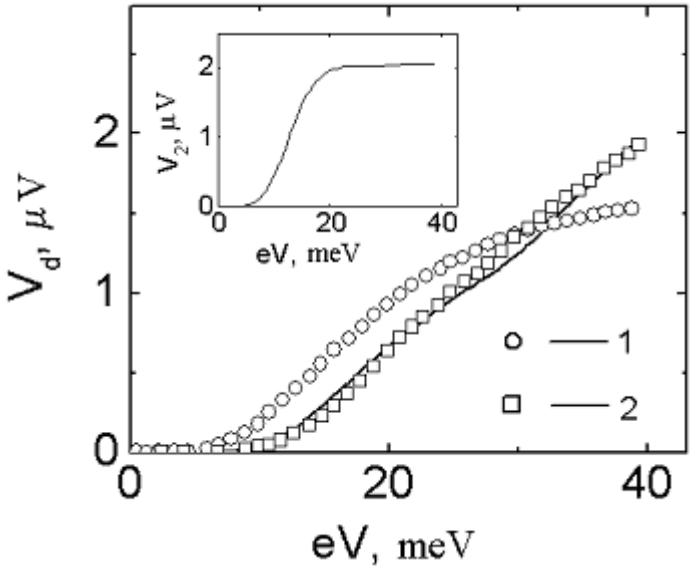

Fig. 4.4 The response of the Cu nanocontact to irradiation with visible light: the solid line represents the experimental data (point-contact spectrum); 1 – response calculated with formula (4.4); 2 – response calculated with formula (4.5). Insert: low frequency (~1 kHz) spectrum of the contact.

increases with the bias voltage (the measurements were performed up to ~170 mV) in contrast with the theoretically predicted saturation.

Line 1 in Fig. 4.4 shows the result of microscopic calculations for the V_d caused by the incident radiation over-heating of the NC (we chose $\Delta T=T_1-T_0=5$ K) and by the bias current. The theoretically predicted saturation (line 1) is easy to understand, if one considers the NC as a bolometric element whose temperature

depends not only on the environment and the incident radiation, but also on the transport current:

$$V_d(V) = I(V)\frac{dR_S}{dT}(V,T)\Delta T\,. \qquad (4.5)$$

With increasing bias voltage, the NC temperature increases as well in agreement with (2.14), but the magnitude of the ΔT under irradiation becomes smaller. This decrease of ΔT compensates the signal increase due to increase of the transport current and brings the response signal to a constant value. However, this is not what is observed experimentally (solid line in Fig. 4.4).

Let us try to explain the experimental results by assuming that the temperature increase ΔT, due to irradiation with a laser beam, is independent of the bias voltage value. Then,

$$V_d(V) = 2L^{1/2}\left[1-\frac{R_s}{R_d}(V)\Delta T\right]. \qquad (4.6)$$

The response values for ΔT=0,16 K calculated in this way are shown in Fig 4.4 (line 2). Our assumption can be motivated by the special contribution of the NC's lateral surfaces to the response signal. These surfaces are heated less by the current because of phonon heat transfer to the environment. Their temperature is not determined by (2.14). On the other hand, the radiation-induced heating of these surfaces is maximal. Certainly, in real conditions the response is due to superposition of (4.5) and (4.6) contributions. Thus, while under HF radiation the induced current heating of the NC itself dominates, for exposure to radiation in the optical range, the direct beam heating of the lateral surfaces gives the main contribution to the response signal. Experiments with sub-millimetre and CO_2 lasers

ascertained that the bias dependence of the response starts to change at a frequency of $2{,}83 \cdot 10^{13}$ Hz.

The nature of the response of a Cu NC in the ballistic regime (Chapter 5) also changes for frequencies higher than $2{,}83 \cdot 10^{13}$ Hz, where radiation heating of the surrounding zone of the NC,becomes important and not only that of the NC itself.

4.5 Conclusions

With increasing radiation frequency in the HF range, a transition from synchronous detection (rectifying) of the external signal at $\Omega < \nu_T$ to bolometric detection at $\Omega > \nu_T$ occurs (ν_T is frequency of thermal relaxation of the NC). According to theoretical models, in the first case ($\Omega < \nu_T$) the temperature of the contact changes with applied alternating voltage and a simple relation determines the bias voltage dependence of the contact temperature in the thermal regime. In the second case ($\Omega > \nu_T$), the influence of the alternating external signal is converted to stationary heating of the contact (bolometric effect). In this regime, the response becomes a smooth function of the bias voltage, proportional to the first derivative of IVC and not to d^2I/dV^2. The higher the irradiation frequency in comparison to the contact relaxation frequency, f_T, less the NC temperature follows the alternating bias.

For Sb and Cu NCs the experiments prove that for $\Omega/2\pi > f_T$ the response signal dependence of the bias corresponds to the 1st, and not to the 2nd derivative of the IVC of the NC.

From the frequency dispersion of response signal a characteristic frequency, f_T, of $\approx 2 \cdot 10^8$ Hz was determined for the thermal relaxation of a given NC of Sb. The thermal relaxation frequency of a Sb NC was also estimated theoretically (based on the determined NC parameters) in two different ways and the

results (0,22 GHz and 0,12 GHz) were in good agreement with experiment.

The experimental response of Cu NCs in the thermal regime to irradiation with light in the visible range differs from calculations according to the bolometric response model. To reach agreement, one has to assume that the direct beam heating of the lateral surfaces (and not only of NC zone) becomes the main contribution to the response signal in the optical range. Significant NC lateral surface heating was experimentally observed for frequencies above $f \approx 2{,}8 \cdot 10^{13}$ Hz.

References

1. O. P. Balkashin, I. I. Kulik. Relaxation kinetics for non-equilibrium quasi-particle excitations in antimony point contacts. Sov. J. Low Temp. Phys. 21 (1995), pp. 32 – 37

2. O. P. Balkashin, I. I. Kulik, M. V. Moskalets. High-frequency response of the metal micro-contacts with small electron mean free path. Sov. J. Low Temp. Phys. 18 (1992), pp. 662-664

3. I. K. Yanson, O. I. Shklyarevskii, N. N. Gribov. Anisotropy of electron-phonon interaction spectra in a magnetic field and quantum interference effects in antimony point contacts. Sov. J. Low Temp. Phys., 1992, v.88, N 1/2, pp. 135-162

4. M. V. Moskalets. High-frequency properties of point contacts induced by nonequilibrium phonon relaxation. Sov. J. Low Temp. Phys. 15 (1989), pp. 271-227

5. I. O. Kulik, I. K. Yanson. Microcontact phonon spectroscopy in the dirty limit. Sov. J. Low Temp. Phys., 1978, v.4, pp. 596-602

HIGH FREQUENCY RELAXATION KINETICS IN METAL AND HIGH-T_C SUPERCONDUCTOR NANOCONTACTS

Chapter 5

NONLINEAR ELECTRICAL CONDUCTIVITY OF METAL NANOCONTACTS IN THE BALLISTIC REGIME

5.1 Abstract

In this PhD project we devoted special efforts to the analysis of the quasiparticles relaxation kinetics of NCs in the ballistic regime for the whole range of excitation energies. The electron-phonon interaction part of the PC spectra ($eV<hf_D$), caused by the spontaneous phonon generation, changes very little for high frequencies, while the background part ($eV>hf_D$), brought about by the reabsorption of non-equilibrium phonons, transforms significantly under HF irradiation.

The interesting phenomenon of the background signal which decreases as the frequency of the radiation increases, discovered earlier by different authors [1, 2], was investigated in details. As will be illustrated below, we could calculate the characteristic frequency for phonon-electron interaction in Cu, and establish the classical and quantum detection frequency ranges as well as the characteristic frequency for the transition to a bolometric response.

Improved resolution of PCS at high frequencies $f>f_T$, $f_{ph\text{-}e}$, (where f_T is the thermal relaxation frequency of the NC, and the $f_{ph\text{-}e}$ is the frequency of non-equilibrium phonon on electron

relaxation) due to reduced reabsorption of non-equilibrium phonons was proved.

Spectra with negative sign of second derivative $d^2V/dI^2<0$ (inversed spectra) for Sb, a semi-metal characterised by a low carrier concentration and a low Fermi energy, and their frequency dispersion were studied.

As for the NCs in the thermal regime, we performed systematic studies of the non-linear properties of ballistic NCs of Cu in the wide frequency range (10^3-$4{,}78\cdot10^{14}$ Hz), and observed the transition from classical to quantum detection regime.

From the frequency dependence of the background reduction coefficient we could deduce the frequency for non-equilibrium phonon relaxation in Cu - an important parameter for the phonon-electron kinetics.

The investigation of the bolometric response when irradiating with visible light established the importance of direct laser heating of the lateral surface of the NC.

The experimental results concerning the response to irradiation in the optical frequency range allowed to establish a special type of PCS, namely Laser Thermal Point-contact Spectroscopy, characterized by a better resolution of spectral singularities.

5.2 Experimental Results and Theoretical Analysis of the Relaxation Kinetics for Cu Nanocontacts in the Ballistic Regime

Phonon and PC spectra of Cu have been studied extensively [1-4]. In the present work, the investigated NCs were of " pin-to-plate" geometry with contact resistances in the range of 0,5-7 Ohm. In each measurement cycle, the PC spectrum of the contact and a series of response signals at HF irradiation were registered. At the end of each cycle, the acoustic frequency (~1 kHz)

spectrum was compared with the initial one to verify the stability of the contact. All spectra were normalised to the maximum intensity of Transverse-phonons (T-phonons) peak, as to neglect the background at this energy.

All NCs reported in this chapter were in the ballistic current regime as proven by the high intensity of the spectral singularities, by the relatively low background level of the response to HF irradiation and also by the calculated characteristic contact parameters. The EPI part of the spectra ($eV<hf_D$) due to spontaneous phonon generation changes very little for HF (Fig. 5.1), while the background part ($eV>hf_D$) due to reabsorption of non-equilibrium phonons varies significantly. The reduction of the background in the HF spectra evidences a new spectral singularity that occurs at a combination of transverse and longitudinal phonon energies, $hf_t + hf_l$, shown in Fig. 5.1 with an arrow. The results for the Cu NCs presented in Figs. 5.1 and 5.2 were obtained earlier by different authors [1, 2]; with the present work these results were completely confirmed. Extensive studies of these phenomena permitted us a detailed analysis of the relaxation kinetics for Cu NCs [5, 14, 19, 20].

A gradual decrease of the background signal at MW frequencies was observed for the bias values $eV>hf_D$ up to 100 meV (Fig. 5.1). Such a behaviour is not predicted by theory. Another unexpected experimental result was the saturation of the background with increasing frequency of the impinging radiation; in fact, (2.23) predicts that the background signal decreases monotonously to zero as the frequency rises.

The response signal, $V_{d,}$ for all NCs was measured at minimal power levels at mW range. With increasing power a linear increase of the response signal (Fig. 5.2) was observed [2, 5] which confirms that the normalisation of the response values to the maximum of the T-phonons peak is correct.

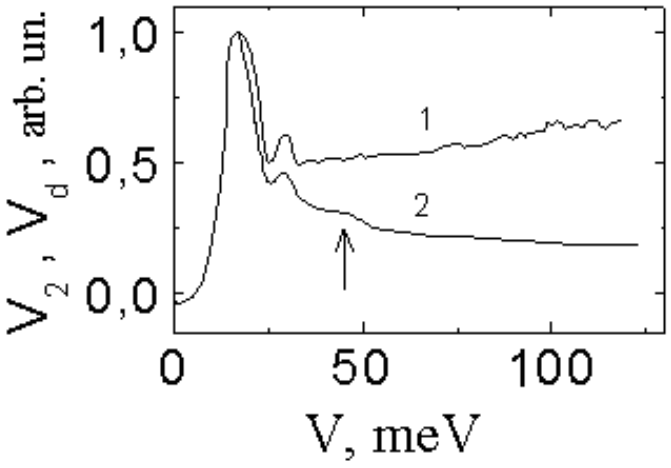

Fig. 5.1 Point-contact spectra of Cu measured [1, 2] at acoustic frequency (~1 kHz) (1) and at microwave frequency (80 MHz) (2).

In the following we focus on the nature of residual background in the PC spectra collected at HFs. The deviation of the experimental results from the theoretically predicted monotonous dependence ($\eta \sim 1/f^2$) can be explained as follows. The measurement of the video-detection signal for a given transport current is performed by registrating the voltage difference V_d on the NC under irradiation and in the dark (3.4). When the IVC does not depend on frequency, the V_d value is determined by the rectification of the alternating HF current on the IVC non-linearities, and for small modulation amplitudes the signal V_d is proportional to the second derivative of the IVC. In the case of HF ($f > f_{ph\text{-}e}$), the IVC are modified because of a different contribution of the phonon reabsorption to electron scattering. The V_d value will not be only due to HF rectification, but also

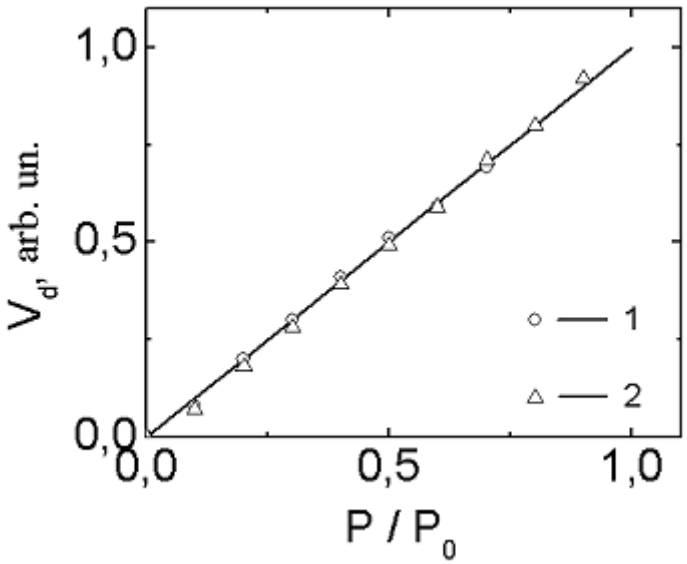

Fig. 5.2 The dependence of response signal on the power (at mW level) of the high frequency radiation for Cu nanocontacts [2], at 17 mV (1) and 60 mV (2) bias voltage.

depends on the modification of the IVC under irradiation. This additional contribution is due to the excessive amount of non-equilibrium phonons generated in the NC by the HF current, at bias $eV>hf_D$. It can be referred to as a bolometric contribution, *i.e.* as modification of the NC resistance with HF irradiation. The higher the irradiation frequency, as smaller the part of non-equilibrium phonons that follows the HF current because of the phonon relaxation inertia.

The NC temperature increases under HF irradiation only in the thermal regime (Chapter 4). The experiments prove and theory confirms that a frequency increase in the range $f>f_T$ (where $f_T \approx sl_i/d^2$ is the thermal relaxation frequency of NC) brings about a non-linear relation between bias and contact temperature. For the contacts in the ballistic regime, the stationary part of the NC temperature is referred to as an effective temperature of the

phonon subsystem, and is higher than the ambient (Helium bath) temperature. The electron subsystem continues to have the ambient temperature.

As theoretical works show, when the elastic mean free paths of phonons and electrons are approximately the same, the thermal relaxation frequency (f_T) is similar to the frequency of non-homogeneous escape of phonons from the NC, and both these frequencies are almost equal to the frequency of phonon-electron interactions $f_{ph\text{-}e}$. As the radiation frequency increases, the rectification part of response signal V_d decreases, while the bolometric contribution grows and finally dominates the response signal. The amplitude of the bolometric component is proportional to the contact current and to the resistance change under irradiation; it grows monotonously with the current. This consideration clarifies the background signal behaviour. At high enough frequencies ($f>f_{ph\text{-}e}$) and small bias ($eV<hf_D$), the video response signal is determined mainly by the rectified HF current. With increasing bias, this part tends to zero, while the bolometric part (proportional to the first derivative of IVC) intensifies. A similar behaviour was described before (Chapter 4) for contacts in thermal regime exposed to alternating electromagnetic fields of frequencies $f>f_T$.

Another characteristic feature of the HF spectra is the intensity decrease of the response at bias voltages in the range $eV>hf_D$. Fig. 5.1 shows a saturation for bias voltages around 100 mV [1, 2], which can be explained with an intermediate phase of phonon gas thermalization occurring through phonon-phonon collisions. The probability of such interactions is of one order of magnitude higher than that of phonon-electron interactions. The effective phonons temperature (2.20), i.e. the number of non-equilibrium phonons increases with bias voltage. The frequency of this process is limited by the thermal capacity of the phonon subsystem. The thermal capacity grows with temperature,

increasing the thermalization time and hence the inertia of the phonon system. The saturation of thermal capacity occurs at the temperatures higher than the Debye temperature $T_{eff}>\Theta_D$, which corresponds to $eV=4k_B\Theta_D=110{,}3$ meV for Cu as seen experimentally in Fig. 5.1.

As noted before, the HF measurements for Cu give evidence for a spectral singularity at $eV\sim45$ meV, absent in the low frequency measurement. One of the reasons for the worse resolution of conventional low frequency Point Contact Spectroscopy is heating of the NC by the transport current. At frequencies $f>f_T$, $f_{ph\text{-}e}$, reabsorption of non-equilibrium phonons and thermal effects are reduced, and hence the resolution of HF spectroscopy is improved. This phenomenon does not influence the spontaneous generation of phonons by non-equilibrium electrons, as soon the operational frequencies $f<<f_{e\text{-}ph}$.

Due to the improved resolution and the fact that additional information that can be retrieved from HF measurements, this method is considered as a new kind of PCS and called High Frequency Point-Contact Spectroscopy.

5.3 Relaxation Kinetics of Non-Equilibrium Phonons in Sb Nanocontacts

The investigation of semi-metallic NC such as Sb, characterised by a low carrier concentration and a low Fermi energy (comparable with phonon energies) permits to discover new effects, for instance trajectory effects for ballistic contacts (when the Larmor orbital radius for electrons is comparable with the NC diameter), and quantum interference effects related to localised electronic states [6, 7]. However, other authors encountered difficulties when trying to explain the background part of the spectra, which is usually attributed to reabsorption processes of non-equilibrium phonons. The nature of the background signal

for Sb was not clear up to now. We performed HF PCS experiments with Sb [8, 9], and explained them based on the big difference in relaxation frequencies for electrons and phonons in metals (~10^3).

The spectra obtained experimentally agree well with the ones known from literature [6, 7] for the same orientation of NC axis relative to crystallographic axis of Sb. The PC spectra of the EPI present (see lines 1 in Fig. 5.3-5.5) a singularity at an energy eV≈2 meV, which can be attributed to intravalley electron scattering processes, as well as two main peaks due to intervalley processes involving acoustic (eV≈7,3 meV) and optical (eV≈17,5 meV) phonon modes. The good quality of the contacts is indicated by the high intensity of the main peaks, as well as by

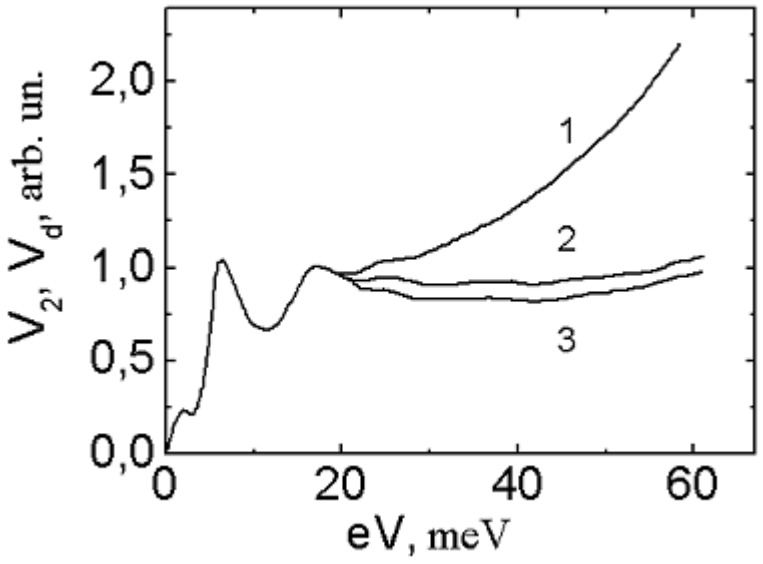

Fig. 5.3 Point-contact spectra of Sb, measured at acoustic frequency (~1 kHz) (1) and in the high frequency range: at 0,6 GHz (2) and at 70 GHz (3). Contact resistance R_0=0,74 Ohm.

the presence of singularities at energies which are a multiple or a sum of of the fundamental ones and hence associated with multi-phonon generation processes. At higher bias $eV \approx 175$ eV a big maximum of thermal nature can be seen; this phenomena was analysed before (section 4.2).

It has been reported elsewhere [6, 7] that for dirty Sb NCs present EPI spectra of a negative sign of second derivative $d^2V/dI^2<0$ (inverse spectra). The same is true or for contacts obtained through multiple contacting of electrodes. The latter procedure implies creating a considerable amount of deformation (cold-work hardening) of the Sb crystal structure. According to [6], the elastic mean free path l_i in these crystals may be of the order of 10 nm, which is comparable with de Broglie wavelength $\lambda_F=2\pi\hbar/p_F$ (p_F is the Fermi momentum) of carriers in Sb due to the small value of p_F ($\varepsilon_F \sim 90$ meV). The condition $l_i \approx \lambda_F$ brings about the possibility of spatial localization of electron states. The scattering of non-equilibrium electrons by phonons in a NC causes a phase lag between electron wave functions, i.e., it violates the quantum localization and hence leads to an increase in the conductivity of the contact ($d^2V/dI^2<0$ with DC bias increasing) and so, to the inverse spectra.

The theory of quantum interference effects in the electrical conductivity of NCs was developed in [10]. Figure 5.4 shows the inverse EPI spectrum obtained after contacting the electrodes repeatedly. The main characteristic features of this spectrum are in good agreement with the data of [6, 7]. As can be seen in Fig. 5.4, the background of the inverse spectrum is negative.

The emergence of a background in PC spectra is associated with the reabsorption of non-equilibrium phonons by the electron flow. For large bias voltages across a contact, the number of non-equilibrium phonons increases with voltage, and so does the number of scattering events of the electrons. In other words, the contact resistance (the first derivative) also increases, and hence

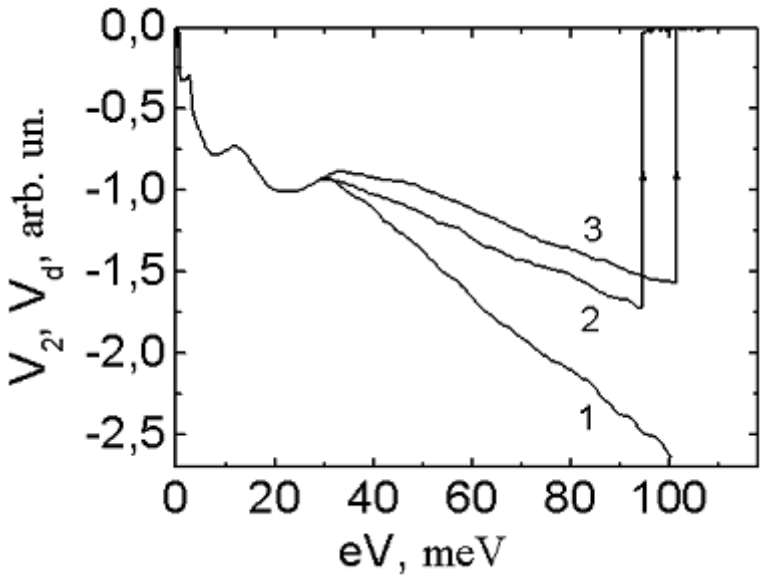

Fig. 5.4 Inverse point-contact spectra of Sb (1) and video response at frequencies 0,59 GHz (2) and 70 GHz (3). Contact resistance R_0=2,05 Ohm.

the second derivative will have a positive nonzero value in this energy range. In the presence of quantum phase-coherent localization effects, the above-mentioned processes violate the localization in the NC, the contact resistance decreases with increasing eV, and the second derivative will be negative.

When the contact is exposed to radiation in the MW wave range, the processes of emission and reabsorption of non-equilibrium phonons by electrons are separated in time due to a considerable difference between the characteristic relaxation times of the electron and phonon subsystems of the metal. This allows us to establish where the background in the PC spectra originates from and to determine the characteristic phonon relaxation times. The phonon-electron relaxation frequency for Debye phonons in Sb can be estimated from (2.22). Using the

values s=3,4·10^5 cm/s for the speed of sound, v_F = 0,7·10^8 cm/s for the Fermi velocity, Θ_D=210 K for the Debye temperature for Sb, and λ=0,09 for the EPI constant obtained from NC studies [6], we obtain $f_{ph\text{-}e}$=1,8 GHz. Taking this value of the characteristic phonon relaxation frequency into account, we measured the microwave PC spectra for exposure to electromagnetic radiation with frequency in the interval 0,1-80 GHz.

The microwave PC spectra of Sb are shown in figures. 5.3 and 5.4 (lines 2,3) for two different frequencies of the impinging radiation. For inverse MW spectra, the radiation was specially screened by an attenuator at the end of recording in order to control the negative sign and its zero level. Fig. 5.5 shows the analogous result for another NC in which a partial spatial

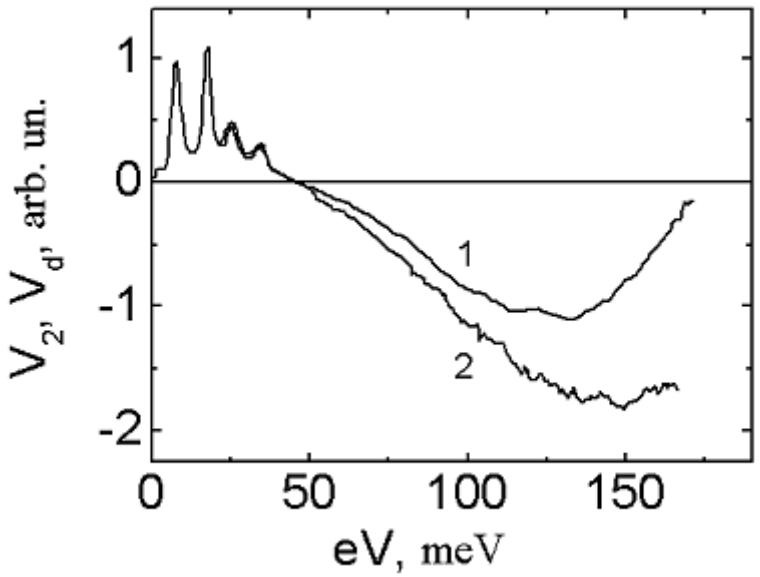

Fig. 5.5 Point-contact spectra of Sb at acoustic frequency (~1 kHz) (1) and at 80 GHz (2). Contact resistance R_0=3,57 Ohm.

localization of electron states appears to take place. For all measurements, the intensity of the MW radiation was chosen in such a way that amplitudes of main EPI peaks at low and high frequencies coincide. Such a normalization of signals correlates the difference between the coefficients of coupling for the NC and external MW field and allows a direct measurement of the frequency dispersion of the response signal.

From the results presented in Figs. 5.3-5.5 follows that for large bias voltages across the contacts, one observes a considerable decrease in video response signal in the background region even for frequencies of the impinging radiation of a few hundred MHz. A further increase in frequency by two orders of magnitude (up to 80 GHz) causes only a slight change. The background signal is found to increase with DC bias voltage across the contact. This increase in background may be observed even in the inverse spectrum region as shown in Fig. 5.5. As noted before (section 4.2), such a behaviour is determined by the contribution of thermal effects.

We shall now analyze the behaviour of the background signal for various radiation frequencies in the energy interval 30-60 meV in the immediate vicinity of the EPI spectrum. It follows from data presented in Figs. 5.3-5.5 that the maximum variation in background amplitude occurs in the acoustic frequency interval up to ~0,6 GHz, and can be attributed to the emergence of thermal effects (see above). Moreover, the frequency dispersion of the background in the interval 0,6-80 GHz is quite insignificant, and a high level of residual background signal is observed even when the measurements are carried out at the limiting frequency of 80 GHz.

The weak dispersion of background in the interval of frequencies close to the characteristic phonon-electron collision frequency in Sb $f_{ph\text{-}e}$~2 GHz points to a low intensity of reabsorption processes of non-equilibrium phonons that can leave the NC region without being scattered by electrons.

In view of this weak reabsorption of non-equilibrium phonons in Sb contacts, we can't attribute the high level of residual background for f~80 GHz to the bolometric effect (i.e., to the presence of non-equilibrium phonons in NC, as it was done before in section 5.2, for Cu NCs). In all probability, the residual background is due to rapid electron-phonon scattering processes with a high characteristic frequency $f_{e\text{-}ph}\sim\lambda f_D\sim10^{13}$ Hz. Therefore we conclude from Fig.s 5.3-5.5 that due to the energy dependence of the electron-phonon relaxation length, Sb NCs undergo a transition from the ballistic ($l_i,\ l_\varepsilon>>d$) or diffusive ($(l_i\ l_\varepsilon)^{1/2}>d$) regime to the thermal one ($l_\varepsilon\ l_i,<<d$). According to the theory of PCS in the dirty limit [11], the intensity of multi-phonon generation processes increases due to energy relaxation of the electrons in the NC. The presence of a background contribution from electron relaxation apparently necessitates the introduction of a phenomenological correction [6], which increases linearly with bias voltage.

All the above considerations concerning possible reasons behind the observation of frequency dispersion of the background signal are also applicable to contacts with localized electron states possessing inverse PC spectra. We can neglect the direct influence of the electromagnetic field on the phase lag between electron wave functions in the NC [12, 13] for energies higher than the Debye energy because of the small characteristic times $\tau_\varphi\sim\tau_{e\text{-}ph}\sim10^{-13}$ s in this energy region. The situation becomes a little more complicated for the contact presented in Fig. 5.5. In spite of a positive EPI spectrum of the NC, the background becomes negative upon increasing the voltage, and then, at even higher values of eV tends to come back to positive values characteristic for a thermal anomaly of the IVC. Such behaviour of the second IVC derivative can be explained by assuming that a fraction of conduction electrons in the NC is localized in space in some part of the contact volume. PC spectral studies for Sb show

that the response of NCs is described correctly by the "T-model" [6] in which impurities are assumed to be concentrated in a narrow layer of thickness $T<d$ at the surface of the contacting electrodes, while the entire remaining NC volume is assumed to be clean. With an increase in the excess energy of the electrons, the EPI overcomes the localization of states in the impurity interlayer, and the resistance begins to decrease ($d^2V/dI^2<0$). However, the NC changes over into a thermal regime upon a further increase in voltage, and thereafter its resistance increases again. The behaviour of the second IVC derivative at HF (line 2 in Fig. 5.5) is determined by the competition between several relaxation mechanisms with different characteristic times ($\tau_{e\text{-}ph}$ at low energies, τ_φ and $\tau_{ph\text{-}e}$ at intermediate energies, τ_T at high energies) and is in good agreement with the proposed model.

5.4 Laser Thermal Point-Contact Spectroscopy of Metals

5.4.1 Experimental Results

In Chapter 4 we showed that the video response of NCs in the thermal regime contains spectral singularities, specific for low frequency spectra. Despite the large energy of optical photons ($\hbar\Omega$~2 eV for λ=0,63 μm), no broadening, characteristic for quantum detection process, of these singularities was observed. In this section we describe the studies of pure ballistic Cu NCs, performed to clarify the physical nature of video detection [5, 14].

To improve the coupling between electromagnetic radiation and NC, we used the "pin-to-plate" geometry. A spear-shaped electrode made of Cu wire of diameter 0,2 mm was sharpened to a diameter ~1 μm. The second electrode was a copper cylinder

with a polished end face or a Cu film of thickness 1,5 μm deposited on a 1,5 mm thick glass substrate. Both electrodes were brought together by a precision mechanism and the NCs were formed directly in liquid Helium.

Optical radiation was generated by a multimode He-Ne current wave laser of nearly 25 mW power at a wavelength λ=0,63 μm ($\Omega/2\pi$=4,75·10^{14} Hz, $\hbar\Omega$=1960 meV). The laser beam was focused through a quartz window in the cryostat walls by a lens to a spot diameter of 0,05 mm in the region of NC. The irradiation of the NC was performed in two different ways as sketched in Fig. 5.6: in the first case (a) the laser beam was directly focused on the NC; in second case (b) it was focused on the backside of the Cu film.

Direct laser beam irradiation of a contact.

For metal NCs, the region of relatively strong non-linearity of IVC associated with electron-phonon interaction extends to Debye energies and covers an interval up to tens of meV (~35 meV for Cu). The energy of a radiation quantum was $\hbar\omega$~2 eV. Hence, in accordance with (3.5), we can expect a monotonic increase in response upon an increase in constant bias voltage across the NC.

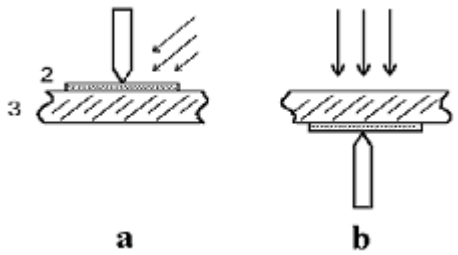

Fig. 5.6 Contact configuration and two methods of laser irradiation: 1 – spear; 2 – copper film; 3 – glass substrate.

The experimental result for the bias voltage dependence of the video response signal , $V_d(V)$, upon direct irradiation of a Cu contact with the laser beam and the corresponding low frequency spectrum are depicted Fig. 5.7 (a). As can be seen from the figure, the detected signal has well-defined spectral singularities whose shape and position coincide with the EPI spectrum of Cu with a slightly enhanced background level. The measurements were made at a NC temperature T=1,7 K in superfluid Helium. In normal Helium ($T>T_\lambda$), the amplitude of the response signal was found to be much larger. Replacement of a thin film electrode by a bulk Cu cylinder [1, 2] practically did not change the result and simply led to a manifold decrease in signal amplitude and to sharper spectral singularities due to a more perfect structure of the metal in a bulk electrode.

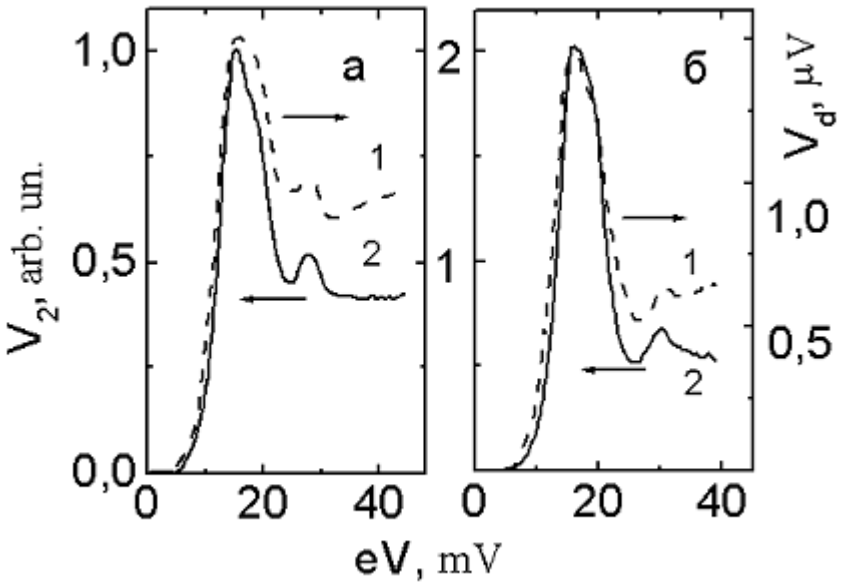

Fig. 5.7 Video response of a Cu contact (1) and its low frequency (~1 kHz) spectrum (2): upon direct irradiation (a) and upon heating (b) with laser beam.

Rotation of the polarization plane of the laser radiation led to a 20-30% variation in response signal amplitude, the maximum being observed when the projection of the electrical component of the external field was parallel to the spear.

The unusual shape of measured signal can be attributed to a broadening of the EPI spectral singularities under the action of the laser irradiation since the light frequency is comparable to the reciprocal time of flight of the electrons through the NC region. It follows from theory [15] that a dispersion of the conductivity should be observed under such conditions. For a contact whose characteristics are described in Fig. 5.7 (a), the reciprocal time of flight is $v_F/d \sim 2{,}2 \cdot 10^{14}$ Hz ($v_F = 1{,}57 \cdot 10^8$ cm/s is the Fermi velocity of electrons in Cu, and the contact diameter $d \sim 7{,}3$ nm is calculated from its resistance $R = 17$ Ohm). Such a broadening results in a smoothing of non-linear IVC regions under irradiation, and hence the difference in IVC measured in the modulation technique experiments assumes its highest value in these regions.

Another mechanism for the broadening of the EPI spectral singularities may be heating of the NC by laser radiation since heating broadens the Fermi edge. This explains the enhancement of the effect in He-I and for a film electrode which has a poorer heat removal from the hot spot as compared to bulk metal. The polarization dependence of the response intensity may be due to antenna properties of the spear or to a change in the absorption and reflection coefficients for different directions of the radiation polarization according to the Fresnel formula, and cannot serve as a proof of the non-thermal nature of the response.

Heating of a contact by a laser beam.

Focussing the laser on the backside of the Cu film (Fig. 5.6 (b)) corresponds to studying the processes associated with heating of the NC. The maximum amplitude of the recorded signal was

attained by scanning the surface of the film with a luminous spot. Under such experimental conditions, the role of the laser beam is reduced to generating a phonon flux on the NC.

Non-equilibrium electrons excited by an external electromagnetic field to energies $\hbar\Omega$~2 eV relax as a result of electron-phonon scattering and generate high-energy non-equilibrium phonons with low group velocities. As these phonons propagate through the film, equilibrium in the phonon subsystem is attained as a result of phonon-phonon scattering. In view of the large thickness and structural heterogeneity of the film, it can be assumed that the phonon distribution at the NC attains its equilibrium which is characterized by certain temperature value $T_0+\Delta T$ exceeding the thermostat (Helium bath) temperature T_0.

The experimentally measured dependence of thermal response on bias voltage is shown in Fig. 5.7 (b) along with the EPI spectrum of this NC. It can be seen that the results are practically the same as in Fig. 5.7 (a) for direct exposure to light. Measurements were carried out on a contact with resistance R=16 Ohm at a temperature T_0=2,8 K and a laser power of 10 mW. In both cases (Fig. 5.7 (a, b)), a broadening of EPI spectral singularities in the signal being detected is visible.

With increasing irradiation power, at least up to ~15 mW, the video response amplitude was proportional to the power.

For temperatures below T_λ=2,17 K, no signal could be registered even for maximum laser power, in contrast to the experiments with direct irradiation of contact. The disappearance of the signal upon an improvement of heat removal due to a transition of Helium to its superfluid state confirms the hypothesis of the thermal nature of the observed effect.

Special experiments were carried out for estimating the heat constant τ of structure “substrate-film-spear”. For this purpose, the response signal was measured for a constant bias voltage V=17 mV across the NC in the static regime by using a compensation DC microvoltmeter and in the dynamic regime in

accordance with the above technique with a modulation frequency f=420 Hz for the radiation intensity. The signal amplitude was found to be exactly twice as high in the static regime. In view of the symmetry of the modulator, it can be concluded from such a result that the structure under consideration has a time constant τ<1/420 s~2,4·10^{-3} s.

The thermal origin of the response V_d measured by us is also confirmed by calculations carried out for the NC presented in Fig. 5.7 (b). Calculations were made by using the experimental values of the IVC, its first and second derivatives, obtained in absence of radiation. The absolute value of the response signals, V_d~10^{-6} V, is 2-3 orders of magnitude smaller than the error in the measurement of the IVC. Hence, more accurate values of the IVC were obtained by doubly integrating the values of the second derivatives. Experimental IVC were used for transforming the voltage dependences into current dependences. The IVC calculated in this way was found to coincide practically with the experimental IVC.

From a comparison of height and half-width of the T-peak in the PC spectra measured under laser irradiation with the PC spectra of Cu recorded in [16] at different temperatures we estimated the temperature increase ΔT to amount to 5 K. The obtained dependences correctly reflect the shape of the experimentally observed signal, although the absolute peak values are slightly higher (see line 1 in Fig. 5.7 (b) and Fig. 5.8). Moreover, calculations show that the amplitude of response signal has a non-linear dependence on temperature increase ΔT. The observed discrepancies with experiment are associated with

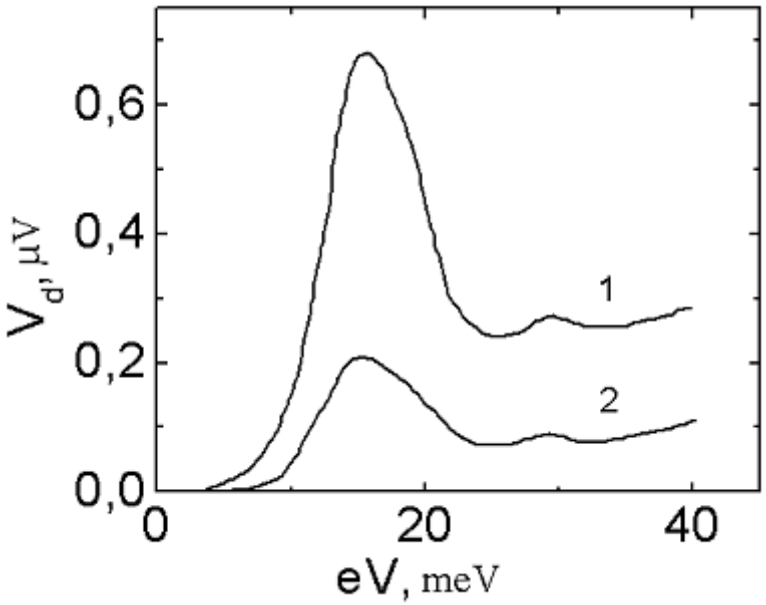

Fig. 5.8 Calculated values of point-contact signal for a temperature increase ΔT=10 K (1) and 5 K (2).

approximations used for simplifying the calculations, and with a nonsymmetric heating of electrodes in the NC region under actual experimental conditions.

So far, we have considered the results for small-size pure NCs with electrons moving in the ballistic regime. Such contacts have a resistance of 10-20 Ohm. For the contact whose PC spectrum is shown in Fig. 5.7 (b), the maximum intensity of spectrum gives a value g_{pc}^{max}~0,24, which is characteristic for the ballistic regime in a Cu contact [4]. An increase in geometrical size of the current concentration region leads to a change in electron-phonon kinetics, and a transition to the diffusive regime. Our measurements show that the shape of the response signal also undergoes a significant change for such contacts as illustrated in Fig. 5.9.

As can be seen in Fig. 5.9, the spectral components are

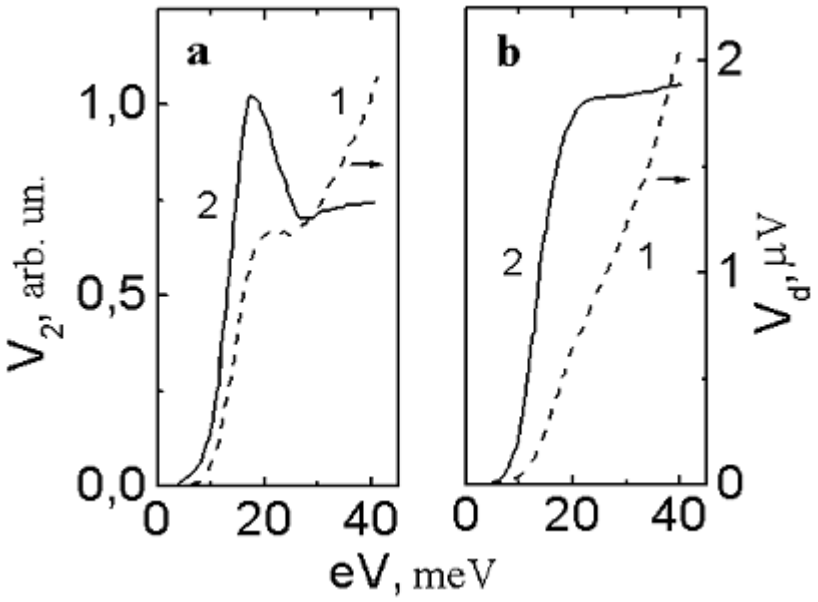

Fig. 5.9 Change in shape of the response signal for different types of Cu NCs: response signal obtained under optical irradiation on the back side of contact (1); point-contact spectrum of the same nanocontact (2).

smoothed upon transition to the thermal regime, and the response signal acquires a monotonic component that increases sharply with increasing of bias voltage. In these conditions, the measured signal cannot be associated only with a smoothing of EPI spectral singularities due to thermal broadening of the Fermi edge as a consequence of irradiation. This is so because the NC temperature in the thermal regime is given by the constant bias (see (2.16)) and is much higher than the quantity ΔT associated with laser heating.

5.4.2 Theoretical Basis of the Laser Thermal Point-Contact Spectroscopy

The entire body of experimental data makes it possible to formulate the basic concepts of a special type of PCS, - the Laser Thermal Point-Contact Spectroscopy. In the modulation temperature spectroscopy technique presented in [17], the change in contact temperature is due to the transport current, and the banks (bulk electrodes) remain cold due to a strong current spreading. Exposure of the NC to the optical laser radiation results in a heating of the electrodes in the immediate vicinity of the constriction, which is equivalent to an increase in the Helium bath temperature by an amount ΔT. The heating asymmetry due to irradiation of only one electrode (Fig. 5.6 (b)) should not affect the results significantly according to the data presented in Fig. 5.7. Apparently, the effect is felt more strongly on the amplitude of the signal being registered than on its shape.

The experimental signal V_d is the difference between two IVC of the NC at the temperatures T and $T+\Delta T$, respectively. To calculate this difference, we use the expression for the IVC of a metal NC from [18]:

$$I(V) = \frac{V}{R_0} - c\int_0^\infty \left[\frac{\varepsilon - eV}{e^{\beta(\varepsilon - eV)} - 1} - \frac{\varepsilon + eV}{e^{\beta(\varepsilon + eV)} - 1} + \frac{2eV}{e^{\beta\varepsilon} - 1} \right] g_{pc}(\varepsilon) d\varepsilon \tag{5.1}$$

where $\beta = (k_B T)^{-1}$, $c = 8d/3ev_F R_0$ and $g_{pc}(\varepsilon)$ - the NC EPI function.

For a small temperature increase ($\delta T << T$), the current response can be presented in the form $\delta I \sim (\partial I(V)/\partial T)\delta T$. Omitting terms in (5.1) that do not have a singularity at the point $\varepsilon = eV$ and

differentiating, we obtain the following expression for the inelastic component of the current:

$$\delta I(V) \cong -c\delta T \cdot T \int_0^\infty g_{pc}(\varepsilon)\chi_1\left(\frac{\varepsilon - eV}{k_B T_0}\right)d\varepsilon\,, \qquad (5.2)$$

where

$$\chi_1(y) = \frac{1}{k_B T}\left(\frac{y}{2sh\left(y/2\right)}\right)^2$$

is the thermal broadening function.

For a crystal where lattice vibrations are represented with the Einstein model ($g(\varepsilon)=g_0\delta(\varepsilon - \varepsilon_0)$), the emergence of a spectral singularity in response to laser irradiation is presented schematically in Fig. 5.10.

In the case of strong heating ($\Delta T>T_0$), we must compute the difference between two expressions (5.1). Assuming that the elastic component of the current does not change upon irradiation and that the temperature is low, we obtain an expression analogous to (5.2) but with a different thermal broadening function:

$$\chi_2(y) = \frac{1}{k_B \Delta T}\frac{|y|}{e^{|y|}-1}\,, \qquad y = \frac{\varepsilon - eV}{k_B \Delta T}\,. \qquad (5.3)$$

The peak half-width for the functions χ_1 and χ_2, is $6k_BT$ and $2{,}5k_BT$, respectively, and not $5{,}44k_BT$ as for conventional low frequency PCS.

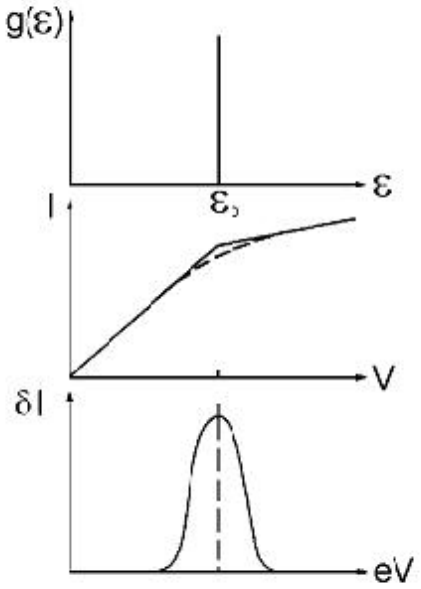

Fig. 5.10 Emergence of spectral singularity in laser response for the Einstein model of crystal lattice vibrations.

5.5 Characteristics of Ballistic Nanocontacts Exposed to Radiation from Acoustic to Optical Frequency Range

The results presented above show that the response of clean ballistic NCs when exposed to electromagnetic radiation can be determined by different mechanisms: the detection of a HF current or contact heating through irradiation in the optical range. To distinguish the frequency ranges for responses of different nature, we systematically studied the non-linear properties of ballistic NCs in the wide frequency range, similarly to what we did for the NCs in thermal regime and described in Chapter 4.

The results of these investigations [19] for the Cu NCs are presented in the remainder of this chapter.

The typical dependencies of the response signal on the bias $V_d(V)$ for different frequencies, shown in Fig. 5.11, are similar, as far as their common features are concerned, to the EPI spectrum of a clean Cu NC where electrons are moving ballistically.

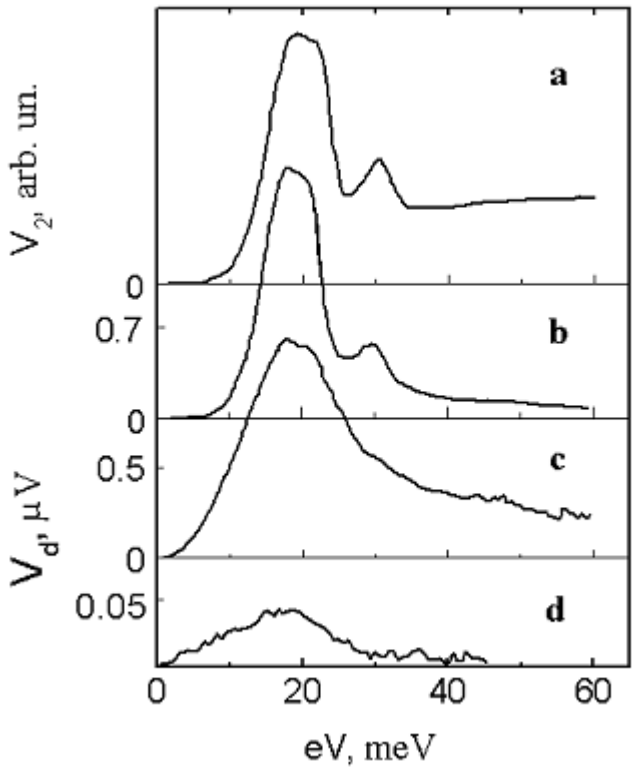

Fig. 5.11 Experimentally measured responses of a Cu nanocontact when exposited to radiation at frequencies $\Omega/2\pi$*: 3746 Hz (a);* $7{,}9\cdot10^{10}$ *Hz (b);* $2{,}5\cdot10^{12}$ *Hz (c);* $4{,}3\cdot10^{12}$ *Hz (d).*

In these measurements of the response when exposed to electromagnetic radiation in different frequency regions, the radiation was supplied to NCs by different methods: with the help of a waveguide in for wavelengths in the microvawe range, employing the light guide in the IR range, through the the windows in the lateral walls of the cryostat and lenses in the visible range. Hence the dependencies $V_d(V)$ presented in Fig. 5.11 refer to different NCs, the only exception being lines (a) and (b), which were obtained for the same NC. For the sake of further comparative analysis, Figs. 5.11 and 5.12 show the results for NCs with analogous PC spectra, similar to line (a) in Fig. 5.11.

The dependence of the response signal on bias voltage is determined by the relation between the frequency of the external field, Ω, and the characteristic relaxation time in the electron-phonon system. Comparing curves (a) and (b) in Fig. 5.11 (a) one can observe a decrease in background signal amplitude when exposing to an electromagnetic field with a frequency of $7{,}9\cdot10^{10}$ Hz. This decrease is associated with the process of reabsorption of non-equilibrium phonons, which determines the level of the background part of the signal in the PC spectrum. The reciprocal time of relaxation for these processes for Cu is equal to $5\cdot10^9$ Hz. This value is calculated from the frequency dependence of background reduction coefficient $\eta(f)$ (2.21), according to the method described in [20]. With this characteristic value we can attribute the dependences (a) and (b) in Fig. 5.11 to two limiting cases, namely line (a) to $\Omega\tau_{ph\text{-}e}<1$ and line (b) to $\Omega\tau_{ph\text{-}e}>1$.

The main part of the signal obtained for bias voltages $eV<30$ meV across NC is attributed to rectification of the alternating HF current at the IVC non-linearities associated with the emission of non-equilibrium phonons during the energy relaxation of electrons. For such processes, $\Omega\tau_{e\text{-}ph}<1$ (where $1/\tau_{e\text{-}ph}\sim10^{13}$-$10^{14}$ Hz) for all frequencies of the external field that were used to

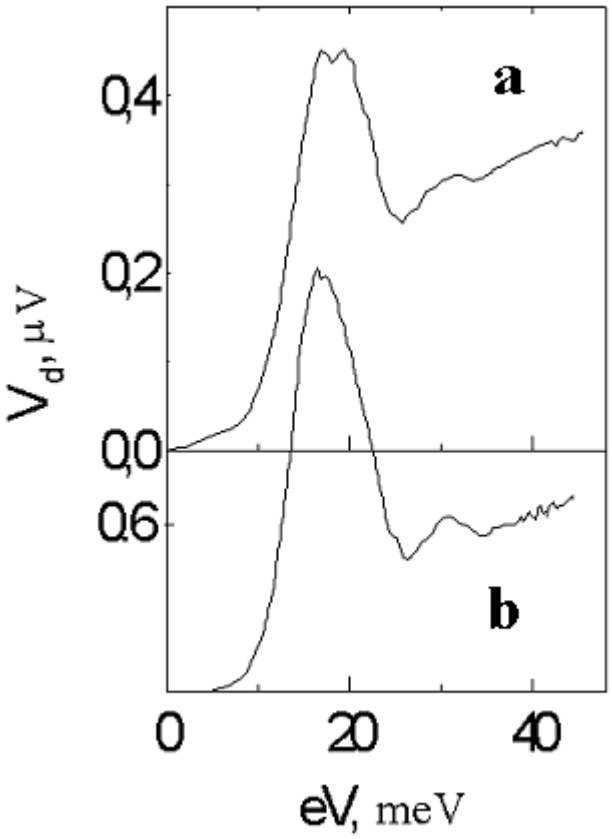

Fig. 5.12 Video response of a Cu contact for frequencies $\Omega/2\pi$*:* $2{,}8\cdot10^{13}$ *Hz (a) and* $4{,}75\cdot10^{14}$ *Hz (b).*

generate the curves presented in Fig. 5.11. The observed broadening of spectral singularities in the bias dependencies of the response with increasing frequency of irradiation, is associated with a transition from the classical to the quantum detection regime. This transition occurs when the quantum energy of the external field (f~$2{,}5\cdot10^{12}$ Hz) becomes comparable to the width of the energy region of a non-linear singularity on the IVC (~10 meV for Cu) of the NC. The decrease in signal

amplitude (Fig. 5.11) with increasing irradiation frequency is naturally associated with a deterioration of the antenna properties of the wire electrode of the NC: decreasing the wave length of the incident radiation, the amplitude of the alternating HF current induced in the NC decreases correspondingly.

Upon a further increase in frequency, the form of bias dependence of $V_d(V)$ changes radically. Fig. 5.12 shows the results obtained for exposure to radiation with frequencies $2{,}8\cdot10^{13}$ Hz and $4{,}75\cdot10^{14}$ Hz. In this range, $\Omega\tau_{e\text{-}ph}\sim1$, and hence we can expect an even stronger broadening of EPI spectrum compared to Fig. 5.11. However, Fig. 5.12 shows that the EPI spectrum as a function of the response becomes still sharper, especially in the visible range. We have shown earlier (section 5.4) that the response of metal NCs to optical radiation is of different nature and associated with thermal broadening of the Fermi edge in the energy distribution of electrons. The results presented in Figs. 5.11 and 5.12 lead to the conclusion that a change in response mechanism from rectification to heating of the NC by external radiation occurs in the frequency range $4{,}3\cdot10^{12}$ - $2{,}8\cdot10^{13}$ Hz.

To analyze the behaviour of a metal NC in a HF electromagnetic field, we use the expression for the IVC obtained in [18] that considers also reabsorption of non-equilibrium phonons,

$$I(V)=\frac{V}{R_0}-C\int_0^{\infty}\left[\frac{\omega-eV}{e^{\beta(\omega-eV)}-1}-\frac{\omega+eV}{e^{\beta(\omega+eV)}+1}+2eVN(\omega)\right]g_{pc}(\omega)d\omega \tag{5.4}$$

where $C=8d/3e\hbar v_F R_0$; $\beta=1/k_BT$; and $N(\omega)$ - the energy distribution function for non-equilibrium phonons for the case of their full reabsorption:

$$N(\omega)=\frac{1}{4\omega}\left[\frac{2\omega}{e^{\beta\omega}-1}+\frac{\omega-eV}{e^{\beta(\omega-eV)}-1}+\frac{\omega+eV}{e^{\beta(\omega+eV)}-1}\right] \tag{5.5}$$

where R_0 is contact resistance at V=0.

With these formulae we can calculate the IVC and the bias voltage dependence of second IVC derivative, d^2I/dV^2 for a Cu NC with resistance R_0=5 Ohm. The NC diameter was determined from (2.2) for a clean orifice, and the value of the Cu EPI function taken from data tabulated in [4] was used for $g_{pc}(\varepsilon)$. The obtained dependence is shown in Fig. 5.13 and agrees well with the real PC spectrum of a Cu NC measured experimentally at acoustic frequency 3746 Hz (Fig. 5.11 (a)).

Line 2 in Fig. 5.13 shows the bias dependence of the effective temperature $T^*(V)$ of non-equilibrium phonons with distribution $N(\omega)$. The effective temperature was determined from the condition that the energy supplied to electron subsystem by the non-equilibrium phonon system, has to be balanced by the energy distribution of equilibrium phonons with the temperature T^*:

$$\int_0^\infty \frac{\varepsilon g_{pc}(\varepsilon)d\varepsilon}{e^{\varepsilon/k_BT^*}-1}=\int_0^{eV}\omega g_{pc}(\omega)N(\omega)d\omega \tag{5.6}$$

The dashed line in Fig. 5.13 shows the simplified dependence $T^*(V)=eV/4k_B$, which was also proposed in [18] for a case of complete reabsorption of non-equilibrium phonons.

The good correspondence of calculated and experimentally measured PC spectra gives the possibility to apply the described above procedure for calculations of the NC response when

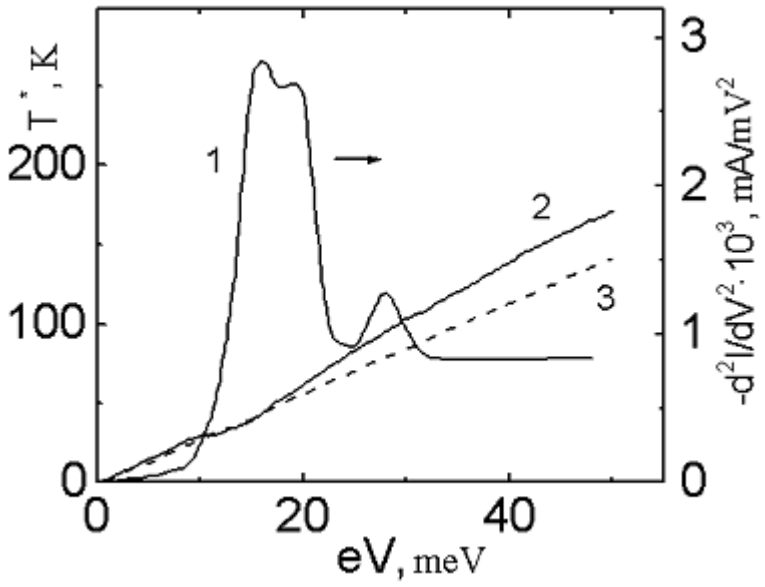

Fig 5.13 Theoretical spectrum of a Cu nanocontact (1) and the dependence of effective temperature of non-equilibrium phonons (2, 3) on bias voltage across the nanocontact, according to different models.

exposed to HF radiation.

Calculations were made without taking into account the changes in coupling between the NC and the external field at different wavelengths, and the alternating HF voltage induced in the NC was assumed to be equal to V_1=1 mV at all frequencies. The obtained dependences $V_d(V)$ for the three electromagnetic fields where $\hbar\Omega$= 0,3 meV, 10,6 meV and 17,6 meV, presented in Fig. 5.14 (a), correspond well to the form of experimental lines in Fig. 5.11. The fitting parameter used in these calculations is the amplitude of the HF voltage on the contact V_1. With the values 0,30 mV; 0,55 mV and 0,19 mV for the frequencies

$7{,}9\cdot10^{10}$ Hz, $2{,}5\cdot10^{12}$ Hz and $4{,}3\cdot10^{12}$ Hz correspondently, we obtained good quantitative agreement with experimental data.

A consideration of non-equilibrium phonons in the NC leads to a nonzero response at high voltages in the calculation, in contrast to [21], where non-equilibrium phonons were neglected.

In the optical frequency range, the response mechanism is of thermal nature. Hence we calculated the differences between the IVC of contacts according to (5.4) and (5.5) for various values of the temperature increase ΔT caused by laser irradiation:

$$V_d(V) = \left[I(V,T) - I(V,T_0)\right]\frac{dV}{dI}(V), \qquad (5.7)$$

where the temperature increase in the NC is $\Delta T = T - T_0$ and the temperature of the Helium bath T_0=2,8K.

The theoretical lines presented in Fig. 5.14 (b) correctly describe the main features of the experimentally obtained dependences shown in Fig. 5.12. The maximum value of the response signal for line 3 in Fig. 5.14 (b) is 7,38 μV.

By absorbing laser radiation in the optical range ($\Omega/2\pi$=$4{,}75\cdot10^{14}$ Hz), the conduction electrons in the metal acquire an excess energy $\hbar\Omega$~2 eV, which is about 70 times higher than the energy of Debye phonons in copper ($\hbar\omega_D$~28 meV). As a result of the subsequent cascades of relaxation processes in the electron-phonon system, a steady non-equilibrium state is established. The extent of deviation of electron and phonon subsystems from equilibrium is determined by the intensity of the laser pumping, as well as by the characteristic velocities of uniform and non-uniform relaxation of

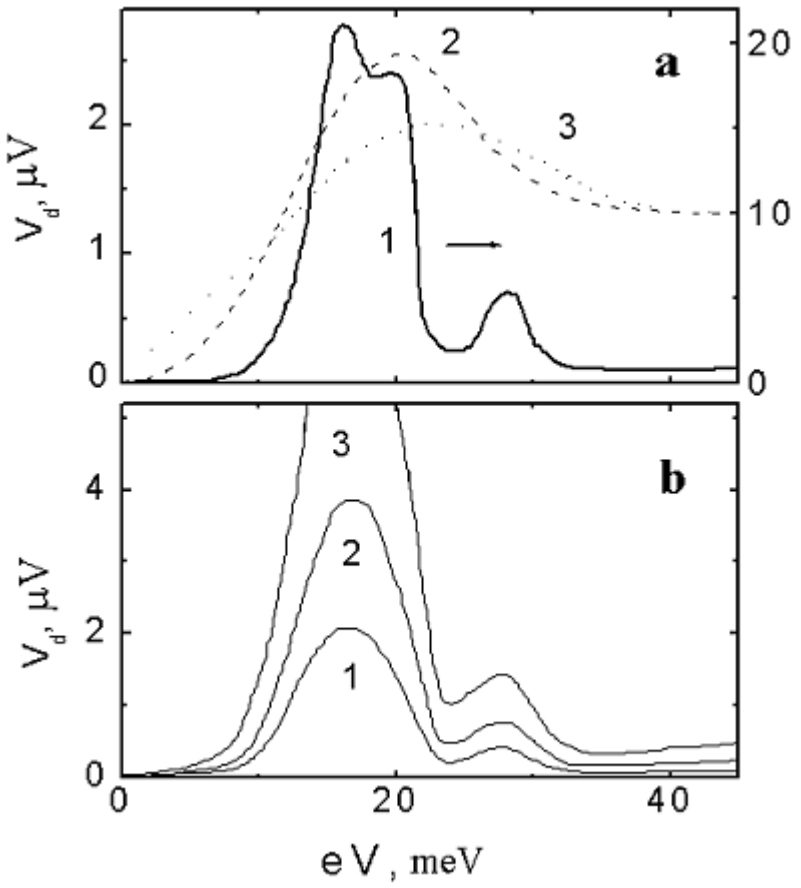

Fig. 5.14 (a) - Response signal calculated for three radiation frequencies Ω/2π: 7,9·10[10] Hz (1), 2,5·10[12] Hz (2) and 4,3·10[12] Hz (3). (b) - Dependences of differences between I-V characteristics on bias for a temperature increase, ΔT, amounting to 1,8 K (1), 2,8 K (2) and 4,1 K (3).

quasiparticles. To simplify calculations, we assumed that in the optical spectral region, the role of radiation is reduced just to a steady heating of NC. The equilibrium energy distribution function is chosen for phonons with a higher value of temperature than that of Helium bath.

A comparison of Figs. 5.12 and 5.14 (b) shows that the calculated response signal is in general (even quantitative) agreement with the experimental results. An exception to this is the high bias region, where there is almost monotonous growth of the measured response amplitude, as for the dirty NC (section 4.3).

An estimate of the NC overheating by laser radiation from the broadening of the low-energy peak of the PC spectrum measured in [14] gives a value of about 1K for ΔT. For a constant intensity of radiation, this quantity may vary slightly in different experiments due to differences in the tuning of laser radiation to the contact region.

Measurements made by us using a CO_2 laser ($\hbar\Omega$=117 meV) gave a response pattern similar to that for the He-Ne laser (see line 1, Fig. 5.14 (b)).

Thus, our experimental results lead to the conclusion that starting from frequencies ~$2{,}8\cdot10^{13}$ Hz, the bolometric response begins to dominate over the signal associated with the rectification of the HF current induced in the NC by an external field.

It should be noted that there is no guarantee that the NC is directly under the laser spot since the contact size (d~10 nm) is much smaller than the diameter of the copper pin (D~1 μm).

Let us now consider in detail the possible reasons why laser heating causes a contribution to the response of a metal NC to emerge, which depends linearly on bias voltage. Fig. 5.15 shows the PC spectrum of a copper contact (a) having a resistance R_0=14,7 Ohm and a dependence of the response to optical radiation (b) for two values of the He-Ne laser power. The expressions for the absolute values of the intensity of PC spectra

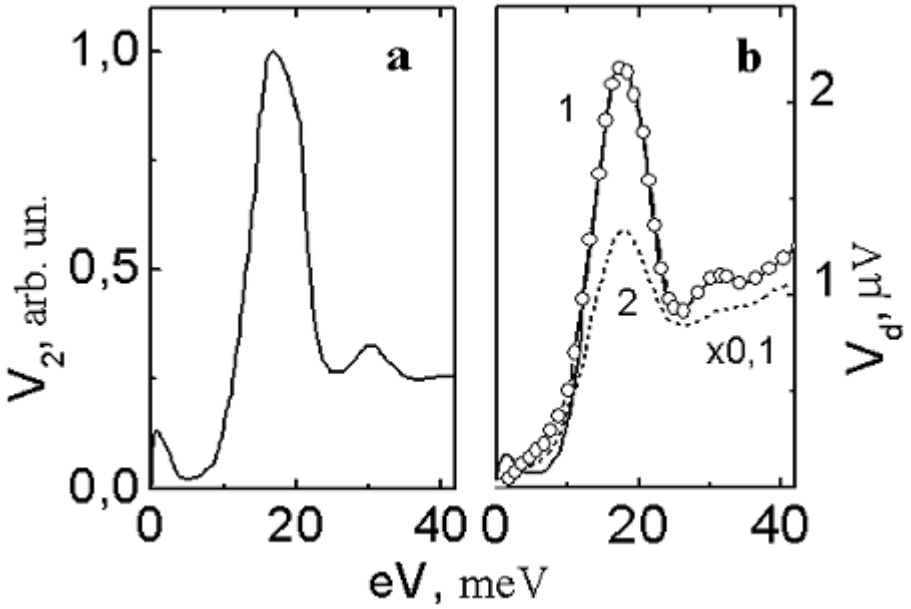

Fig. 5.15 Spectrum of a Cu nanocontact in the ballistic regime (a) and its response to optical radiation (b) for a laser power of 3,8 mW (1) and 25 mW (2). The solid lines correspond to experimental results while the points indicate the results of calculations. The vertical scale for the line (2) is reduced 10 times.

for copper and the contact resistance (Wexler's equation (2.3)) were used to calculate the elastic mean free path of electrons and the contact diameter (l_i=1300 nm, d=7,8 nm). Since $l_i/d>>1$, the contact is clean and the electrons follow the ballistic regime. This conclusion is also confirmed by the good quality of the spectrum in Fig. 5.15 (a).

In analogy with the response of a dirty contact (Chapter 4) to optical radiation, we assume that clean contacts also make a linear bolometric contribution to the signal being measured:

$$V_d^b(V) = I\frac{dR}{dT}\Delta T = V\alpha_T\Delta T \qquad (5.8)$$

where V is the voltage, ΔT the increase in temperature as a result of irradiation, and $\alpha_T=R_0^{-1}\cdot(dR/dT)$ the thermal coefficient of the metal resistance in the NC region. In the case of a complete reabsorption of non-equilibrium phonons for large bias voltages across the contact (phonon signal region), there exists a simple relation between α_T and the background level $\alpha_V=R_0^{-1}\cdot(dR/dV)$ in the low-frequency PC spectrum. The relation α_T/α_V determines the level of phonon overheating in the NC. For clean contacts, we obtain the theoretical estimation α_T/α_V =0,172 mV/K [20]. Using this value, α_V=3,85·10^{-3} mV^{-1} calculated from the experimental line in Fig. 5.15 (a) for V>35 mV, and putting ΔT=2 K, we obtain V_d^b=66 μV for V=50 mV, which is about two orders of magnitude higher than the experimental values presented by line 1, Fig. 5.15 (b).

If we assume only a partial reabsorption of non-equilibrium phonons by the electron flow, as is usually the case with clean contacts of small geometrical dimensions, the relation between the phonon gas temperature T^* and the voltage will be weaker than that shown in Fig. 5.13 (line 2). In this case, the experimental value [21] of the ratio α_T/α_V is about twice as large as the theoretical value. Hence the response signal also must increase by a factor of two.

It is more reasonable to assume that the linear bolometric contribution to the NC response $V_d^b(V)$ is associated not with the contact itself, but with the region surrounding it, *i.e.* the volume of the bulk electrodes around the contact (~0,1 mm) over which the transport current spreads. The voltage drop in this region is much smaller than the one across the NC, and the value of α_T is also different. Both these quantities are position depended. Hence

an exact calculation of $V_d^b(V)$ requires a solution of the spatially non-uniform relaxation problem.

Under actual conditions, the experimental measurements of the response of a NC to laser heating are carried out by registering the sum of the signals $V_d(V)=V_d^b(V)+V_d^T(V)$, where $V_d^T(V)$ is defined by formula (5.7) and $V_d^b(V)$ by expression (5.8). We calculated the dependence $V_d(V)$ for the case ΔT=2 K by introducing a fitting parameter A=1,73·10^{-5} K^{-1} ($V_d^b(V)=A\cdot\Delta T\cdot V$) which takes into account the change in voltage as well as the thermal resistance coefficient in the vicinity of the contact. The results of such calculations are marked by circles in Fig. 5.15 (b) and are in good agreement with the experimental data.

To interpret the experimental results, we should apparently take into account the possible steady deviation from the equilibrium values of the distribution functions for electrons and phonons under the action of laser radiation with a high energy $\hbar\Omega>>\hbar\omega_D$, instead of reducing the effect of irradiation just to heating of the contact.

Without laying any claim to the rigorous nature of the model chosen by us, we calculated the difference $V_d(V)$ between two IVC of a copper NC described by expression (5.4). The action of the laser radiation for the perturbed IVC was taken into consideration not only by replacing T_0 by $T_0+\Delta T$, but also by adding to the non-equilibrium phonon distribution function (5.5) a term

$$M(\varepsilon)=\gamma(B-\varepsilon)\frac{\Theta(B-\varepsilon)}{\varepsilon}. \qquad (5.9)$$

The results of calculations for the values B=30 meV and $\gamma\sim10^{-4}$ were found to be practically the same as for the dependence shown by circles in Fig. 5.15 (b). Although the function $M(\varepsilon)$ is close to the phonon equilibrium distribution function, its value

becomes much larger at high energies for the chosen values of parameters. The final conclusion about the possible extent of the deviation from equilibrium in the electron-phonon system in a NC exposed to laser radiation can be drawn after carrying out a more rigorous theoretical analysis.

5.6 Conclusions

The response V_d to irradiation in the HF range is found to be not only due to rectification of the HF current, but also to a bolometric effect which modifies the IVC. For contacts in the ballistic regime this effect is attributed to an increase in the effective temperature of the phonon subsystem, while the electron subsystem continues to be at ambient temperature. At the high enough frequencies $f>f_{ph\text{-}e}$ ($f_{ph\text{-}e}$ is phonon-electron relaxation frequency), at small bias ($eV<hf_D$) the response signal is determined mainly by the rectified HF current. With increasing bias, this part tends to zero, while the bolometric part, proportional to the first derivative of the IVC, grows.

Improved resolution of PCS at frequencies $f>f_T, f_{ph\text{-}e}$, due to the reduced reabsorption of non-equilibrium phonons was established and allowed to consider the High Frequency Point-Contact Spectroscopy as a new type of PCS.

The non-equilibrium Debye phonons relaxation on electrons occurs at the inter-atomic scale, while the NC dimension is about 10-100 inter-atomic distances. Thus, the value for relaxation frequency of such a process for copper, $f_{ph\text{-}e}=5\cdot10^9$ Hz, experimentally obtained by us from High Frequency Point-Contact Spectroscopy studies, is valid for bulk copper.

A significant increase in the background part as a function of bias was observed for normal and inverse ($d^2V/dI^2<0$) spectra for Sb. The registered weak frequency dispersion of the background in the Sb PC spectra points towards a low intensity of

reabsorption processes of non-equilibrium phonons. This means the latter can leave the NC region without being scattered by electrons. Observed high level of residual background for f~80 GHz can't be attributed to the bolometric effect. In all probability, the residual background is due to rapid electron-phonon scattering processes with a high characteristic frequency $f_{e\text{-}ph} \sim \lambda f_D \sim 10^{13}$ Hz.

Copper NCs were investigated under irradiation in a wide frequency range, from acoustic to optical frequencies (10^3-$4{,}78 \cdot 10^{14}$ Hz). The main part of the response signal obtained for frequencies up to ~$4{,}3 \cdot 10^{12}$ Hz at, low bias voltages (eV<30 meV) is attributed to classical rectification of the alternating HF current at the non-linearities in the IVC, associated with the emission of non-equilibrium phonons during energy relaxation of the electrons. The observed broadening of spectral singularities at frequencies above f=$2{,}5 \cdot 10^{12}$ Hz is associated with a transition from classical to quantum detection. For f>$2{,}8 \cdot 10^{13}$ Hz the response signal is attributed to the bolometric effect.

Exposure of the NC to the optical laser radiation (λ=0,63 μm) results in a heating of the electrodes in the immediate vicinity of the constriction, which is equivalent to an increase in the Helium bath temperature. The entire body of experimental data makes it possible to formulate the basic concepts of a special type of Point-Contact Spectroscopy for the optical range of frequency, - the Laser Thermal Point-Contact Spectroscopy. The mechanism for the video response of the NC for low bias voltages (eV<hf_D) under optical radiation is attributed to the heating of the NC by laser radiation since heating broadens the Fermi edge.

We obtained a good agreement between experimental data and theoretical calculations, except for the response to radiation in the optical range obtained for high bias voltages (eV>hf_D). In analogy with the response to optical radiation of NCs in the thermal regime, we assume that the bolometric contribution is associated

not with the NC itself, but with its surrounding region, *i.e.* with the volume of bulk electrodes (~0,1 mm) around NC, over which the transport current spreads.

References

1. I. K. Yanson, O. P. Balkashin, Yu. A. Pilipenko. Non-equilibrium phonon relaxation in metal microcontacts. Sov. Phys. JETP Lett. vol. 41, No. 7, p. 373 (1985)

2. O. P. Balkashin, I. K. Yanson, Yu. A. Pilipenko. Relaxation kinetics of non-equilibrium phonons in copper and gold. Sov. J. Low Temp. Phys. 13, 222 (1987)

3. A. G. M. Jansen, A. P. van Gelder, P. Wyder. Point–contact spectroscopy in metals. J. Phys. C, 1980, v.13, N 33, p.6073-6118

4. A. V. Khotkevich and I. K. Yanson. Atlas of Point Contact Spectra of Electron-Phonon Interaction in Metals. Kluver Academic Publishers, Boston/Dordrecht/London (1995)

5. O. P. Balkashin, I. I. Kulik. Laser thermal point-contact spectroscopy of metals. Sov. J. Low Temp. Phys. 16 (1990), pp. 166–171

6. I. K. Yanson, O. I. Shklyarevskii, N. N. Gribov. Anisotropy of electron-phonon interaction spectra in a magnetic field and quantum interference effects in antimony point contacts. Sov. J. Low Temp. Phys., 1992, v.88, N 1/2, pp. 135-162

7. I. K. Yanson, N. N. Gribov, O. I. Shklyarevskii. Trajectory effects in microcontact spectroscopy of the electron-phonon interaction. JETP Lett. 42, 195 (1985)

8. O. P. Balkashin, I. I. Kulik. Relaxation kinetics for non-equilibrium quasi-particle excitations in antimony point contacts. Sov. J. Low Temp. Phys. 21 (1995), pp. 32-37

9. O. P. Balkashin, I. I. Kulik. Quasi-particle relaxation kinetic in Sb point contacts. Proc. 2nd International Conference Of The Point Contact Spectroscopy. Physica B 218 (1996) 50-53

10. I. F. Itskovich, I. O. Kulik, R. I. Shekhter. Effect of Localization and Inelastic Scattering of Electrons in Point-Contact Electric Conductivity. Sov. J. Low Temp. Phys. 13, 659 (1987)

11. I. O. Kulik, M. V. Moskalets. Nonlinear electrical conductivity of metal point contacts in the dirty limit. Sov. J. Low Temp. Phys. 15, 229 (1989)

12. G. Bergmann, W. Wei, Z. Yao, R.M. Mueller. Non-equilibrium in metallic structures in the presence of high current density. Phys. Rev. B, 1990, v.41, n 11, p. 7386-7396

13. J. Liu, N. Giordano. Weak localization, electron-electron interactions and Joule heating in the presence of a microwave electric field in thin metal films. Phys. Rev. B, 1991, v.43, n 2, p. 1385-1390

14. O. P. Balkashin, I. I. Kulik. The interaction of laser radiation with copper microcontacts. Proc. Young Scientist's Conference, Kharkov, 1989, pp. 96-97. Institute for Low Temperature Physics & Engineering Ukr. SSR Acad. Sci. (in Russian)

15. I. O. Kulik, A. N. Omel'yanchuk, I. G. Tuluzov. Motional inductance of the point-contacts between normal metals. Sov. J. Low Temp. Phys, 8, 386 (1982)

16. A. P. van Gelder, A.G.M. Jansen, and P. Wyder, Temperature dependence of point-contact spectroscopy in copper. Phys. Rev. B, 1980, v.22, n 4, p. 1515-1521

17. B. I. Verkin, I. K. Yanson, I. O. Kulik, O. I. Shklyarevskii, A. A. Lysykh, Yu. G. Naidyuk.. Singularities in d^2V/dI^2 dependences of point contacts between ferromagnetic metals. Solid State Commun. 30, 215 (1979)

18. I. O. Kulik. Non-equilibrium current states in the metal micro-contacts. Sov. J. Low Temp. Phys. 11, 516 (1985).

19. O. P. Balkashin, I. I. Kulik. The characteristics of the metal point contacts (PC) in the range between acoustic and optical frequencies. Sov. J. Low Temp. Phys. 18 (1992), pp. 946–952

20. I. O. Kulik, I. K. Yanson, O. P. Balkashin, Yu. A. Pilipenko, I. I. Kulik. A method for the determination of the relaxation time for non-equilibrium excitations. USSR Patent No. 1581138, March 22, 1990

21. I. O. Kulik, A. N. Omel'yanchuk, I. G. Tuluzov, T. Z. Sarkisyants. Effects of high frequency detection in microcontacts between normal metals. Sov. J. Low Temp. Phys. 10 (1984), p. 463

22. I. O. Kulik, A. N. Omel'yanchuk, I. K. Yanson. Non-equilibrium phonons in the point-contacts between the normal metals. Sov. J. Low Temp. Phys. 7, 129 (1991)

23. A. I. Akimenko, A. B. Verkin, N. M. Ponomarenko, I. K. Yanson. Dependence of point-contact spectra on contact parameters. Sov. J. Low Temp. Phys. 8 (1982), p. 130

Chapter 6

NON-STATIONARY PROCESSES IN NANOCONTACTS WITH HIGH-T_C SUPERCONDUCTORS

6.1 Abstract

The conductivity of ceramic samples is determined by their structure and their superconductive coherence length is rather small (ξ~2-3 nm). The ceramics can be described as a system of randomly distributed, randomly oriented and weakly bound mono- and polycrystalline grains. The characteristic dimensions of crystals are much larger than ξ, and the grain boundaries resulting in normal or semiconductor character. The inter-grain zones behave as tunnel contacts. Thus, the superconductive metal oxide ceramics could be considered as Josephson media with S-I-S, S-N-S or S-N-I-N-S grain transitions. The transport properties of such media are quite sensitive to the structure which in turn depends on the preparation technique. Hence, in order to formulate general conclusions, it is important to investigate the superconductive parameters of both single grains and entire structures, produced by different recipes.

High-T_C superconducting ceramics ($YBa_2Cu_3O_{7-y}$, $Bi_2Sr_2CaCu_2O_y$) were investigated by PCS, namely by means of NCs in "shift" geometry between the ceramics bars, or in "pin-to-plate" geometry, with a pin electrode of normal or superconducting metal. We investigated the IVC of the superconducting ceramic NCs at small bias voltage as well as the

large jump-like hysteresis for large bias voltages. The results for frequency dispersion of these singularities at small and large bias and their dependencies both for HF and optical range irradiation are discussed in the light of the thermal model for non-homogeneous media that has a characteristic length for thermal processes l~10 nm.

6.2 Non-Stationary Josephson Effect in High-T_C Superconductors under High Frequency Radiation

The samples of high-T_C superconducting ceramics ($YBa_2Cu_3O_{7-y}$, $Bi_2Sr_2CaCu_2O_y$) were prepared according to the standard technology of solid phase synthesis with multi-stage grinding, pressing and annealing. The wire electrodes were attached to the opposite ends of the ceramic bars (2x2x10 mm) by applying springs and Indium gaskets, or they were glued with Ag paste. We characterized samples in both "shift" and "pin-to-plate" geometries, with the opposite electrode (bar or pin) consisting of superconducting (Nb, Ta) or normal (Cu, Ag) metals. High-T_C films of 1-100 μm thickness were also measured. The latter were produced by suspension deposition on MgO or SrTi substrates and subsequent annealing. Bridges of dimensions w<30 μm and l<40 μm of high-T_C superconductors were made by scribing of the films.

When NC between superconducting metal and high-T_C ceramic is made, the Josephson structure (see Chapter 1.2) is realised due to the presence of dielectric (oxide on the metal electrode) or semiconductor phase (of high-T_C ceramic) in between the superconducting zones (superconductive metal and superconductive grain of ceramics). At these conditions the Josephson effect will occurs, characterised by the critical

superconductive current I_c at zero bias (V=0) and by supercurrent (nondissipative current) at V>0.

The difference between the high-T_C and the low-T_C superconductors is in that the former display the d-wave pairing with the anisotropic energy gap vanishing at certain symmetry points on the Fermi surface. In particular, NCs of $YBa_2Cu_3O_{7-y}$ ceramics differ from traditional superconductor NCs in that they have very low critical currents I_c. The characteristic voltage $V_c=I_cR_N$ which defines the maximal frequency of Josephson tunnelling current between two superconductive zones, is about 1 mV (see Fig. 6.1 and 6.2). This value is much smaller than expected ($V_c=\pi\Delta/e$), taking into account that the energy gap Δ for $YBa_2Cu_3O_{7-y}$ is equal to 20-40 meV [1].

The thermal fluctuations in the contact further reduce and can apparently vanish the static Josephson response of the contact. The informative study of high-T_C contacts can be achieved with the high-frequency modulation of the resistive state at nonzero voltages. Exposure of the NC to an external electromagnetic field induces current steps in the IVC (Josephson non-stationary effect). These steps were observed for bias voltages up to only 4 mV, even at the maximum of radiation intensity. The position of the induced steps is defined by the well known Josephson equation

$$V_n = nhf / 2e, \quad n = 0, 1, 2, 3, \ldots \tag{6.1}$$

where n is the number of the step, f is the frequency of the impinging radiation and $2e$ the charge of the superconducting pair.

In Fig. 6.1, the initial IVC of a Ta–$YBa_2Cu_3O_{7-y}$ (1) NC and its modification upon MW irradiation (2) is shown. It should be noted that at large bias voltages, the IVC is shifted upwards from

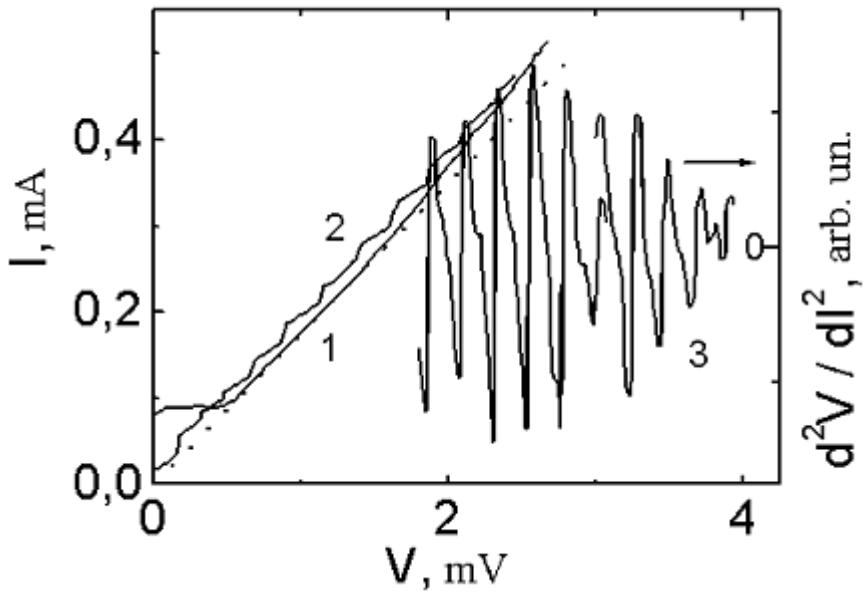

Fig. 6.1 I-V characteristic of a Ta–$YBa_2Cu_3O_{7-y}$ nanocontact at T=4,2 K without radiation (1) and when Ta–$YBa_2Cu_3O_{7-y}$ underexposed to the microwave radiation with $\Omega/2\pi$=78 GHz (2). On the right the second derivative of the I-V characteristic (3) is shown for the same contact under identical irradiation conditions, to evidence the steps generated on I-V characteristic.

the linear dependence by an amount which grows monotonously with increasing bias. This behaviour is typical for semiconductors and therefore we have to conclude that semiconducting phase is present in ceramic samples.

For improved resolution of the current steps, the signal of the second derivative of the IVC (3) was measured with the help of the standard low frequency (~1 kHz) modulation method [2, 3]. The positions of the first steps which occur as the bias is increased correspond well to the Josephson equation (6.1), but at larger bias the distance between the adjacent steps expands, and

their slope increases. In other words: the dynamic resistance increases for larger bias voltage.

For the highest observable step (corresponding to n=19), we obtain V_n=3,1 mV (f_n~1,5·10^{12} Hz) from the Josephson equation (6.1), while the corresponding experimental value is 3,9 mV. Hence we must take into account the effect of the external radiation on the resistive (semi-conducting) regions of the contact zone.

Fig. 6.2 illustrates that the step-like changes in resistance are a characteristic phenomenon for high-T_C ceramic contacts not exposed to radiation. Several resistive regions with a resistance that varies in a stepwise fashion can be identified in the IVC of a contact between Ta and a $YBa_2Cu_3O_{7-y}$ ceramic (Fig. 6.2).

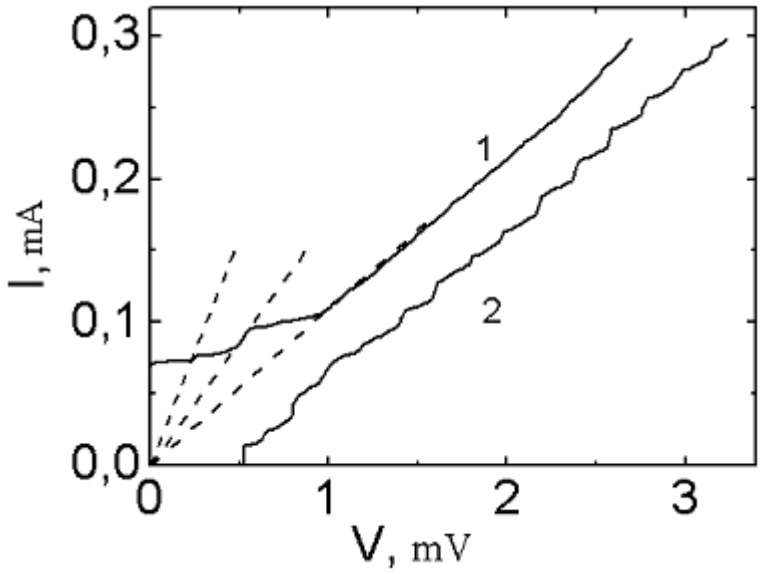

Fig. 6.2 I-V characteristic of a Ta-$YBa_2Cu_3O_{7-y}$ ceramics contact without irradiation (1) and under irradiation with f=7,8·10^{10} Hz (2). T=4,2 K.

The resistances of the IVC for the 3 different steps indicated by the dashed lines in Fig. 6.2 are (going from left to right) 3,42 Ohm, 6,05 Ohm and 9,37 Ohm. These experimental data are close to nR_0 with n=1, 2, 3 and the average value of R_0 amounting to 3,14 Ohm. Exposure to HF radiation induces current steps in the IVC of the contact (line 2 in Fig. 6.2 is shifted along the voltage axis by 0,5 mV). However, in contrast with the samples of Fig. 6.1, the steps are not regular at low bias voltages. For large bias voltages across the contact, the distance between steps becomes regular. In all probability, the resistance regions on the IVC are not associated with thermal effects, because the Josephson step structure on IVC is still observed and extends to quite high voltages (~4 mV), and so, the sample is still in superconductive state. The multiplicity in the variation of resistance suggests the existence of phase slip centres in long superconducting channels in the ceramic, but the size of the single crystallites in our samples significantly exceeds the coherence length, which is quite small for these materials: $\xi \sim 10^{-7}$ cm. A possible reason for the resistive regions can be formation of three-dimensional phase slip centres which one can imagine as phase separation surfaces [4] appearing in damaged regions in the ceramic near the contact with a metal electrode.

In contrast to the contacts made of a ceramic and a normal superconductor (Nb, Ta), the NC of Cu and the high-T_C superconductor presents a slope in the critical current [5] and induced steps (see insert on the Fig. 6.3), both caused by the presence of resistivity in the circuit.

When the impinging radiation is in the MW range, the relative values of the critical current are correctly described by the modulus of the zero-order Bessel function (solid line in Fig. 6.3). This function is given by the expression

$$I_n = I_c \left| J_n(eV_1 / hf) \right|, \tag{6.2}$$

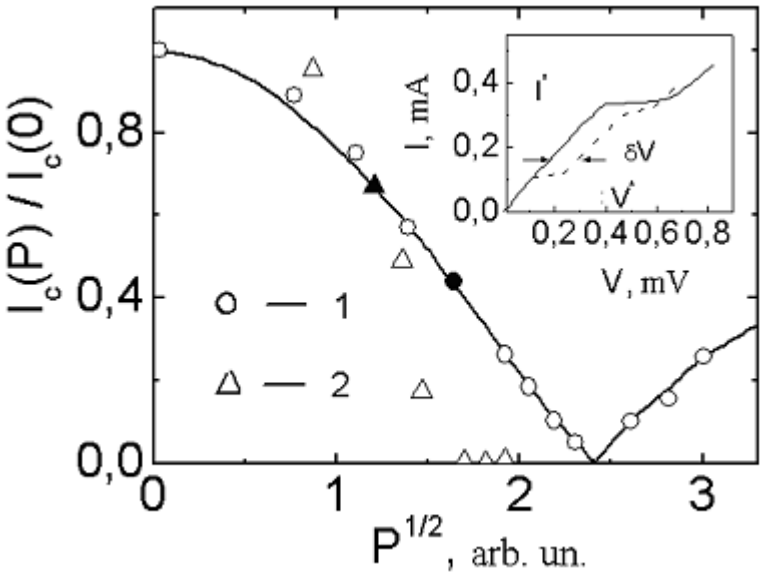

Fig. 6.3 Effect of the incident radiation power on the critical current: 1- the contact Cu-$YBa_2Cu_3O_{7-\delta}$ ceramics ($f_1=7{,}9\cdot10^{10}$ Hz, T=4,2 K); 2 – the contact Ta-$YBa_2Cu_3O_{7-\delta}$ ceramic ($f_2=4{,}75\cdot10^{14}$ Hz, T=2,15 K). The insert shows the I-V characteristic of the Cu-$YBa_2Cu_3O_{7-\delta}$ ceramics contact (the solid line was obtained without radiation, and the dashed line under radiation of frequency f_1).

where *n* is the order of the function and $V_1 \sim \sqrt{P}$ is the amplitude of the alternative voltage, induced on the contact by the external HF field. To determine the scale along the abscissa axis, the experimental and theoretical dependences were made to coincide at the filled points.

In the case of a Cu electrode, a weak link in the superconducting circuit emerged in the ceramic itself, probably at the boundary between grains, near the point of the contact between the electrodes. In such contacts, however, the non-stationary Josephson effect is reliably observed at liquid N_2 temperature. Quite often the resistive parts (their existence can be considered the reason of the finite slope of critical current) are connected in series. This was observed also for the contacts with superconducting metals. The slope is associated with the fact that metal oxide ceramics have a multi-phase granular structure (especially near the surface) consisting of superconducting and normal phases. In view of such a heterogeneous composition, the obtained contacts can be represented as a series-parallel circuit formed by elements with different conductivity.

The equivalent circuit [6] for a NC in this case can be drawn as a parallel circuit, where one arm contains the Josephson element and a resistance R_1, while the parallel arm contains the resistance R_2. It is assumed that the resistive elements have linear IVC and that the incident radiation power is quite low, so that bolometric effects are not observed. Applying Kirchhoff's laws to such a circuit, we can easily show that

$$I^* = I_c\left(R_1 + R_2\right)R_2^{-1}, \quad V* = I_c R_1, \quad \delta V = V_j R_2 (R_1 + R_2)^{-1} \tag{6.3}$$

where $V_1 = hf/2e$ in accordance with (1.8).

The notation used in these expressions can be followed from the insert in Fig. 6.3. Formula (6.3) leads to expressions for the values of R_1 and R_2 as a function of the experimentally measured quantities:

$$R^* = V^*/I^*, \quad R_1 = R^* V_j/\delta V, \quad R_2 = R_1 (V_j/\delta V - 1)^{-1} \tag{6.4}$$

For $R_2 \neq \infty$, we always have $V_j > \delta V$. Applying this technique to a Cu-high-T_C superconductor contact whose IVC are presented in the insert in Fig. 6.3, we obtain R_1=1,75 Ohm and R_2=3,63 Ohm.

6.3 Bolometric Response of Nanocontacts with High-T_C Superconductors Exposed to Electromagnetic Radiation with Frequencies in the Optical Range

A completely different behaviour of the critical current under irradiation with a power $I_c(P)$ was observed in the optical frequency range ($\Omega/2\pi=4{,}75\cdot10^{14}$ Hz). As can be seen from Fig. 6.3, the increase in radiation intensity caused a monotonic decrease in the critical current for the Ta-$YBa_2Cu_3O_{7-\delta}$ contact. At a certain level of radiation power, the critical current becomes equal to zero. We can assume that the laser radiation heats the contact in this frequency range. It is well known [7, 8] that in S_1-Constriction–S_2 structures formed from different superconductors with quite different energy gaps ($\Delta_1 << \Delta_2$), the temperature dependence of the critical current is similar to that for the material with the smaller gap. In our case [9], the gaps for Ta and $YBa_2Cu_3O_{7-\delta}$ differ by more than an order of magnitude. Hence we can expect that $I_c(T) \sim \Delta_1(T)$, where $\Delta_1(0)$=0,7 meV for Ta. To determine the temperature increase ΔT (in the contact exposed to laser radiation) with respect to the He bath temperature (T_0=2,15 K), a linear dependence of the temperature increase on the laser power was assumed. When the sample is heated to above the λ-point of He (T_λ=2,17 K), the steepness of this dependence increases considerably, due to a decrease in the heat removal from the contact. The radiation power required for heating the contact to a temperature T_λ was chosen empirically to be equal to

1,7 mW. The destruction of superconductivity in Ta (T_c=4,48 K) gives another point on the second segment of the dependence

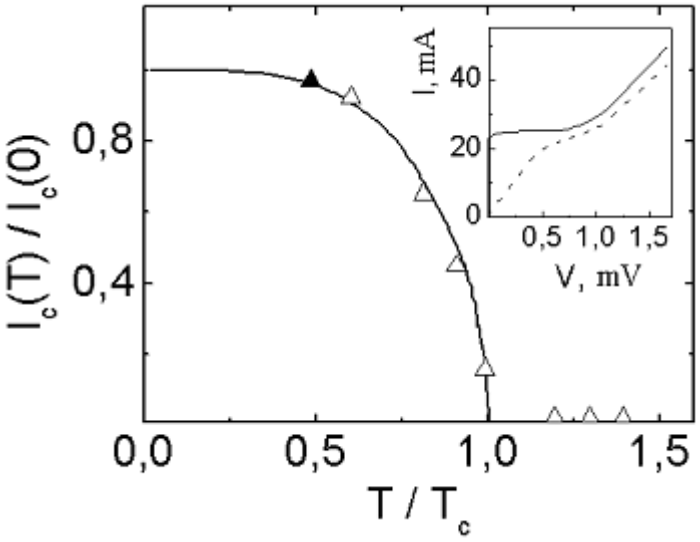

Fig 6.4 Temperature dependence of the critical current in a Ta-$YBa_2Cu_3O_{7-\delta}$ contact. The solid line is calculated according to BCS theory. The insert shows the change in I-V characteristics upon irradiation with a frequency $f_2=4,75\cdot10^{14}$ Hz.

ΔT(P). The slope of the linear dependence was found to be 0,21 K/mW.

Since the contact temperature was higher than T_λ for all values of laser power used in our experiments, the temperature increase above T_λ was calculated from the formula

$$\Delta T = 0,21\left(P - 1,7\right) \tag{6.5}$$

Fig 6.4 shows the dependence of the critical current of the contact temperature determined in this way [10]. The solid line corresponds to the temperature dependence of the energy gap of

Ta calculated according to BCS theory. The scales along the ordinate axis for both dependences were made to coincide at T=2,17 K (filled point in Fig. 6.4). The experimental and theoretical values are found to be in good agreement. This fact validates the thermal mechanism of radiation detection assumed for this frequency range.

The insert in Fig. 6.4 shows the IVC of a similar contact measured in the absence of radiation (solid line) and when exposed to the maximum laser radiation power. The nonlinearity in the region 0,5-1,0 mV under irradiation may be due to the contribution of superconductive inclusions along the path of the transport current, or to the response of the resistive ceramic regions to the external radiation.

Irradiation of high-T_C ceramic-Nb contacts (T_c=9,2 K) by a laser beam at the maximum power reduced the critical current to only half of its value. This means that the temperature increase in these contacts, as in the contacts with Ta, was not more than 4-5 K.

Thus, unlike what was observed for irradiation in the MW range, the response to light with a frequency of $4{,}75 \cdot 10^{14}$ Hz is of bolometric origin and associated with a steady heating of the contact by the electromagnetic radiation.

6.4 Local State Switching in Heterogeneous High-T_C Superconductors

6.4.1 Experimental Results for Superconducting Ceramics

Many authors have reported the existence of considerable hysteresis effects in the electrical conductivity of $Bi_2Sr_2CaCu_2O_y$ contacts. Large current-voltage characteristics were observed for

various types of conducting structures with a current concentration, such as tunnel contacts, contacts with direct conductivity, and microbridges [11, 12, 13, 14]. Several mechanisms were proposed to explain the observed effects, including the formation of the phase slip centres, suppression of superconductivity of tunnel junctions between individual superconducting grains, and thermal effects.

Here we report investigations of step-like singularities and hysteresis effects [15, 16] in different IVC of contacts formed by high-T_C superconductors. The measurements were carried out over a wide range of temperatures and HF radiation frequencies. The IVC were recorded using a circuit containing a current source as well as a circuit with a given voltage. The main experimental results were obtained for $Bi_2Sr_2CaCu_2O_y$ high-T_C superconductors. The initial ceramic samples and bulk bridges with geometric dimensions exceeding 50 μm had a superconducting transition temperature of about 86 K. The resistance decreased with temperature, i.e., the temperature dependence of the resistivity was of that of a metal. The stationary Josephson effect was not observed in comparatively narrow bridges (w<30 μm) and high-T_C material contacts with superconducting metals (Nb and Ta).

The IVC of the contacts measured in our experiments practically coincide with the analogous characteristics of narrow bridges. They also vary in a similar manner with the changing frequency of electromagnetic radiation and temperature. The characteristics of contacts formed with pins made of superconducting and normal metals are also identical. Replacement of a ceramic by high-T_C films of various thicknesses also left the general form of IVC unchanged. Hence the experimental results mainly correspond to the contacts formed between Ta and $Bi_2Sr_2CaCu_2O_y$ high-T_C films.

Typical IVC of the investigated samples are shown in Fig. 6.5. A region of gradually decreasing supercurrent is formed on the initial part of the IVC. In some samples, a region of negative

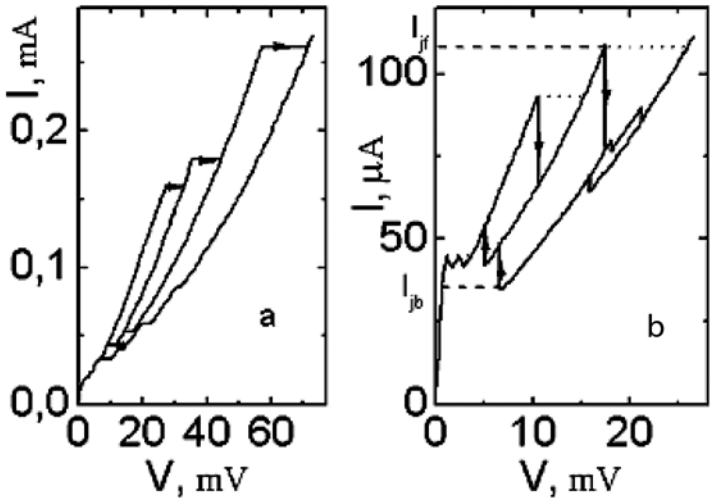

Fig. 6.5 I-V characteristics of contacts between Nb and $Bi_2Sr_2CaCu_2O_y$ high-T_C superconducting ceramics measured with a current source (a) and between Ta and a $Bi_2Sr_2CaCu_2O_y$ high-T_C film measured with a voltage source (b). The dashed line shows the I-V characteristics of the same contact obtained with the current source.

differential resistance (Fig. 6.5, b) was observed for bias voltages V~5 mV. This segment of IVC was reversible with respect to the change in direction of the voltage sweep applied to the contact.

For voltages V>10 mV, the IVC are divided into a set of individual exponential branches, which are described quite well by functional dependences of the form:

$$I_n = I_0\left[\exp\left(|V|/a_n\right)-1\right], \qquad (6.6)$$

which are characteristic for metal-semiconductor contacts. Here n is the number of the branch. The constants a_n are of the order of a fraction of 1 V. Upon a change in DC bias voltage, transitions from one branch to another (shown by arrows in Fig. 6.5) occur abruptly when certain critical current or voltage values are attained, and the resistance varies by 10-30% in the transition. Special experiments involving an alternating bias voltage and IVC recording on an oscilloscope with a resolution 10^{-5} s have failed to reveal any time dependence of the signal in the regions of the resistance jumps. Each resistance jump during a transition from one exponential branch to another is accompanied by a strong hysteresis in the IVC and, when the bias voltage decreased, a corresponding reverse jump to a much lower voltage takes place. This correspondence is difficult to trace because of electromagnetic stray currents, which cause a transition to occur simultaneously through several stable states. The quantities I_{jf} and I_{jb} in Fig. 6.5 correspond to the values of the current passing through the sample for forward and backward passage of current in the same hysteresis loop. As a rule, the first jump in the resistance occurs for a current of the order of tens of μA passing through the sample.

The IVC undergo considerable alteration upon heating from 4,2 to 200 K. The resistance increases in the initial segment of IVC, the excess current gradually decreases to zero for $T \sim T_C$, and the sample resistance than begins to decrease. For large bias voltages in the region of hysteresis loops, the values of the critical current for forward and backward transitions gradually approach each other with increasing temperature, and the hysteresis loop degenerates into a reversible transition for T~40 K. Upon subsequent increase in temperature, a reversible voltage switchover occurs for higher and higher current values. Decreasing gradually, it disappears as the temperature

approaches T_C. The temperature dependence $R_S(T)$ of the static resistance of a contact measured at a constant bias voltage V~20

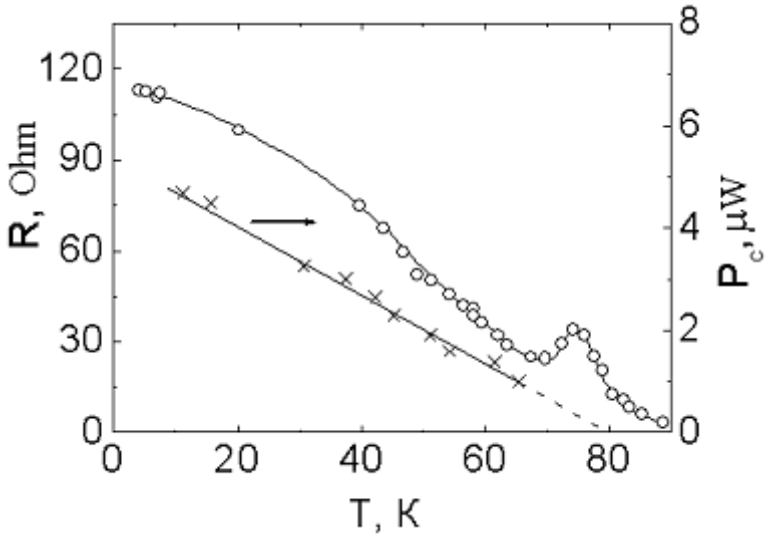

Fig. 6.6 Temperature dependence of the static resistance R_S and the critical power P_C, dissipated in the contact at the first switching of the resistance.

mV is shown in Fig. 6.6. It can be seen from this figure that a local minimum is observed against the background of a monotonic resistance decrease as the temperature approaches T_C. For some samples, this singularity is observed in the temperature interval $40<T<120$ K.

The HF modulation of the voltage applied to the contact revealed the existence of the frequency dispersion in the behaviour of the IVC upon irradiation in the interval from acoustic frequencies to 80 GHz. For irradiation frequencies $f<f_0$, where f_0=30-50 GHz for various samples, a reversal of the sign of curvature is observed upon a gradual increase in the power of

the radiation incident on the contact (Fig. 6.7). The curvature does not reverse its sign at frequencies $f>f_0$.

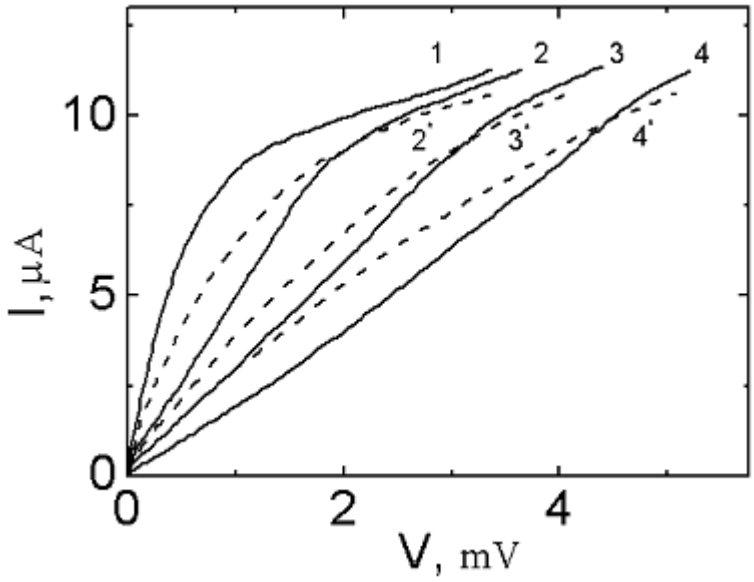

Fig. 6.7 Effect of irradiation on the initial segment of the IVC: the IVC in the absence of radiation (line 1), under the irradiation of frequency $f=\Omega_1/2\pi=9{,}6$ GHz (lines 2-4), and $f=\Omega_2/2\pi=78$ GHz (lines 2'-4'). The radiation power (at level of mW) increases from zero level with the increasing of number of the lines. T=4,2 K.

Fig. 6.8 illustrates that for high voltages in the region of multiple-valued IVC, a gradual increase in power (at mW level) leads to a degeneracy of the hysteresis into a reversible voltage jump (for measurements with a current source), whose value decreases to zero upon a further increase in the radiation intensity. The value of the frequency f_0 mentioned above is the boundary value for IVC rearrangement in the hysteresis region.

For f_0, the hysteresis degenerates with increasing MW irradiation power in the interval of currents $I_{if}>I>I_{ib}$ (Fig. 6.8, a). The

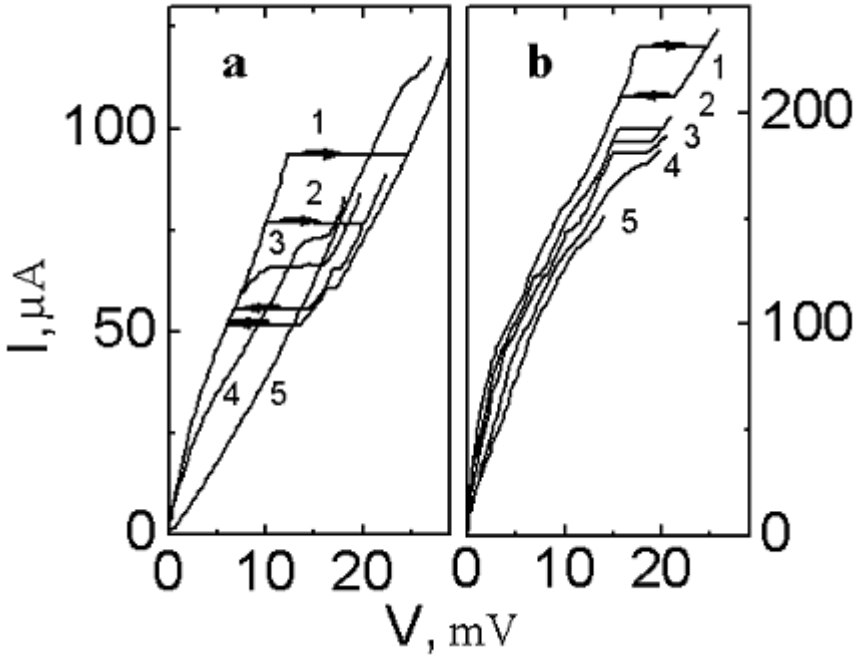

Fig. 6.8 Influence of irradiation on the multiple-valued region of the I-V chacteristics at T=4,2 K: (a) refers to radiation with frequency f =9,6 GHz and (b) to an electromagnetic field which varies with f=78 GHz; the radiation power is of mW level and increases from zero with increasing number of curves.

voltage step remaining in the IVC is shifted upon further power increase towards larger currents, and the sample resistance diminishes. In the frequency range $f>f_0$ a hysteresis degeneracy is observed for currents $I<I_{ib}$ (Fig. 6.8, b), after which the voltage jump is displaced towards lower values of current, and the sample resistance grows.

The multiple-valued IVC described above were also observed on the bridges prepared from polycrystalline $YBa_2Cu_3O_{7-\delta}$ high-

T_C films, but the samples displaying such IVC were not so frequent.

The presence of a semiconducting phase in our samples is confirmed by the thermally activated nature of the $R(T)$ curve in Fig. 6.6. The semiconducting energy gap calculated from similar dependences for various samples in the temperature range 40-80 K vary from fractions of meV to several meV.

The initial regions of IVC presented in Fig. 6.5 indicate that our samples have no continuous superconducting current channel, and that the conduction is accomplished through the semiconducting layer. Although the IVC in this region for some contacts can be described by a power function ($V \sim I^{\alpha}$), where the exponent a is slightly greater than 2 (which is typical of a transition to the resistive state for a network of weak Josephson links [17]), we did not observe a non-stationary Josephson effect in the contacts exposed to HF radiation. With the increasing temperature, the superconducting component of the transport current reduces, while the conduction through the semiconducting layer increases.

As mentioned above, the resistance jumps and the IVC hysteresis loops at DC bias V>10 mV gradually disappear as the temperature approaches T_C. No new singularities were observed on IVC for higher bias voltages and temperatures up to $T \leq T_C$. Therefore, these singularities should be attributed to the degradation of the superconducting state in individual grains.

The experimental data indicate that the electric power $P_c=I_jV_j$ dissipated in the contact at the bias voltage corresponding to the characteristic jumps decreases with increasing temperature (Fig. 6.6). If we assume that the resistance jumps have a thermal origin and that the temperature in the vicinity of the individual grains is determined by the temperature of the thermostat (He bath) and also by the Joule heating of that region, the relation between the critical power and the thermostat temperature must have the form

$\beta P_C + T = T_C$. Fig. 6.6 presents this kind of dependence for the NC between the superconducting electrode and $Bi_2Sr_2CaCu_2O_y$ ceramics.

The thermal mechanism of the observed effects is also confirmed by the anomalous behaviour of the temperature dependences of the excess current in the initial segment of the IVC. Another fact that also confirms this conclusion, is the temperature dependence of the critical power P_C up to $T=T_\lambda$. These phenomena could be attributed to a significant changes in the conditions of heat removal from the hot contact region at $T<T_\lambda$.

6.4.2 Hysteresis in the I-V Characteristics of High-T_C Superconductors

The evolution of the contact state can be visualized as follows: the weak inter-granular links cease to be superconducting for small bias voltages when a critical current density is attained; in some cases (see, for example, Fig. 6.5, b), the normal region expands with increasing bias voltage and the IVC acquires a segment with a negative differential resistance. This segment is completely reversible for measurements with a voltage source. Due to the presence of a layer connected in series which exhibits a semiconductor-type conductivity, the initial segment of the IVC always has a finite slope. As the current increases, the Joule-heating of semiconducting regions becomes more important. The temperature of over-heating is maximal near superconducting grains due to the concentration of current lines. After the attainment of T_C, individual grains go to the normal state, and the sample resistance increases abruptly, even in measurements with a voltage source. When an individual grain ceases to be superconducting, the transport current is redistributed in the bulk

of the high-T_C material, but Joule-heating is still insufficient to maintain all the volume in the normal state. Subsequently, the overheated region expands due to transitions in neighbouring grains. To return the sample to a superconducting state, the transport current must be reduced significantly in order to cool the entire normal region (which includes several grains) below T_C. Obviously, the real situation at the contact is complicated in view of the spread of current from the contact, the presence of voids in the material, and the change in the conditions of heat removal from the hot region during the phase transition of the various grains.

It should be noted that similar IVC with hysteresis loops spanning over several resistive transitions were observed [18] during thermal degradation of the superconducting state due to the action of the transport current in composite conductors based on Nb-Ti alloys.

Let us now turn to the results of experiments concerning the exposure of the contacts to HF radiation. Taking into account the observed dispersion of the response at frequencies $f>f_0$=30-50 GHz, we first consider the data for the frequency range $f<f_0$. The behaviour of IVC for various levels of radiation power in this frequency range is correctly described by classical rectification of the HF alternating current. In the quasi-static approximation, the IVC of the non-linear element, exposed to electromagnetic radiation, is described by equation (3.3). The results of the corresponding calculations are presented in Fig. 6.9 (a) for several values of the AC voltage V_1. The calculations were made for a model IVC (line 1 in Fig. 6.9, a), coinciding in shape with experimental curves obtained with a small bias voltage across the contact. A comparison of the family of curves in Fig. 6.9 (a) with the experimental data for the radiation frequency f=9,6 GHz (Fig. 6.7) indicates that the behaviour of the IVC in the region where

$V \rightarrow 0$ is indeed determined by classical detection processes of electromagnetic radiation.

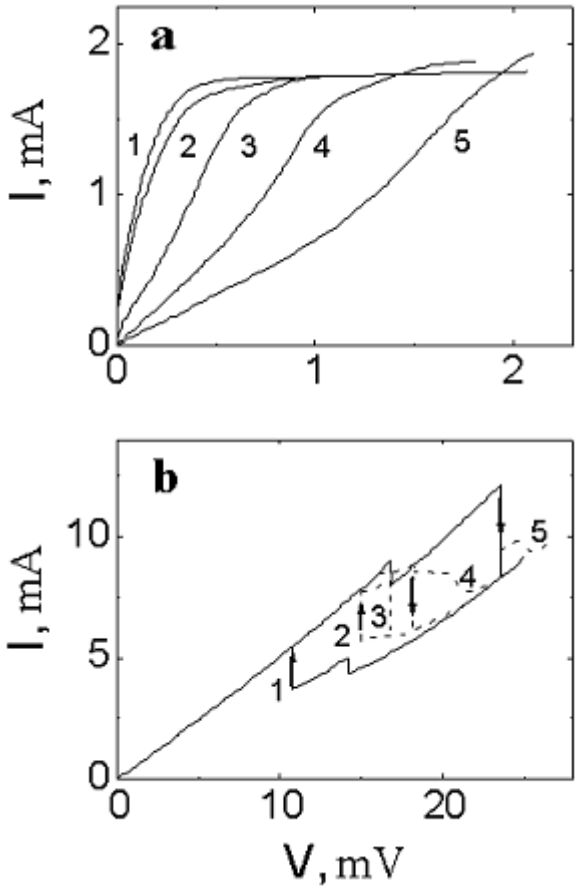

Fig. 6.9 The effect of bias voltage modulation on the I-V characteristics: a) the results of calculations for the initial segment of model I-V characteristics for modulation amplitudes V_1, of : 0 (line 1); 0,2 mV (line 2); 0,4 mV (line 3); 1,0 mV (line 4) and 1,8 mV (line 5).

b) experimental results obtained for the bias voltage modulated by the acoustic frequency (~1 kHz) with modulation amplitudes V_1: 0 (line 1); 0,36 mV (line 2); 0,5 mV (line 3); 1,0 mV (line 4) and 1,3 mV (line 5).

The multi-valued nature of IVC in the hysteresis region complicates a similar analysis for large bias voltages across the contact. For this reason, special experiments were performed to detect the low-frequency signal from an audio-frequency oscillator (f=1,9 kHz). The results of these experiments are presented in Fig. 6.9 (b). It can be seen that as the amplitude V_1 of low-frequency modulation increases, the hysteresis loop degenerates into a reversible jump for a certain voltage, lying between V_{jf} and V_{jb}, or in a current jump that is displaced towards higher voltages upon a further increase in V_1. Such signal behaviour is in a good agreement with the IVC modification in the hysteresis region under MW irradiation at frequencies $f < f_0$ (see Fig. 6.8, a).

The behaviour of the IVC when irradiated in the frequency range $f>f_0$ is completely different. As the radiation intensity increases, the differential resistance in the initial region of the IVC increases, and the hysteresis loop is displaced towards smaller currents and voltages (see Figs. 6.7 and 6.8, b). A comparison of these results with the data obtained for various temperatures leads to the conclusion that exposure to MW radiation with $f>f_0$ results in heating of the whole contact region or of several of its individual zones.

6.5 Conclusions

The characteristic voltage $V_C=I_CR_N$ that defines the Josephson current frequency, is found to be about 1 mV. This value is much smaller than expected ($V_C=\pi\Delta/e$), taking into account the energy gap Δ for $YBa_2Cu_3O_{7-\delta}$ (20-40 meV).

Exposure to electromagnetic radiation induces current steps on the initial part of IVC (non-stationary Josephson effect) for bias voltages up to 4 mV. In the microwave range, the behaviour of the critical current is correctly described by zero-order Bessel

function. We found that the response of contacts of high-T_C superconductors to mm range radiation is of Josephson nature, at least up to frequencies of ~$1{,}5 \cdot 10^{12}$ Hz. Unlike the behaviour in the microwave range, the response to radiation in the optical frequency range is of bolometric origin and associated with a steady radiation heating of the contact. The behaviour of the critical current with increasing laser radiation power is correctly described by the temperature dependence of the energy gap.

Given the heterogeneous composition of the ceramics, the NCs can be presented as a series-parallel circuit formed by elements with different types of conductivity. The observed hysteresis singularities in the IVC can be attributed to the degradation of the superconducting state in individual grains. The experimental data confirm that a thermal mechanism is the origin of the observed effects.

Exposure of the NCs to HF radiation resulted in a frequency dispersion also in the hysteresis part of IVC. The behaviour of IVC for irradiation in the range $f<f_0$ (f_0=30-50 GHz) is correctly described by a classical rectification model of the HF alternating current. The behaviour of the IVC in the frequency range $f>f_0$ (microwave and optical range) is completely different and can be attributed to heating of the whole contact region or of several of its individual zones by the radiation.

Other authors [19] also observed the effects of large-amplitude voltage switching in poly-crystalline high-T_C films of $Bi_2Sr_2CaCu_2O_y$. The characteristic time of the switching process was found to be ~1 μs. These results were interpreted on the basis of a thermal model, as a consequence of the transition of superconducting grains to the normal state. In our experiments, much shorter characteristic times $1/\tau \approx f_0 \sim 4 \cdot 10^{10}$ s^{-1} were registered, which are considerably smaller than the thermal relaxation time for individual grains with a size of 1-10 μm. Using the standard values of the thermodynamic characteristics

of $Bi_2Sr_2CaCu_2O_y$ high-T_C superconductors at $T \sim T_C$, we can estimate the typical geometric size d as $\approx(\lambda/c\rho f_0)^{1/2} \sim 10$ nm [20], where we considered the following values: thermal conductivity λ=0,04 J/(cm·s·K), specific heat c=0,2 J/(g·K), and density ρ=4,5 g/cm^3. Such nano-sized regions, overheated under HF radiation, can be attributed to thin semiconducting layers that separate the superconducting grains. The state of these layers impacts the behaviour of the entire contact zone.

The independence of the IVC shape on the type of the sample (a bridge or a contact with either a normal or a superconducting metal all give the same results) indicates that the observed effects are associated with the properties of the high-T_C material in the small volume in which the transport current is concentrated. It is well known that the polycrystalline films and ceramic samples under investigation have the form of a multiply connected disordered system of superconducting grains of various geometrical size, connected through weak Josephson links with a statistical spread of the binding energy of inter-grain junctions. The spatial heterogeneity of metal oxide ceramics is enhanced by the important (~20 %) porosity of ceramics and by the presence of inclusions with semiconductor-type conductivity. The strong spatial heterogeneity in superconductive properties of high-T_C superconductors is due to a small coherence length of the order parameter ξ that is, typically, of the order of several nm. Consequently, any structural and phase differences in the material having a size of the order of atomic separation are responsible for significant spatial variations in the superconducting energy gap.

References

1. I. K. Yanson, L. F. Ribal'chenko, V. V. Fisun et al. The study of the High-T_c superconductor by the micro-contact method. Sov. J. Low Temp. Phys. 14, 402 (1988)

2. O. P. Balkashin, I. I. Kulik, I. K. Yanson et al. Nature of response to electromagnetic radiation in contacts with superconducting oxides. Sov. J. Low Temp. Phys. 16 (1990), pp. 176-178

3. O. P. Balkashin, I. I. Kulik, I. K. Yanson. Superconducting oxide point contacts in the high-frequency field. 1st Soviet-German Symposium on HTSC. Sov. J. Low Temp. Phys. 16 (1990), p. 389

4. I. K. Yanson, L. F. Ribal'chenko, V. V. Fisun et al. Spatially non homogeneous discrete states of the superconductor at the injection of non equilibrium quasi-particles from point-contact with normal metal. Sov. J. Low Temp. Phys. 14, 639 (1988)

5. O. P. Balkashin, I. I. Kulik, I. K. Yanson et al. Electromagnetic response of the contacts with metal-oxide superconductors. Proc. 2d Soviet Conference on High-T_c Superconductivity, Kiev, 1989, vol. 1, pp. 243-244, Inst. of Metal Physics of the Ukr. SSR Acad. Sci.

6. J. A. Pals, W. van Haeringen, M. H. van Maaren. Josephson effect between superconductors in possibly different spin-pairing states. Phys. Rev. B, 1977, v.15, N 5, pp. 2592-2599

7. I. O. Kulik, I. K. Yanson. Josephson effect in superconducting bridges. Nauka, Moscow (1970) 272 p. (in Russian)

8. I. O. Kulik, A. N. Omel'yanchuk. The Josephson effect in the superconducting bridges: microscopic theory. Sov. J. Low Temp. Phys. 4, 142 (1978)

9. O. P. Balkashin, I. I. Kulik, I. K. Yanson et al. The response of the metal-YBaCuO ceramics contacts under the high-frequency and optical radiation. Proc. 3d Soviet Conference on Non-homogeneous Electronic States, Novosibirsk, 1989, pp. 190-191, Institute for Inorganic Chemistry of Sib. Dep. of USSR Acad. Sci.

10. O. P. Balkashin, I. I. Kulik, I. K. Yanson. Laser radiation heat detector with the metal microcontact base. Proc. 7th Soviet Conference on the Heat Detectors of Radiation, Leningrad, 1990, pp. 36-37, Government Optical Institute (in Russian)

11. A. T. M. de Waele, W. A. Draisma, H. J. van Schevicoven, R. W. van der Heijden, D. M. de Leeuv, C. A. Mutsaers, G. P. J. Geelen. Point-contacts from $BiCaSrCu_2O_x$. Physica C, 1988, v. 153-155, pp. 621-622

12. L. F. Ribal'chenko, V. V. Fisun, N. L. Bobrov et al. Micro-contact spectroscopy of high-T_c BiSrCaCuO. Sov. J. Low Temp. Phys. 15, 54 (1989)

13. T. Walsh, J. Moreland, R. H. Ono. Bi-Sr-Ca-Cu-O thin-film energy gap as a function of temperature and force applied to squeezable-electron-tunneling junctions. Phys. Rev. B, 1991, v.143, p. 11492

14. O. V. Karpov, M. S. Chubarov, V. A. Shilov. The studies of IVC of the Josephson transitions of the High-T_c ceramics. Sov. Tech. Phys. Lett. 17, 584 (1991)

15. O. P. Balkashin, I. I. Kulik. The switching and hysteresis phenomena in conductivity of BiSrCaCuO compound. Proc. 3d Soviet Conference on High-T_c Superconductivity, Kharkov, 1991, pp. 23-24, Institute for Low Temperature Physics & Engineering Ukr. SSR Acad. Sci.

16. I. I. Kulik, O. P. Balkashin. Local switching of states in non-homogeneous HTS materials. Sov. J. Low Temp. Phys. 21 (1995), pp. 146-151

17. V. N. Skokov, V. P. Koverda, N. M. Bogdanov, A. A. Dik. Thermal destruction of the superconducting state in thin films of $YBa_2Cu_3O_{7-y}$. Sov. Phys. JETP Lett. 16, 630 (1990)

18. A. A. Akhmetov, V. P. Baev. Current voltage characteristics of composite superconductors with high contact resistance. Cryogenics, 1984, v. 24, N 2, pp. 67-72

19. V. L. Bakumenko, E. D. Bekeshko, L. N. Kurbatov, V. I. Mikhas'ko. Voltage switching and N-type voltage-current characteristics of polycrystalline Bi-high-T_c superconducting films. Sverhprov: Fiz. Him. Teh. (SPCT) vol. 4, No. 8, p. 1594 (1991) (in Russian).

20. G. Karlsruhe, D. Eger. Thermal conductivity of solids. Nauka, Moscow, 1964, 87 p. (in Russian)

Chapter 7

SUMMARY

The presented work deals with an interesting and relatively simple experimental method, called Point Contact Spectroscopy that permits to study the behaviour of quasiparticles (phonons) in conductive solids: their generation, interactions with electrons, disappearance. We could investigate by this technique also more exotic processes for other quasiparticles (conduction electrons), such as their trapping in a semi metal crystal lattice (Sb), the pairing in superconducting solids, and the absorption of phonons by electrons. Point Contact Spectroscopy consists in the creation of a nanocontact (10-100 nm in diameter) between two conductors and in monitoring its response to electromagnetic fields. When kept in liquid helium, an enormous current density in the range of 10^9 A/cm^2 can be created in such a constriction and in these conditions, the contact becomes an instrument for revealing the quantum properties of electrons and phonons.

This Dissertation is dedicated particularly to High Frequency Point Contact Spectroscopy. This novel method uses the modulation of probe current at the frequencies from acoustic to optical range where the nanocontact is placed in a microwave waveguide or in a light guide for infra-red and optical irradiation. By this method we could experimentally determine the frequency (GHz range) at which the generated phonons will no longer influence the electrons. Apart from giving this scientifically important result, these measurements at higher frequencies were also proven to have much better precision. Other interesting phenomena were observed when irradiating with infra-red light,

namely the transition of the radiation detection mechanism from classical to the quantum regime and an increase of the phonon gas temperature. On the other hand, irradiation in the optical range was found to heat the whole nanocontact, changing the mechanism of the events (Laser Thermal Point Contact Spectroscopy).

We also focused on nanocontacts of high-T_C ceramics, which are materials with special superconductive properties and could explain the mechanism of the big jump-like hysteresis on their I-V characteristics.

The obtained results concerning the high frequency properties of nanocontacts are of importance not only from the fundamental solid state physics point of view, they are also highly relevant for the development of nano- and micro-electronics.

The main results of this PhD project can be formulated as follows:

1. The resolution of Point-Contact Spectroscopy is increased with High Frequency Point-Contact Spectroscopy - a new approach in solid-state physics.

2. The characteristic frequency of the inelastic phonon-electron scattering of phonons at the Debye energy in Cu is found to be equal to $5 \cdot 10^9$ Hz.

3. When exposed to radiation with frequencies above $2{,}8 \cdot 10^{13}$ Hz, the response of Cu nanocontacts is due to radiation-heating of the electrode surfaces next to the contact, and not only to heating of the nanocontact itself, caused by the induced current.

4. A special regime of Laser Thermal Point-Contact Spectroscopy was developed for ballistic nanocontacts irradiated in the optical range. This technique is associated with the thermal broadening of the Fermi edge in the electronic density of states.

5. Steps and hysteresis loops observed in the conductivity of contacts with high-T_C ceramics are well described by the thermal model for heterogeneous media that considers a characteristic length for thermal processes l~10 nm.

SAMENVATTING

In dit proefschrift beschrijven wij ons onderzoek waar punt-contact spectroscopie wordt ingezet om het gedrag van quasideeltjes (fononen) in geleidende materialen te onderzoeken: hun ontstaan, hun wisselwerking met elektronen en hun verval. Bijzondere aandacht wordt ook geschonken aan meer exotische processen voor andere quasideeltjes (conductie-elektronen); namelijk hoe de elektronen ingevangen worden door het rooster in de semimetal Sb, het breken van Cooper paren in een supergeleider na een initiële fotonabsorptie, en de absorptie van fononen door elektronen. De punt-contact spectroscopie bestaat in het maken van een nanocontact - een 10-100 nm brede connectie tussen twee elektroden. Als dit nanocontact in vloeibare helium wordt gehouden, kan daarin een enorme stroomdichtheid van 10^9 A/cm^2 gecreëerd worden en het contact wordt een instrument om de kwantumeigenschappen van elektronen en trillingen te meten.

In dit proefschrift besteden wij speciale aandacht aan hoge frequentie punt-contact spectroscopie. Deze nieuwe methode maakt gebruik van de stroommodulatie met frequenties van akoestische golven tot het optische bereik. Het nanocontact wordt in een microgolfgeleider geplaatst of in een optische lichtgeleider voor bestraling met infrarood of zichtbaar licht. Met behulp van deze methode konden wij experimenteel vaststellen bij welke frequentie (GHz bereik) de gegenereerde fononen de elektronen niet meer beïnvloeden. Behalve dit wetenschappelijk belangrijke resultaat te leveren, zijn deze metingen met hoge frequentie ook veel precieser. Andere interessante fenomenen worden waargenomen bij bestraling met infrarood licht, te weten de overgang van de klassieke naar het kwantum detectieregime en een stijging van de fonongastemperatuur. Anderzijds vonden wij dat optische straling het hele nanocontact verwarmt en zo het responssignaal verandert (laser thermische punt-contact spectroscopie).

We hebben de punt-contact spectroscopie ook toegepast op Hoge-T_c supergeleidende keramieken, te weten materialen met bijzondere supergeleidende eigenschappen. Daarmee hebben wij het mechanisme van de grote sprongsgewijze hysterese in de I-V karakteristieken van de nanocontacten gevormd door hoge-T_c supergeleiders, kunnen verklaren.

De gepresenteerde resultaten met betrekking tot de hoge frequentie-eigenschappen van nanocontacten zijn niet alleen belangrijk voor de fundamentele fysica, maar ook interessant uit praktisch oogpunt voor de ontwikkeling van nano- en microelektronica.

De belangrijkste resultaten van dit promotieonderzoek kunnen als volgt geformuleerd worden:

1. Hoge frequentie punt-contact spectroscopie verbetert de resolutie van punt-contact spectroscopie en toont een nieuwe aanpak in de vaste stof fysica.
2. De karakteristieke frequentie van de inelastische fonon-elektron verstrooiing van fononen met de Debye energie in Cu blijkt $5 \cdot 10^9$ Hz te zijn.
3. Bij bestraling met frequenties boven $2{,}8 \cdot 10^{13}$ Hz is de respons van de Cu nanocontacten veroorzaakt door de stralingsverwarming van de elektrodeoppervlakken vlakbij het contactpunt, en niet alleen door de verwarming van nanocontact die ontstaat bij geïnduceerde stroom.
4. Een speciaal regime van laser thermische punt-contact spectroscopie werd ontwikkeld voor ballistische nanocontacten bestraald in het optische bereik. Deze techniek is geassocieerd met thermische verbreding van de Fermi-rand in de elektronische toestandsdichtheid.
5. Stappen en hystereselussen, waargenomen in de geleidbaarheid van de contacten met hoge-Tc keramiek, zijn goed beschreven door het thermische model voor heterogene media. In dit model is de karakteristieke lengte voor thermische processen $l \sim 10$ nm.

ACKNOWLEDGEMENTS

The author would like to express his warm gratitude to Prof. P. Rudolf for her valuable comments in discussions and her big help with the presentation of this thesis, as well as for her kindness and attention during the preparation and elaboration of the text.

I wish express my deep gratitude to Prof. I. K. Yanson for his continued support and attention to this research. His supervision of the work and in particular his help in the interpretation of the experimental results was essential for the success of this project.

I am deeply indebted to Prof. O. P. Balkashin for his support at all stages of this work. His professionalism and personal participation were of great importance for obtaining the results presented here and for their critical analysis.

I would like to thank the members of the reading committee, Prof. B. J. van Wees, Prof. J. M. van Ruitenbeek and Prof. A. Barone for their constructive criticisme. I am very grateful to Fei Pei for translating the summary into Dutch and to Sonja Heimink-Groot for all her great help with administrative and organisational matters.

I deeply thank my parents Igor and Tamara, my wife Olga and my daughter Caterina, for their appreciation and love.

Many thanks to the colleagues of the Nanocontact Laboratory. The collaborative and friendly spirit of the group contributed a lot at all stages of the work.

LIST OF PUBLICATIONS

1. O. P. Balkashin, I. I. Kulik. Laser thermal point-contact spectroscopy of metals. Sov. J. Low Temp. Phys. 16 (1990), pp. 166–171

2. O. P. Balkashin, I. I. Kulik, M. V. Moskalets. High-frequency response of metal microcontacts with small electron mean free path. Sov. J. Low Temp. Phys. 18 (1992), pp. 662-664

3. O. P. Balkashin, I. I. Kulik, I. K. Yanson et al. Nature of response to electromagnetic radiation in contacts with superconducting oxides. Sov. J. Low Temp. Phys. 16 (1990), pp. 176-178

4. O. P. Balkashin, I. I. Kulik, I. K. Yanson. Superconducting oxide point contacts in a high-frequency field. 1st Soviet-German Symposium on HT_cS. Sov. J. Low Temp. Phys. 16 (1990), pp. 389

5. I. O. Kulik, I. K. Yanson, O. P. Balkashin, Yu. A. Pilipenko, I. I. Kulik. A method for the determination of the relaxation time of non-equilibrium excitations. USSR Patent No. 1581138, March 22, 1990

6. O. P. Balkashin, I. I. Kulik. Relaxation kinetics for non-equilibrium quasi-particle excitations in antimony point contacts. Sov. J. Low Temp. Phys. 21 (1995), pp. 32-37

7. I. I. Kulik, O. P. Balkashin. Local switching of states in non-homogeneous HTS materials. Sov. J. Low Temp. Phys. 21 (1995), pp. 146-151

8. O. P. Balkashin, I. I. Kulik. Quasiparticle relaxation kinetics in Sb point contacts. Proc. 2nd International Conference On Point Contact Spectroscopy. Physica B 218 (1996) 50-53

9. O. P. Balkashin, I. I. Kulik. The characteristics of the metal point contacts (PC) in the range between acoustic and optical frequencies. Sov. J. Low Temp. Phys. 18 (1992), pp. 946–952

10. O. P. Balkashin, I. I. Kulik, I. K. Yanson, Yu. G. Litvinenko, V. T. Zagoskin. Electromagnetic response of contacts with metal-oxide superconductors. Proc. 2d Soviet Conference on High-T_c Superconductivity, Kiev, 1989, vol.1, pp. 243-244, Inst. of Metal Physics of the Ukr.SSR Acad.Sci. (in Russian)

11. O. P. Balkashin, I. I. Kulik. The switching and hysteresis phenomena in the conductivity of a BiSrCaCuO compound. Proc. 3d Soviet Conference on High- T_c Superconductivity, Kharkov, 1991, pp. 23-24, Institute for Low Temperature Physics & Engineering Ukr.SSR Acad.Sci. (in Russian)

12. O. P. Balkashin, I. I. Kulik, I. K. Yanson. Laser radiation heat detector based on metal microcontacts. Proc. 7th Soviet Conference on the Heat Detectors of Radiation, Leningrad, 1990, pp. 36-37, Government Optical Institute (in Russian)

13. O. P. Balkashin, I. I. Kulik, I. K. Yanson et al. The response of the metal-YBaCuO ceramic contacts to high-frequency and optical radiation. Proc. 3d Soviet Conference on Non-homogeneous Electronic States, Novosibirsk, 1989, pp. 190-191, Institute for Inorganic Chemistry of Sib. Dep. of USSR Acad.Sci. (in Russian)

14. O. P. Balkashin, I. I. Kulik. The interaction of laser radiation with copper microcontacts. Proc. Young Scientists Conference, Kharkov, 1989, pp. 96-97, Institute for Low Temperature Physics & Engineering Ukr.SSR Acad.Sci. (in Russian).